Editor's Comments:

- *Though the referee viewed the difference between the real topography and the 4 km-resolution case as a minor issue, I am not fully convinced because of the steep terrain condition. It has been suggested that really high resolution in the vertical and in the horizontal are both needed to accurately represent the complex topography (Seaman et al. 2009; Saide et al. 2011). Could you further justify if the 4-km resolution can represent the real transport in comparison to even higher resolution simulations (e.g., 2 km).*
  Reference:
  Seaman, N., Gaudet, B., Zielonka, J., Stauffer, D., 2009. Sensitivity of Vertical Structure in the Stable Boundary Layer to Variations of the WRF Model's MELLORYAMADA-JANJIC Turbulence Scheme. 9th WRF Users' Workshop, Boulder, 23e27 June, pp. 7
  Saide et al. (2011) Forecasting urban PM10 and PM2.5 pollution episodes in very stable nocturnal conditions and complex terrain using WRFeChem CO tracer model, doi:10.1016/j.atmosenv.2011.02.001

Thanks for this comment. It is a very important point. It is for sure that 4-km resolution still cannot fully resolve the complex topography of Himalayas. Previous studies have found that ~4 km and ~1 km simulations can produce generally consistent features over the Himalayas, but the simulation at ~1 km with better representation of topography can produce a little better meteorological fields compared to the observations (e.g., Karki et al., 2017). We also conducted the sensitivity experiment at 1.5 km resolution and found the difference between 1.5 km resolution and 4 km resolution is relatively smaller. However, it should be noted that the 1.5 km resolution simulation is only conducted over a much smaller region for a shorter period due to the computational cost. All the previous studies with the simulations at the resolutions higher than 4 km (~1 km or ~2 km) around the study region can only conduct the simulations covering a small part of the Himalayas. We select 4 km instead of 1.5 km resolutions to conduct the final experiments and analysis due to the balance of the reasonable results and computational cost. Please note, this study conducted the simulations with full chemistry at 4 km resolution covering the entire Himalayas (first time as far as we are aware) that is much more computationally expensive than the meteorology-only simulation with WRF. In fact, it may need even sub-1 km resolution to fully resolve the complex topography of Himalayas. However, at this moment, it is not computationally affordable to conduct the simulation at such high resolution covering the entire Himalayas with full chemistry for even a month simulation.

Therefore, the purpose of this study is to examine the potential impact of complex topography on pollutant transport and hence the aerosol forcing over the TP instead of producing a so-called "realistic" simulation (in fact, none of modeling studies can produce a "realistic" simulation without any assumption and simplification). We selected the 4-km

resolution as it is also considered as the convection-permitting scale that can be used for future studies to investigate the impact of aerosols on regional climate of TP and is also proved to better resolve convection system and its interaction with aerosols without convective parameterization. This study can be considered as the one-step forward investigation in this field, because most of previous studies about modeling aerosol climatic impacts over the TP applied the horizontal resolutions of tens of kilometers. In future, if computational resource allows, higher resolution than 4-km is definitely needed in a region with such complex topography.

Now we discuss the limit of 4-km resolution for the complex topography of Himalayas in the revised manuscript as "In addition, although the topography at 4-km resolution resolves much better topography of Himalayas than that at 20-km resolution, it still cannot fully resolve the complexity of topography of Himalayas. The higher resolution (e.g., 1 km or sub-1 km) may be needed. Previous studies have found that the simulations at the resolutions between 1 km and 4 km can produce generally consistent features, but the simulation at 1 km with better representation of topography can produce a little better meteorological field compared to the observations (e.g., Karki et al., 2017). One sensitivity experiment at 1.5-km resolution is also conducted in this study and found the difference between the simulations at 1.5-km and 4-km resolutions is relatively small. However, it should be noted that the simulation at 1.5-km resolution is only conducted covering a much smaller region for a shorter period due to the computational cost. The experiment at 4-km instead of 1.5-km resolution is conducted finally for the study region and period due to the balance of resolving the complex topography to some extent and affordable computational cost."

Anonymous Referee #1

We thank the reviewer again for keeping helping to improve the quality of manuscript. The comments suggest that there are still some unclear discussion in the manuscript. We feel sorry not to explain our methodology more clearly. We further clarify them in this revision. For Methodology, we add more explanation to justify its validity and include the discussion about wet deposition. For results to conclusion, we revise part of conclusion to include more discussion about the comparison with previous studies and add more convincing results. Please see our detailed response below.

Specific comments:
- *1, METHODOLOGY:*
  i) The authors replaced the 20-km simulation by a 4-km simulation but with 'smooth' topography to be compared with. As I argued in the last round of review, the such topography (identically over 5 by 5 grid cells) cannot represent the smooth one of 20-km resolution. Taking the slope between neighboring grid cells as example, the values will be 0, 0, 0, 0, dz/4, which definitely defer from those of 20-km resolution (dz/20). Thus, we cannot say that the such topography is smoothened, but stepped. In fact, it is rather unrealistic. The authors did not provide any reasonable explanation but argued that some other studies applied such a method. Following others but without a respect to the truth cannot be acceptable in the science. Moreover, it is not appropriate that the 4-km topography refers to as 'original' topography. But this is a minor issue.

To explain the smoothing effect, let's follow the example provided by the reviewer to figure out what we miss and what we get in below. To simplify the example of a mountain case as reviewer suggested in one dimension, if there are 15 grid cells at 4 km resolution that represent 3 grid cells at 20 km resolution, their terrain heights are (0, 0, 0, 0, 0), (0, 0, 1 km, 0, 0), (0, 0, 0, 0, 0) at 4 km and 0, 0.2 km, 0 at 20 km. In this case, the slopes between neighboring grid cells will be (0, 0, 0, 0), (0, 0, 1/4, 1/4, 0, 0), (0, 0, 0, 0) (14 slopes within 15 grids) at 4 km and 0.2/20 and 0.2/20 at 20 km. After applying the terrain heights at 20-km resolution for the 4-km resolution simulation, the terrain heights of these 15 grid cells will be (0, 0, 0, 0, 0), (0.2 km, 0.2 km, 0.2 km, 0.2 km, 0.2 km), (0, 0, 0, 0, 0). The slopes will become (0, 0, 0, 0), (0.2/4, 0, 0, 0, 0, 0.2/4), (0, 0, 0, 0). It is evident that after applying the 20-km resolution topography, the 4-km simulation has smoother terrain and slope (smaller values) compared to the original 4-km simulation. The terrain height distributions within the same distance between the two simulations are same, although the slopes between neighboring grids at the 20-km resolution and the smooth 4-km resolution simulations are still different.

Therefore, we agree that the sensitivity (or idealized) experiment at 4-km resolution with smooth topography does not exactly represent the simulation at 20-km resolution. Since they are two experiments at different resolutions, there is no way to create identical impact from the topography between the two experiments. That's why we revised our manuscript to focus on the impact of smoothing topography on simulated results instead of comparing the simulations at two resolutions. In the revised manuscript, we did not focus on using the difference between the two experiments at 4-km resolution to explain the difference between the simulations at resolutions of 4 km and 20 km. The focus of this study has switched to understand the impact of complex topography resolved by 4 km. In our designed experiments, we believe that the difference between the two 4-km experiments with different topography can reflects the impact of complex topography against the smooth topography, at least to some extent. Using 20-km resolution topography is just one example to smooth the topography. We can also smooth the topography to 50 km or 100 km resolution if necessary. In fact, we also conducted the sensitivity experiment at 4-km resolution with the topography from one-degree resolution. The result is consistent that the complex topography will increase the transport of BC over the TP although the magnitudes are different. We selected 20-km topography as the smooth topography for the 4-km simulation, because a majority of climate and air quality modeling studies around this region used the horizontal resolutions of tens of kilometers. Therefore, the results found in this study can provide some evidence that the modeling at relatively coarse resolutions may underestimate the transport due to the smooth topography of Himalayas during our study period.

Now, we add the clarification in the methodology part of the revised manuscript as "It is noteworthy that this study focuses on understanding the impact of complex topography resolved by 4 km instead of the difference between 4-km and 20-km simulations. Prescribing the topography at 4 km following the 20-km resolution distribution is just one way to smooth the topography. In fact, the sensitivity experiment at 4-km resolution with the topography from the one-degree resolution dataset is also conducted, and the result is consistent."

In terms of reality, we never call a sensitivity experiment as the "realistic" simulation. It is generally designed to compare with the control simulation that can be considered as a "realistic" simulation, at least relatively if we don't argue that models are never perfect. We cited others' studies with the similar methodology is not meant to say that we just followed previous studies. Instead, we would like to say that this kind of methodology through comparing the control and sensitivity (idealized) numerical experiment to isolate the impact of one factor out of many influential factors is reasonable and acceptable in modeling community. In fact, this is one of the unique features of modeling studies compared to observational studies that is normally hard to isolate different influential

factors. Therefore, definitely, the results from this study will contribute to the community. Now, we specifically highlight that the sensitivity experiment is idealized in the revised manuscript as "Therefore, besides this control experiment, one sensitivity (idealized) experiment is also conducted with the same configuration as the control one ……"

Finally, in the revised manuscript, we have replaced "original topography" to "complex topography" in the main text and figures. We are not sure why the reviewer still has this concern. Please provide more specific places so that we can further revise.

- ***ii) The authors intended to investigate the impact of topography (particularly valley) -representation on the BC transport and further the local climate (precipitation) via radiative forcing. However, the precipitation can also influence the BC concentration via wet deposition, which is totally ignored in the MS.***

First of all, we agree that aerosol (including BC) and precipitation have two-way feedback. They can affect each other in the atmosphere. In our study, we did include this feedback in the experiment. We described it in the methodology part as

"Aerosol-cloud interactions were included in the model by Gustafson et al. (2007) for calculating the activation and re-suspension between dry aerosols and cloud droplets. The wet removal of grid-resolved stratiform clouds/precipitation includes two aspects, namely in-cloud removal (rainout) and below-cloud removal (washout) by Easter et al. (2004) and Chapman et al. (2009), respectively."

Although the wet deposition is included in the simulations, we didn't emphasize this process because its impact is quite small during our simulation period. During the pre-monsoon season, precipitation over the region to the south of Himalayas is quite small (Fig. S9). Along the Himalayas and over the TP, the precipitation is relatively large. We have discussed in our last revised manuscript that, based on our analysis of the contribution of each model process (transport, dry-deposition, emission, PBL mixing, and wet deposition) to the increase of BC column mass averaged over the TP during the simulation period, the two main processes affecting the BC column mass over the TP during the period are transport and dry deposition. The impact of wet deposition between the two experiments with different topography is different, however, the difference is much smaller than that of transport (source) and dry deposition (sink). That's why we didn't emphasize the analysis of wet deposition impacts. Now, we further clarify this in the revised manuscript as

"Although the impacts of PBL mixing and wet deposition on the BC column mass over the TP are also different between the simulations with different topography, their impacts are much smaller than those of transport and dry deposition during the study period."

One reason of relatively small impact of wet deposition may be because of inactive convection during the pre-monsoon season. We have discussed in the revised manuscript

that the aerosol-climate interaction with the consideration of complex topography during the monsoon season deserves further investigation, as following:

"In addition, the active convection during the monsoon season may also play an important role on pollutant transport across the Himalayas, which deserves further investigation. Furthermore, aerosol impact on cloud and precipitation, particularly during the monsoon season, and thus on the latent heat in the atmosphere and the associated responses may also depend on the complex topography."

- *2. RESULTS to CONCLUSIONS:*
  i), Their results obviously show that the BC transport difference between two simulations is due to the higher BC concentration simulated by the 4-km resolution rather than wind speed (fig 11, 14, s4, s5a,b, s6, s7), although I was confused by their bi-yaxis (do not know which, pressure or height, the plots relate to and whether they made interpolation. Do they mean that pressure level can be certainly converted to height?) of their cross-section plots and wind directions (do they take vertical wind into consideration?).

Sorry for the confusion. In last revision, the figures used two Y-axis to show both pressure and height coordinates, however the modeling results were only interpolated to the pressure levels. The heights of the figures were estimated based on the pressure-height relationship in the situation of Standard Atmosphere. This method is suggested by the official website of NCL plotting program (https://www.ncl.ucar.edu/Applications/height_lat.shtml) for demonstration. We agree that this includes a few assumptions. Therefore, according to your comment, now, we revise all figures to have one single coordinate of height to be more straightforward. Now the modeling results are interpolated into the height coordinate and then plot. In the revised manuscript, the vertical wind is included in the cross-section plots of Fig. 10-11.

We would like to kindly remind the reviewer again that both simulations in the revised manuscript are at 4 km resolution. The only influential factor leading to the difference is topography. It is not quite appropriate to conclude that the transport difference is due to the BC concentration difference based on the results along the Himalayas or over the TP. This is like the question of "which come first, chicken or egg?". The Himalayas and TP are not the source of BC. The BC there comes from the transport. The higher concentration along the Himalayas and over the TP in the simulation with the complex topography is due to the stronger transport from the source region instead of causing the stronger transport. The higher BC concentration over the TP from the simulation with complex topography is the main point of this study, which is resulted from the stronger transport. It can be partly reflected from Fig. 5. It shows that the BC column mass loading is actually lower over the source region from the simulation with the complex topography but higher over the Himalayas and TP areas. This indicates that the stronger transport reduces the mass loading
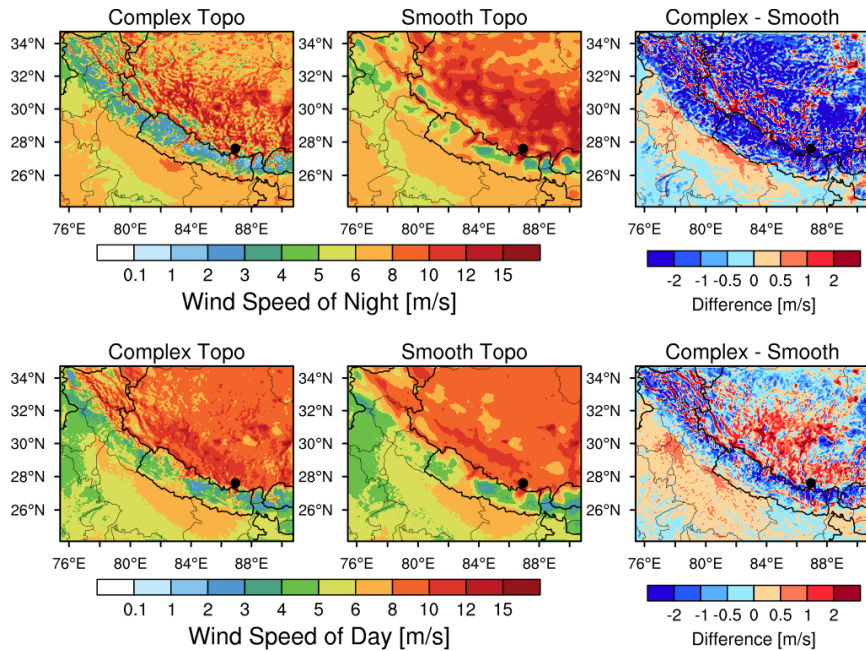
over the source region and increases the mass loading over the relatively clean region. Now we add the clarification in the revised manuscript as "In general, the column BC mass loading from the simulation with complex topography is higher over the TP and lower over the region to the south of Himalayas compared with the smooth topography, reflecting the stronger transport of BC from the source region to the Himalayas and TP due to the complex topography (see the discussion in Section 3.2)."

In terms of wind speed, we agree that the wind speed can be reduced overall except along some valley channels. With the new analysis added in this revised manuscript, we found the stronger transport is not necessarily linked with overall stronger wind speed but with stronger southerly wind towards the TP, which also depends on the wind direction. Now we add more discussion about the impacts on wind speed and transport in the revised manuscript. See our response to your comments below about the details.

- *Again, weaker wind speeds are expected from finer-resolution simulation according to previous study considering that gravity-wave-drag and turbulence-orographic-form-drag to be explicitly resolved. The authors intended to emphasize the more valleys represented by finer-resolution, but they ignored the blocking effect of more and higher mountains. They discussed only one paper (Lin et al. 2018), but there are more studies addressing the weaker near-surface (and lower-model-level) including ones focusing on a broader domain.*

Yes, we agree that the complex topography could weaken the near-surface wind speed. Now, we clarify it in the revised manuscript and add our analysis of near-surface wind in the revised manuscript. More comparison with previous related studies and the discussion about the difference are added as well.

In the revised manuscript, one new figure (Fig. S4) is added into the supporting material about the changes of near-surface wind speed (no direction), and another new figure (Fig. 13) is added into the main text about the changes of near-surface meridional wind (with direction), during our simulation period due to the impacts of complex topography. As shown in Fig. S4, what we found is that the overall near-surface wind speed is reduced over the mountainous regions with the complex topography compared to with the smooth topography, which is consistent with previous studies. However, the near-surface southerly wind during the daytime of simulation period is increased with the complex topography over the Himalayas (Fig. 13), which indicates that the transport towards the TP is strengthened with the complex topography in the study period, particularly over the central and eastern Himalayas where the BC mass loading is higher. Therefore, although the complex topography weakens the overall near-surface wind speed around the Himalayas, it favors the BC transport across the Himalayas in the study period.

Figure S4. Spatial distributions of wind speed averaged within 500 m above the ground for daytime and nighttime of April 1-20, 2016 from the simulations with complex and smooth topography. The difference between the two is also shown. Nighttime is local time 21:00-6:00, and daytime is 9:00-18:00.

Figure 13. Spatial distributions of meridional wind speed averaged within 500 m above the ground for day and night during April 1-20, 2016 from the simulations with complex and smooth topography. The difference between the two is also shown. Nighttime is defined as local time 21:00-6:00, and daytime is defined as 9:00-18:00. Positive value denotes southerly, and negative value denotes northerly.

Since some previous studies showed the overall moisture transported across the Himalayas towards the TP should be weaker with the complex topography due to the orographic drags, we further investigate the difference between this study and previous ones, although this study focuses on air pollutants instead of moisture. We found most of previous studies focused on monsoon season instead of pre-monsoon season. Therefore, we also conducted the meteorological simulations (WRF instead of WRF-Chem to reduce significantly the computational cost) for monsoon season (June-July-August) at different resolutions (4 km versus 20 km). We found that the moisture transport and precipitation in monsoon season are reduced at the higher resolution with complex topography and the meridional wind is overall weakened particularly over the central and eastern Himalayas and TP, which is consistent with previous studies. This may indicate that the different large-scale circulations between the two seasons may also lead to different impacts of complex topography on meridional winds and hence cross-Himalayas transport. This further indicates a longer-term study should be conducted to examine the impacts of topography on aerosol climatic effect over the TP in both pre-monsoon and monsoon seasons as we acknowledged in the discussion part.

Now we clarify this in the Section 3.2 of revised manuscript as

"However, it is noteworthy that previous studies have found that the orographic drag (including gravity wave drag and turbulence orographic form drag) over the region with complex topography, such as the Himalayas and other mountainous areas, would weaken the overall near-surface wind speed (e.g., Beljaars et al., 2004; Horvath et al., 2012; Jiménez and Dudhia, 2012; Zhou et al., 2017, 2018; Lin et al., 2018; Wang et al, 2020). Therefore, the near-surface wind speed is also examined. The complex topography does lead to the overall reduction of near-surface wind speed over the Himalayas area (Fig. S4 in the supporting material), which is consistent with previous studies. However, it is interesting to note that the near-surface southerly wind during the daytime of the simulation period is overall increased over the Himalayas area with the complex topography (Fig. 13), which indicates that the transport towards the TP is strengthened with the complex topography in the daytime, particularly over the central and eastern Himalayas where the BC mass loading is higher (Fig. 5). During the night, the meridional wind is dominated by northerly over the Himalayas region in the simulation with the smooth topography. The complex topography weakens the transport away from the TP or change the wind direction from northerly to southerly over some areas of Himalayas. Both effects enhance the overall transport efficiency across the Himalayas towards the TP. Therefore, although the complex topography weakens the overall near-surface wind speed around the Himalayas, it induces more realistic small-scale mountain-valley circulation that favors the BC transport across the Himalayas towards TP during the study period."

In the conclusion part of revised manuscript as

"Previous studies also found the induced change of circulation and transport due to the complex topography at convection-permitting scales with the focus on the meteorological fields over the Himalayas and TP regions (e.g., Karki et al., 2017; Zhou et al., 2017, 2018; Lin et al., 2018; Wang et al., 2020). Most of them either conducted the sub-10 km simulations covering a relatively smaller region (e.g., 101×96 grids at 5 km in Karki et al., 2017; 181×121 grids at 2 km in Lin et al., 2018; ~330×230 grids at 3 km in Wang et al., 2020) compared to this study (400×300 grids at 4 km) or conducted the simulations covering the entire Himalayas but at the resolutions above 10 km and with the sub-grid orographic drag parameterization to consider the impact of complex topography. Although some of previous studies also showed that the resolved complex topography yielded more realistic small-scale mountain-valley circulations and enhanced valley winds over the Himalayas region compared to the smoother topography, the overall moisture transport across the Himalayas towards the TP was weaker with the complex topography due to the orographic drags.

The difference between previous studies and this study can be due to several factors. First, previous studies focused on moisture instead of air pollutants. The spatial (horizontal and vertical) distributions between air pollutants and moisture are different and may contribute to the different impacts of topography on the overall transport flux across the Himalayas. However, the analysis of the moisture from the simulations in this study shows the increase of moisture transport (not shown) and hence the increase of precipitation over the TP with the complex topography (Fig. S9). Second, most of previous studies focused on monsoon season instead of pre-monsoon season. Therefore, the meteorological simulations for monsoon season (June-July-August) at different resolutions are also conducted in this study. The results show that the moisture transport and precipitation are reduced at the higher resolution with complex topography and the meridional wind is overall weakened particularly over the central and eastern Himalayas and TP (not shown), which is consistent with previous studies. This may indicate that the different large-scale circulations between the two seasons (much stronger southerly during the monsoon season) may also lead to different impacts of complex topography on meridional winds and hence cross-Himalayas transport."

- *ii) The author revised their conclusions as the enhanced BC transport in their finer resolution simulation is due to deeper-valleys plus PBL height and small-scale circulations. I did not find in any part of their results they have investigated the quantified difference in PBL height or circulations between the simulations. It can be agreed that the PBL height can somehow influence the BC transport but this study cannot lead to this conclusion. The case for resolved small-scale circulations is likewise. To diagnose the BC transport, the BC transport and wind are direct (and sufficient) factors. The resolved small-scale circulations may only mean the more realistically-simulated local winds but not stronger wind speeds.*

We did mention the effects of deeper-valleys and small-scale circulation, however, we found the PBL effect is relatively small. We discussed about its impact only for daytime and nighttime difference that is not the focus of this study. Now we clarify it in the revised manuscript as "The strong transport is primarily within the PBL during the daytime, and the deeper PBL during the daytime allows BC over the source region mixed to higher altitude, which also leads to stronger import transport during the day than the night. The relatively small difference in simulated PBL heights and structure between the two experiments can be due to their different surface heating resulted from different topography complexity (e.g., Wagner et al., 2014)."

We agree that the eventual factors influencing the BC transport should be BC mass and wind. In terms of favorable small-scale circulation, now we demonstrate it more clearly in the revised manuscript as we respond to your comment above. The results show that the near-surface southerly wind is increased during the daytime of the simulation period over the Himalayas with the complex topography, which indicates that the transport towards the TP is strengthened with the complex topography in the study period, particularly over the central and eastern Himalayas where the BC mass loading is higher.

In terms of BC mass, we mentioned deeper valley in the manuscript that does not mean deeper PBL. What we mean is that the resolved deeper valleys lead to the higher volume of relatively-high-concentration BC, which can also result in stronger transport towards the TP even with similar near-surface wind speed. For example, the altitude (above the ground) below which the BC mass concentration is larger than 0.3 ug/m^3 is much higher along the valleys with the complex topography than with the smooth topography. We add a figure (Fig. S6) in the supporting material to demonstrate this. The correlation coefficient between the difference of terrain heights of valleys and of volumes of relatively high-concentration BC can reach -0.76, indicating the lower the valleys are, the higher the volumes of BC mass can be transported across the Himalayas. This is clarified in the revised manuscript as "Another effect of resolving valleys is that the volume of relatively-high-concentration BC could be higher with deeper valleys (Fig. S5 in the support material), which can also result in stronger transport towards the TP even if the wind condition is similar. For example, the altitude (above the ground) below which the BC mass concentration is larger than 0.3 ug/m^3 is much higher along the valleys with the complex topography than with the smooth topography (Fig. S6 in the support material). The correlation coefficient between the difference of terrain heights of valleys and of volumes of relatively-high-concentration BC can reach -0.76, indicating that the lower the valleys are, the higher the volumes of BC mass can be transported across the Himalayas. The combined influence of these factors results in significantly enhanced BC transport towards the TP with the complex topography (Fig. 12), which can also be demonstrated by the distributions of wind

and BC mass concentration along the longitudinal cross section (Fig. S7a, b in the support material)."

Now we further clarify this part of our conclusions in the Highlight, Abstract, and Conclusion as
"The complex topography results in stronger overall crossing-Himalayas transport during the study period primarily due to the strengthened efficiency of near-surface meridional transport towards the TP, enhanced wind speed at some valleys, and deeper valley channels associated with larger transported BC mass volume."

"The complex topography results in stronger overall crossing-Himalayas transport during the simulation period primarily due to the strengthened efficiency of near-surface meridional transport towards the TP, enhanced wind speed at some valleys, and deeper valley channels associated with larger transported BC mass volume."

"The complex topography results in 50% higher overall transport flux across the Himalayas during the simulation period than that with the smooth topography, primarily due to the strengthened efficiency of near-surface meridional transport towards the TP, enhanced wind speed at some valleys, and deeper valley channels associated with larger BC mass volume that can be transported into the TP, although the overall wind speed is weakened due to the orographic drags with the complex topography."

Editor's Comments:

- *Though the referee viewed the difference between the real topography and the 4 km-resolution case as a minor issue, I am not fully convinced because of the steep terrain condition. It has been suggested that really high resolution in the vertical and in the horizontal are both needed to accurately represent the complex topography (Seaman et al. 2009; Saide et al. 2011). Could you further justify if the 4-km resolution can represent the real transport in comparison to even higher resolution simulations (e.g., 2 km).*
  Reference:
  Seaman, N., Gaudet, B., Zielonka, J., Stauffer, D., 2009. Sensitivity of Vertical Structure in the Stable Boundary Layer to Variations of the WRF Model's MELLORYAMADA-JANJIC Turbulence Scheme. 9th WRF Users' Workshop, Boulder, 23e27 June, pp. 7
  Saide et al. (2011) Forecasting urban PM10 and PM2.5 pollution episodes in very stable nocturnal conditions and complex terrain using WRFeChem CO tracer model, doi:10.1016/j.atmosenv.2011.02.001

Thanks for this comment. It is a very important point. It is for sure that 4-km resolution still cannot fully resolve the complex topography of Himalayas. Previous studies have found that ~4 km and ~1 km simulations can produce generally consistent features over the Himalayas, but the simulation at ~1 km with better representation of topography can produce a little better meteorological fields compared to the observations (e.g., Karki et al., 2017). We also conducted the sensitivity experiment at 1.5 km resolution and found the difference between 1.5 km resolution and 4 km resolution is relatively smaller. However, it should be noted that the 1.5 km resolution simulation is only conducted over a much smaller region for a shorter period due to the computational cost. All the previous studies with the simulations at the resolutions higher than 4 km (~1 km or ~2 km) around the study region can only conduct the simulations covering a small part of the Himalayas. We select 4 km instead of 1.5 km resolutions to conduct the final experiments and analysis due to the balance of the reasonable results and computational cost. Please note, this study conducted the simulations with full chemistry at 4 km resolution covering the entire Himalayas (first time as far as we are aware) that is much more computationally expensive than the meteorology-only simulation with WRF. In fact, it may need even sub-1 km resolution to fully resolve the complex topography of Himalayas. However, at this moment, it is not computationally affordable to conduct the simulation at such high resolution covering the entire Himalayas with full chemistry for even a month simulation.

Therefore, the purpose of this study is to examine the potential impact of complex topography on pollutant transport and hence the aerosol forcing over the TP instead of producing a so-called "realistic" simulation (in fact, none of modeling studies can produce a "realistic" simulation without any assumption and simplification). We selected the 4-km resolution as it is also considered as the convection-permitting scale that can be used for future studies to investigate the impact of aerosols on regional

climate of TP and is also proved to better resolve convection system and its interaction with aerosols without convective parameterization. This study can be considered as the one-step forward investigation in this field, because most of previous studies about modeling aerosol climatic impacts over the TP applied the horizontal resolutions of tens of kilometers. In future, if computational resource allows, higher resolution than 4-km is definitely needed in a region with such complex topography.

Now we discuss the limit of 4-km resolution for the complex topography of Himalayas in the revised manuscript as "In addition, although the topography at 4-km resolution resolves much better topography of Himalayas than that at 20-km resolution, it still cannot fully resolve the complexity of topography of Himalayas. The higher resolution (e.g., 1 km or sub-1 km) may be needed. Previous studies have found that the simulations at the resolutions between 1 km and 4 km can produce generally consistent features, but the simulation at 1 km with better representation of topography can produce a little better meteorological field compared to the observations (e.g., Karki et al., 2017). One sensitivity experiment at 1.5-km resolution is also conducted in this study and found the difference between the simulations at 1.5-km and 4-km resolutions is relatively small. However, it should be noted that the simulation at 1.5-km resolution is only conducted covering a much smaller region for a shorter period due to the computational cost. The experiment at 4-km instead of 1.5-km resolution is conducted finally for the study region and period due to the balance of resolving the complex topography to some extent and affordable computational cost."

Anonymous Referee #1

We thank the reviewer again for keeping helping to improve the quality of manuscript. The comments suggest that there are still some unclear discussion in the manuscript. We feel sorry not to explain our methodology more clearly. We further clarify them in this revision. For Methodology, we add more explanation to justify its validity and include the discussion about wet deposition. For results to conclusion, we revise part of conclusion to include more discussion about the comparison with previous studies and add more convincing results. Please see our detailed response below.

Specific comments:
- *1, METHODOLOGY:*
  i) The authors replaced the 20-km simulation by a 4-km simulation but with 'smooth' topography to be compared with. As I argued in the last round of review, the such topography (identically over 5 by 5 grid cells) cannot represent the smooth one of 20-km resolution. Taking the slope between neighboring grid cells as example, the values will be 0, 0, 0, 0, dz/4, which definitely defer from those of 20-km resolution (dz/20). Thus, we cannot say that the such topography is smoothened, but stepped. In fact, it is rather unrealistic. The authors did not provide any reasonable explanation but argued that some other studies applied such a method. Following others but without a respect to the truth cannot be acceptable in the science. Moreover, it is not appropriate that the 4-km topography refers to as 'original' topography. But this is a minor issue.

To explain the smoothing effect, let's follow the example provided by the reviewer to figure out what we miss and what we get in below. To simplify the example of a mountain case as reviewer suggested in one dimension, if there are 15 grid cells at 4 km resolution that represent 3 grid cells at 20 km resolution, their terrain heights are (0, 0, 0, 0, 0), (0, 0, 1 km, 0, 0), (0, 0, 0, 0, 0) at 4 km and 0, 0.2 km, 0 at 20 km. In this case, the slopes between neighboring grid cells will be (0, 0, 0, 0), (0, 0, 1/4, 1/4, 0, 0), (0, 0, 0, 0) (14 slopes within 15 grids) at 4 km and 0.2/20 and 0.2/20 at 20 km. After applying the terrain heights at 20-km resolution for the 4-km resolution simulation, the terrain heights of these 15 grid cells will be (0, 0, 0, 0, 0), (0.2 km, 0.2 km, 0.2 km, 0.2 km, 0.2 km), (0, 0, 0, 0, 0). The slopes will become (0, 0, 0, 0), (0.2/4, 0, 0, 0, 0, 0.2/4), (0, 0, 0, 0). It is evident that after applying the 20-km resolution topography, the 4-km simulation has smoother terrain and slope (smaller values) compared to the original 4-km simulation. The terrain height distributions within the same distance between the two simulations are same, although the slopes between neighboring grids at the 20-km resolution and the smooth 4-km resolution simulations are still different.

Therefore, we agree that the sensitivity (or idealized) experiment at 4-km resolution with smooth topography does not exactly represent the simulation at 20-km resolution. Since they are two experiments at different resolutions, there is no way to create identical impact from the topography between the two experiments. That's why we

revised our manuscript to focus on the impact of smoothing topography on simulated results instead of comparing the simulations at two resolutions. In the revised manuscript, we did not focus on using the difference between the two experiments at 4-km resolution to explain the difference between the simulations at resolutions of 4 km and 20 km. The focus of this study has switched to understand the impact of complex topography resolved by 4 km. In our designed experiments, we believe that the difference between the two 4-km experiments with different topography can reflects the impact of complex topography against the smooth topography, at least to some extent. Using 20-km resolution topography is just one example to smooth the topography. We can also smooth the topography to 50 km or 100 km resolution if necessary. In fact, we also conducted the sensitivity experiment at 4-km resolution with the topography from one-degree resolution. The result is consistent that the complex topography will increase the transport of BC over the TP although the magnitudes are different. We selected 20-km topography as the smooth topography for the 4-km simulation, because a majority of climate and air quality modeling studies around this region used the horizontal resolutions of tens of kilometers. Therefore, the results found in this study can provide some evidence that the modeling at relatively coarse resolutions may underestimate the transport due to the smooth topography of Himalayas during our study period.

Now, we add the clarification in the methodology part of the revised manuscript as "It is noteworthy that this study focuses on understanding the impact of complex topography resolved by 4 km instead of the difference between 4-km and 20-km simulations. Prescribing the topography at 4 km following the 20-km resolution distribution is just one way to smooth the topography. In fact, the sensitivity experiment at 4-km resolution with the topography from the one-degree resolution dataset is also conducted, and the result is consistent."

In terms of reality, we never call a sensitivity experiment as the "realistic" simulation. It is generally designed to compare with the control simulation that can be considered as a "realistic" simulation, at least relatively if we don't argue that models are never perfect. We cited others' studies with the similar methodology is not meant to say that we just followed previous studies. Instead, we would like to say that this kind of methodology through comparing the control and sensitivity (idealized) numerical experiment to isolate the impact of one factor out of many influential factors is reasonable and acceptable in modeling community. In fact, this is one of the unique features of modeling studies compared to observational studies that is normally hard to isolate different influential factors. Therefore, definitely, the results from this study will contribute to the community. Now, we specifically highlight that the sensitivity experiment is idealized in the revised manuscript as "Therefore, besides this control experiment, one sensitivity (idealized) experiment is also conducted with the same configuration as the control one ……"

Finally, in the revised manuscript, we have replaced "original topography" to "complex topography" in the main text and figures. We are not sure why the reviewer still has this concern. Please provide more specific places so that we can further revise.

- *ii) The authors intended to investigate the impact of topography (particularly valley) -representation on the BC transport and further the local climate (precipitation) via radiative forcing. However, the precipitation can also influence the BC concentration via wet deposition, which is totally ignored in the MS.*

First of all, we agree that aerosol (including BC) and precipitation have two-way feedback. They can affect each other in the atmosphere. In our study, we did include this feedback in the experiment. We described it in the methodology part as

"Aerosol-cloud interactions were included in the model by Gustafson et al. (2007) for calculating the activation and re-suspension between dry aerosols and cloud droplets. The wet removal of grid-resolved stratiform clouds/precipitation includes two aspects, namely in-cloud removal (rainout) and below-cloud removal (washout) by Easter et al. (2004) and Chapman et al. (2009), respectively."

Although the wet deposition is included in the simulations, we didn't emphasize this process because its impact is quite small during our simulation period. During the pre-monsoon season, precipitation over the region to the south of Himalayas is quite small (Fig. S9). Along the Himalayas and over the TP, the precipitation is relatively large. We have discussed in our last revised manuscript that, based on our analysis of the contribution of each model process (transport, dry-deposition, emission, PBL mixing, and wet deposition) to the increase of BC column mass averaged over the TP during the simulation period, the two main processes affecting the BC column mass over the TP during the period are transport and dry deposition. The impact of wet deposition between the two experiments with different topography is different, however, the difference is much smaller than that of transport (source) and dry deposition (sink). That's why we didn't emphasize the analysis of wet deposition impacts. Now, we further clarify this in the revised manuscript as

"Although the impacts of PBL mixing and wet deposition on the BC column mass over the TP are also different between the simulations with different topography, their impacts are much smaller than those of transport and dry deposition during the study period."

One reason of relatively small impact of wet deposition may be because of inactive convection during the pre-monsoon season. We have discussed in the revised manuscript that the aerosol-climate interaction with the consideration of complex topography during the monsoon season deserves further investigation, as following:

"In addition, the active convection during the monsoon season may also play an important role on pollutant transport across the Himalayas, which deserves further investigation. Furthermore, aerosol impact on cloud and precipitation, particularly

5

during the monsoon season, and thus on the latent heat in the atmosphere and the associated responses may also depend on the complex topography."

- *2. RESULTS to CONCLUSIONS:*
  i), Their results obviously show that the BC transport difference between two simulations is due to the higher BC concentration simulated by the 4-km resolution rather than wind speed (fig 11, 14, s4, s5a,b, s6, s7), although I was confused by their bi-yaxis (do not know which, pressure or height, the plots relate to and whether they made interpolation. Do they mean that pressure level can be certainly converted to height?) of their cross-section plots and wind directions (do they take vertical wind into consideration?).

Sorry for the confusion. In last revision, the figures used two Y-axis to show both pressure and height coordinates, however the modeling results were only interpolated to the pressure levels. The heights of the figures were estimated based on the pressure-height relationship in the situation of Standard Atmosphere. This method is suggested by the official website of NCL plotting program (https://www.ncl.ucar.edu/Applications/height_lat.shtml) for demonstration. We agree that this includes a few assumptions. Therefore, according to your comment, now, we revise all figures to have one single coordinate of height to be more straightforward. Now the modeling results are interpolated into the height coordinate and then plot. In the revised manuscript, the vertical wind is included in the cross-section plots of Fig. 10-11.

We would like to kindly remind the reviewer again that both simulations in the revised manuscript are at 4 km resolution. The only influential factor leading to the difference is topography. It is not quite appropriate to conclude that the transport difference is due to the BC concentration difference based on the results along the Himalayas or over the TP. This is like the question of "which come first, chicken or egg?". The Himalayas and TP are not the source of BC. The BC there comes from the transport. The higher concentration along the Himalayas and over the TP in the simulation with the complex topography is due to the stronger transport from the source region instead of causing the stronger transport. The higher BC concentration over the TP from the simulation with complex topography is the main point of this study, which is resulted from the stronger transport. It can be partly reflected from Fig. 5. It shows that the BC column mass loading is actually lower over the source region from the simulation with the complex topography but higher over the Himalayas and TP areas. This indicates that the stronger transport reduces the mass loading over the source region and increases the mass loading over the relatively clean region. Now we add the clarification in the revised manuscript as "In general, the column BC mass loading from the simulation with complex topography is higher over the TP and lower over the region to the south of Himalayas compared with the smooth topography, reflecting the stronger transport of BC from the source region to the Himalayas and TP due to the complex topography (see the discussion in Section 3.2)."

In terms of wind speed, we agree that the wind speed can be reduced overall except along some valley channels. With the new analysis added in this revised manuscript, we found the stronger transport is not necessarily linked with overall stronger wind speed but with stronger southerly wind towards the TP, which also depends on the wind direction. Now we add more discussion about the impacts on wind speed and transport in the revised manuscript. See our response to your comments below about the details.
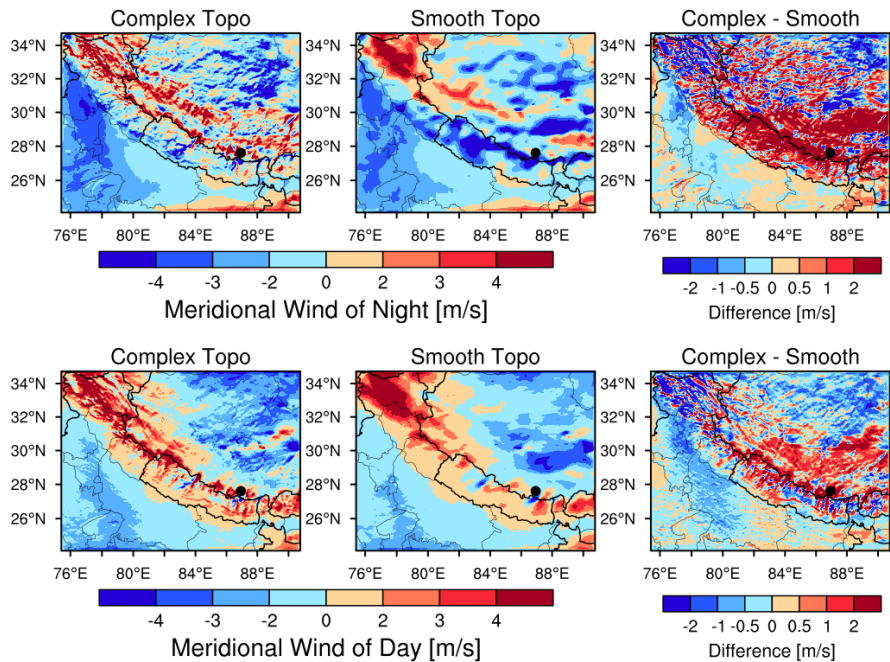
- *Again, weaker wind speeds are expected from finer-resolution simulation according to previous study considering that gravity-wave-drag and turbulence-orographic-form-drag to be explicitly resolved. The authors intended to emphasize the more valleys represented by finer-resolution, but they ignored the blocking effect of more and higher mountains. They discussed only one paper (Lin et al. 2018), but there are more studies addressing the weaker near-surface (and lower-model-level) including ones focusing on a broader domain.*

Yes, we agree that the complex topography could weaken the near-surface wind speed. Now, we clarify it in the revised manuscript and add our analysis of near-surface wind in the revised manuscript. More comparison with previous related studies and the discussion about the difference are added as well.

In the revised manuscript, one new figure (Fig. S4) is added into the supporting material about the changes of near-surface wind speed (no direction), and another new figure (Fig. 13) is added into the main text about the changes of near-surface meridional wind (with direction), during our simulation period due to the impacts of complex topography. As shown in Fig. S4, what we found is that the overall near-surface wind speed is reduced over the mountainous regions with the complex topography compared to with the smooth topography, which is consistent with previous studies. However, the near-surface southerly wind during the daytime of simulation period is increased with the complex topography over the Himalayas (Fig. 13), which indicates that the transport towards the TP is strengthened with the complex topography in the study period, particularly over the central and eastern Himalayas where the BC mass loading is higher. Therefore, although the complex topography weakens the overall near-surface wind speed around the Himalayas, it favors the BC transport across the Himalayas in the study period.

Figure S4. Spatial distributions of wind speed averaged within 500 m above the ground for daytime and nighttime of April 1-20, 2016 from the simulations with complex and smooth topography. The difference between the two is also shown. Nighttime is local time 21:00-6:00, and daytime is 9:00-18:00.

Figure 13. Spatial distributions of meridional wind speed averaged within 500 m above the ground for day and night during April 1-20, 2016 from the simulations with complex and smooth topography. The difference between the two is also shown. Nighttime is defined as local time 21:00-6:00, and daytime is defined as 9:00-18:00. Positive value denotes southerly, and negative value denotes northerly.

Since some previous studies showed the overall moisture transported across the Himalayas towards the TP should be weaker with the complex topography due to the orographic drags, we further investigate the difference between this study and previous ones, although this study focuses on air pollutants instead of moisture. We found most

of previous studies focused on monsoon season instead of pre-monsoon season. Therefore, we also conducted the meteorological simulations (WRF instead of WRF-Chem to reduce significantly the computational cost) for monsoon season (June-July-August) at different resolutions (4 km versus 20 km). We found that the moisture transport and precipitation in monsoon season are reduced at the higher resolution with complex topography and the meridional wind is overall weakened particularly over the central and eastern Himalayas and TP, which is consistent with previous studies. This may indicate that the different large-scale circulations between the two seasons may also lead to different impacts of complex topography on meridional winds and hence cross-Himalayas transport. This further indicates a longer-term study should be conducted to examine the impacts of topography on aerosol climatic effect over the TP in both pre-monsoon and monsoon seasons as we acknowledged in the discussion part.

Now we clarify this in the Section 3.2 of revised manuscript as
"However, it is noteworthy that previous studies have found that the orographic drag (including gravity wave drag and turbulence orographic form drag) over the region with complex topography, such as the Himalayas and other mountainous areas, would weaken the overall near-surface wind speed (e.g., Beljaars et al., 2004; Horvath et al., 2012; Jiménez and Dudhia, 2012; Zhou et al., 2017, 2018; Lin et al., 2018; Wang et al, 2020). Therefore, the near-surface wind speed is also examined. The complex topography does lead to the overall reduction of near-surface wind speed over the Himalayas area (Fig. S4 in the supporting material), which is consistent with previous studies. However, it is interesting to note that the near-surface southerly wind during the daytime of the simulation period is overall increased over the Himalayas area with the complex topography (Fig. 13), which indicates that the transport towards the TP is strengthened with the complex topography in the daytime, particularly over the central and eastern Himalayas where the BC mass loading is higher (Fig. 5). During the night, the meridional wind is dominated by northerly over the Himalayas region in the simulation with the smooth topography. The complex topography weakens the transport away from the TP or change the wind direction from northerly to southerly over some areas of Himalayas. Both effects enhance the overall transport efficiency across the Himalayas towards the TP. Therefore, although the complex topography weakens the overall near-surface wind speed around the Himalayas, it induces more realistic small-scale mountain-valley circulation that favors the BC transport across the Himalayas towards TP during the study period."

In the conclusion part of revised manuscript as
"Previous studies also found the induced change of circulation and transport due to the complex topography at convection-permitting scales with the focus on the meteorological fields over the Himalayas and TP regions (e.g., Karki et al., 2017; Zhou et al., 2017, 2018; Lin et al., 2018; Wang et al., 2020). Most of them either conducted the sub-10 km simulations covering a relatively smaller region (e.g., 101×96 grids at 5 km in Karki et al., 2017; 181×121 grids at 2 km in Lin et al., 2018; ~330×230 grids at

3 km in Wang et al., 2020) compared to this study (400×300 grids at 4 km) or conducted the simulations covering the entire Himalayas but at the resolutions above 10 km and with the sub-grid orographic drag parameterization to consider the impact of complex topography. Although some of previous studies also showed that the resolved complex topography yielded more realistic small-scale mountain-valley circulations and enhanced valley winds over the Himalayas region compared to the smoother topography, the overall moisture transport across the Himalayas towards the TP was weaker with the complex topography due to the orographic drags.

The difference between previous studies and this study can be due to several factors. First, previous studies focused on moisture instead of air pollutants. The spatial (horizontal and vertical) distributions between air pollutants and moisture are different and may contribute to the different impacts of topography on the overall transport flux across the Himalayas. However, the analysis of the moisture from the simulations in this study shows the increase of moisture transport (not shown) and hence the increase of precipitation over the TP with the complex topography (Fig. S9). Second, most of previous studies focused on monsoon season instead of pre-monsoon season. Therefore, the meteorological simulations for monsoon season (June-July-August) at different resolutions are also conducted in this study. The results show that the moisture transport and precipitation are reduced at the higher resolution with complex topography and the meridional wind is overall weakened particularly over the central and eastern Himalayas and TP (not shown), which is consistent with previous studies. This may indicate that the different large-scale circulations between the two seasons (much stronger southerly during the monsoon season) may also lead to different impacts of complex topography on meridional winds and hence cross-Himalayas transport."

- *ii) The author revised their conclusions as the enhanced BC transport in their finer resolution simulation is due to deeper-valleys plus PBL height and small-scale circulations. I did not find in any part of their results they have investigated the quantified difference in PBL height or circulations between the simulations. It can be agreed that the PBL height can somehow influence the BC transport but this study cannot lead to this conclusion. The case for resolved small-scale circulations is likewise. To diagnose the BC transport, the BC transport and wind are direct (and sufficient) factors. The resolved small-scale circulations may only mean the more realistically-simulated local winds but not stronger wind speeds.*

We did mention the effects of deeper-valleys and small-scale circulation, however, we found the PBL effect is relatively small. We discussed about its impact only for daytime and nighttime difference that is not the focus of this study. Now we clarify it in the revised manuscript as "The strong transport is primarily within the PBL during the daytime, and the deeper PBL during the daytime allows BC over the source region mixed to higher altitude, which also leads to stronger import transport during the day than the night. The relatively small difference in simulated PBL heights and structure between the two experiments can be due to their different surface heating resulted from different topography complexity (e.g., Wagner et al., 2014)."

We agree that the eventual factors influencing the BC transport should be BC mass and wind. In terms of favorable small-scale circulation, now we demonstrate it more clearly in the revised manuscript as we respond to your comment above. The results show that the near-surface southerly wind is increased during the daytime of the simulation period over the Himalayas with the complex topography, which indicates that the transport towards the TP is strengthened with the complex topography in the study period, particularly over the central and eastern Himalayas where the BC mass loading is higher.

In terms of BC mass, we mentioned deeper valley in the manuscript that does not mean deeper PBL. What we mean is that the resolved deeper valleys lead to the higher volume of relatively-high-concentration BC, which can also result in stronger transport towards the TP even with similar near-surface wind speed. For example, the altitude (above the ground) below which the BC mass concentration is larger than 0.3 ug/m^3 is much higher along the valleys with the complex topography than with the smooth topography. We add a figure (Fig. S6) in the supporting material to demonstrate this. The correlation coefficient between the difference of terrain heights of valleys and of volumes of relatively high-concentration BC can reach -0.76, indicating the lower the valleys are, the higher the volumes of BC mass can be transported across the Himalayas. This is clarified in the revised manuscript as "Another effect of resolving valleys is that the volume of relatively-high-concentration BC could be higher with deeper valleys (Fig. S5 in the support material), which can also result in stronger transport towards the TP even if the wind condition is similar. For example, the altitude (above the ground) below which the BC mass concentration is larger than 0.3 ug/m^3 is much higher along the valleys with the complex topography than with the smooth topography (Fig. S6 in the support material). The correlation coefficient between the difference of terrain heights of valleys and of volumes of relatively-high-concentration BC can reach -0.76, indicating that the lower the valleys are, the higher the volumes of BC mass can be transported across the Himalayas. The combined influence of these factors results in significantly enhanced BC transport towards the TP with the complex topography (Fig. 12), which can also be demonstrated by the distributions of wind and BC mass concentration along the longitudinal cross section (Fig. S7a, b in the support material)."

Now we further clarify this part of our conclusions in the Highlight, Abstract, and Conclusion as
"The complex topography results in stronger overall crossing-Himalayas transport during the study period primarily due to the strengthened efficiency of near-surface meridional transport towards the TP, enhanced wind speed at some valleys, and deeper valley channels associated with larger transported BC mass volume."

"The complex topography results in stronger overall crossing-Himalayas transport during the simulation period primarily due to the strengthened efficiency of near-surface meridional transport towards the TP, enhanced wind speed at some valleys, and deeper valley channels associated with larger transported BC mass volume."

"The complex topography results in 50% higher overall transport flux across the Himalayas during the simulation period than that with the smooth topography, primarily due to the strengthened efficiency of near-surface meridional transport towards the TP, enhanced wind speed at some valleys, and deeper valley channels associated with larger BC mass volume that can be transported into the TP, although the overall wind speed is weakened due to the orographic drags with the complex topography."

Impact of topography on black carbon transport to the southern Tibetan Plateau during pre-monsoon season and its climatic implication

[1]Meixin Zhang, [1]Chun Zhao*, [2,3]Zhiyuan Cong, [1]Qiuyan Du, [1]Mingyue Xu, [1]Yu Chen, [4]Ming Chen, [1]Rui Li, [1]Yunfei Fu, [1]Lei Zhong, [3,5]Shichang Kang, [6]Delong Zhao, [6]Yan Yang

[1]School of Earth and Space Sciences, University of Science and Technology of China, Hefei, China

[2]Key Laboratory of Tibetan Environment Changes and Land Surface Processes, Institute of Tibetan Plateau Research, Chinese Academy of Sciences (CAS), Beijing 100101, China

[3]CAS Center for Excellence in Tibetan Plateau Earth Sciences, Institute of Tibetan Plateau Research, CAS, Beijing 100101, China

[4]National Center for Atmospheric Research, Boulder, CO, USA

[5]State Key Laboratory of Cryosphere Science, Northwest Institute of Eco-Environment and Resources, CAS, Lanzhou 730000, China

[6]Beijing Weather Modification Office, Beijing 100101, China

*Corresponding author: Chun Zhao (chunzhao@ustc.edu.cn)

Key points:

1. The black carbon (BC) transport across the Himalayas can overcome a majority of mountain ridges, but the valley transport is much more efficient during the pre-monsoon season.

2. The complex topography results in stronger overall crossing-Himalayas transport during the study period primarily due to the strengthened efficiency of near-surface meridional transport towards the TP, enhanced valley wind, speed at some valleys, and deeper valley channels, and induced small scale favorable circulation associated with larger transported BC mass volume.

3. The complex topography generates 50% higher transport flux of BC across the Himalayas and 30-50% stronger BC radiative heating in the atmosphere up to 10 km over the Tibetan Plateau (TP) than that with the smoother topography, which implies that global climate models with relatively coarse resolution may introduce significant negative biases in estimating BC radiative forcing over the TP due to smooth topography.

4. The different topography also leads to different distributions of snow cover and BC forcing in snow over the TP.

Abstract

Most of previous modeling studies about black carbon (BC) transport and impact over the Tibetan Plateau (TP) conducted simulations with horizontal resolutions coarser than 10 km that may not be able to resolve well the complex topography of the Himalayas. In this study, the two experiments covering entire Himalayas with the Weather Research and Forecasting Model coupled with chemistry (WRF-Chem) at the horizontal resolution of 4 km but with two different topography datasets (4-km complex topography and 20-km smooth topography) are conducted for pre-monsoon season (April, 2016) to investigate the impacts of topography on modeling the transport and distribution of BC over the TP. Both experiments show evident accumulation of aerosols near the southern Himalayas during the pre-monsoon season, consistent with the satellite retrievals. The observed episode of high near-surface BC concentration at the station near the Mt. Everest due to heavy biomass burning near the southern Himalayas is well captured by the simulations. The simulations indicate that the prevailing up-flow across the Himalayas driven by the large-scale ~~circulation~~westerly and small-scale southerly circulations during the daytime is the dominant transport mechanism of South Asian BC into the TP, and is much stronger than that during the nighttime. The simulation with 4-km topography resolves more valleys and mountain ridges, and shows that the BC transport across the Himalayas can overcome a majority of mountain ridges but the valley transport is more efficient. The complex topography results in stronger overall crossing-Himalayas transport during the simulation period primarily due to the strengthened efficiency of near-surface meridional transport towards the TP, enhanced ~~valley~~ wind~~,~~ speed at some valleys, and deeper valley channels~~, and induced small-scale favorable circulation~~ associated with larger transported BC mass volume. This results in 50% higher transport flux of BC across the Himalayas and 30-50% stronger BC radiative heating in the atmosphere up to 10 km over the TP from the simulation with 4-km complex topography than that with 20-km smoother topography. The different topography also leads to different distributions of snow cover and BC forcing in snow. This study implies that global climate models generally with even coarser resolutions than 20 km and therefore relatively smoother topography may introduce significant negative biases in estimating light absorbing aerosol radiative forcing over the TP.

1. Introduction

The Tibetan Plateau (TP) is the highest plateau in the world with an average elevation over 4 km and an area of approximately 2.5×10^6 km^2, known as the world's third pole (Qiu, 2008), and its enormous dynamic and thermal effects have a huge impact on large-scale atmospheric circulation through the energy exchange with the atmosphere especially the troposphere, such as Asian monsoon (e.g., Ye and Wu, 1998; Duan and Wu, 2005; Wu et al., 2007, 2012a; Boos and Kuang, 2013; Chen and Bordoni, 2014; He et al., 2019; Zhao et al., 2019). In addition, the glacial melting water of TP is one of the important sources of water resources of the Indus River, Ganges River, Yangtze River, and Yellow River in Asia (e.g., Singh and Bengtsson, 2004; Barnett et al., 2005; Immerzeel et al., 2010; Lutz et al., 2014). Previous studies found aerosols in the atmosphere over/around the TP could change the regional climate of Asia (e.g., Qian et al., 2011, 2015; Lau et al., 2017, 2018). Model simulations showed that the absorptive aerosols changed the surface radiative flux over the TP by 5-25 W m^{-2} during the pre-monsoon season in April and May and led to the changes in summer monsoon circulations (Qian et al., 2011). Meanwhile, aerosol may affect the atmosphere by modulating the vertical structure of cloud and precipitation around the TP, and thus change the distribution of atmospheric latent heat around the TP, which is the main driving force of regional atmosphere circulations (e.g., Li et al., 2010, 2017, 2019). Moreover, when absorbing aerosols settle on the snow-covered areas, they will blacken the surface of snow cover and glacier to a large extent (e.g., Hansen and Nazarenko, 2004; Ramanathan and Carmichael, 2008; Lau et al., 2010, 2018; Lee et al., 2013; Zhang et al., 2017, 2018), reduce the snow albedo so as to absorb more solar radiation and cause the consequences of accelerated melting (e.g., Ramanathan et al., 2007; Ming et al., 2009; Yasunari et al., 2010; Ji et al., 2015; Zhang et al., 2015). According to the Intergovernmental Panel on Climate Change Fifth Assessment Report (IPCC AR5), the radiative forcing caused by the important component of absorbing aerosols, black carbon (BC), on the surface snow is 0.04 W m^{-2} (0.02-0.09 W m^{-2}) on global average, and the regional forcing (such as over the Arctic and the Himalayas) can be considerably large.

The TP is surrounded by various sources of pollutants. Over the South of TP, previous studies have suggested that South Asia was the main source of pollutants transported to the plateau (e.g., Cong et al., 2009, 2015a, b; Kopacz et al., 2011; Lu et al., 2012; Zhao et al., 2013; Wang et al., 2015; Zhang et al., 2015; Kang et al., 2016, 2019; Li et al., 2016; Chen et al., 2018). A huge blanket or layer of "haze" composes of light-absorbing carbonaceous aerosol

107 particles that often erupts in the pre-monsoon season over South Asia and has a significant
108 influence on the plateau (e.g., Prasad and Singh, 2007; Engling and Gelencser, 2010). Among
109 them, biomass burning emission reaching the maximum in pre-monsoon season over South
110 Asia is one of the dominant sources (e.g., Cong et al., 2015b). Many studies investigated the
111 transport mechanisms of South Asian pollutants to the TP and found that the pollutants
112 transported across the Himalayas were mainly due to the combination of large-scale circulation
113 and regional wind (e.g., Hindman and Upadhyay, 2002; Cao et al., 2010; Dumka et al., 2010;
114 Marinoni et al., 2010; Cong et al., 2015a; Kang et al., 2016; Lüthi et al., 2015; Zhang et al.,
115 2017). Cong et al. (2015a) conducted seven-day backward air-mass trajectories experiment and
116 found2015b) suggested that strong large-scale westerly and local small-scale mountain-valley
117 wind passed through western Nepal, northwest India and Pakistan (i.e., southern Himalayas)
118 in the pre-monsoon season. Dumka et al. (2010) and Kang et al. (2016) inferred from the
119 trajectory analysis that long-distance transport from Africa and Europe may also affect the BC
120 concentration of Himalayas in addition to the influence of regional pollution. The synoptic
121 troughs and ridges were also found favoring the transport of pollutants into the TP from South
122 Asia (Lüthi et al., 2015).
123   Although previous studies have confirmed the transport of pollutants across the Himalayas,
124 the complex topography of Himalayas complicates transport mechanisms. On one hand, Cao
125 et al. (2010) revealed that the Himalayas acted as a huge barrier to the transport of a large
126 amount of BC over the plateau based on model simulations. On the other hand, some studies
127 found that the valleys across the Himalayas served as channels for efficient transport of
128 pollutants (e.g., Hindman and Upadhyay, 2002; Marinoni et al., 2010). Marinoni et al. (2010)
129 analyzed the observation of wind at a station of the southern Himalayas and found that a distinct
130 valley wind system with the prominent southerly continuously transported pollutants to the
131 plateau. Most of these studies used observations and back-trajectory models to demonstrate the
132 transport pathways of pollutants to the TP, which cannot explicitly reveal the transport
133 mechanisms underneath, in particular quantifying the impacts of complex topography.
134   A few of modeling studies investigated the pollutant transport mechanisms using 3-D
135 chemical transport models (e.g., Kopacz et al., 2011; Liu et al., 2015; Zhang et al., 2017; Yang
136 et al., 2018). However, most of them simulated transport processes at relatively coarse
137 horizontal resolutions (e.g., 20-100 km), which cannot resolve well the complex topography of
138 Himalayas. It is noteworthy that studies about the aerosol climatic impact over the TP also used
139 climate models at relatively coarse horizontal resolutions (e.g., Flanner and Zender, 2005;
140 Menon et al., 2010; Kopacz et al., 2011; Qian et al., 2011, 2015; He et al., 2014; Zhang et al.,

141 2015; Ji et al., 2016). So far, there is only one study that used a chemical transport model at a
142 horizontal resolution of sub-10 km to investigate pollutant transport mechanisms over the
143 eastern Himalayas (Cao et al., 2010). Furthermore, none of studies assessed quantitatively the
144 impacts of topography on modeling the pollutant transport across the Himalayas and hence on
145 estimating aerosol distribution and radiative forcing over the TP.

146   In order to examine the potential impacts of complex topography on pollutant transport
147 across the Himalayas over the TP, this study conducts multiple experiments with the Weather
148 Research and Forecasting Model coupled with chemistry (WRF-Chem, Grell et al., 2005;
149 Skamarock et al., 2008). The WRF-Chem model is selected because it includes the interaction
150 between meteorology and aerosol and is widely used for regional modeling of aerosol and its
151 climatic impact (e.g., Cao et al., 2010; Zhao et al., 2010, 2011, 2012, 2014; Wu et al., 2013;
152 Gao et al., 2014; Huang et al., 2015; Fan et al., 2015; Feng et al., 2016; Zhong et al., 2017;
153 Sarangi et al., 2019; Liu et al., 2020). The model has also been used to investigate the aerosol
154 transport and climatic impact over the Himalayas region (e.g., Feng et al., 2016; Cao et al.,
155 2010; Sarangi et al., 2019). The model is suitable for simulations at hydrostatic and non-
156 hydrostatic scales and thus can be used for investigating the impacts of resolution-dependent
157 feature, such as topography, on modeling results. In particular, the meteorological part of the
158 model (WRF) has been systematically evaluated and used to investigate the impacts of
159 resolutions on simulations of moisture transport and climate over the Himalayas region (e.g.,
160 Shi et al., 2008; Karki et al., 2017; Lin et al., 2018).; Zhou et al., 2017, 2018; Wang et al.,
161 2020). All of these previous studies with the model lay the foundation for this modeling study.

162   Two experiments with different topography representations are conducted to investigate
163 the impacts of topography complexity on the pollutant transport across the Himalayas and the
164 resulting radiative forcing over the TP. The simulations are conducted for April 2016 in pre-
165 monsoon season, because South Asia is seriously polluted during this period and the pollutants
166 transported to the TP during the period may have significant impacts on Asian monsoon system
167 (e.g., Lau et al., 2006a, b; Ding et al., 2009; Kuhlmann and Quaas, 2010; Qian et al., 2011,
168 2015). In addition, the observed concentration of BC at the observation station besides Mt.
169 Everest shows an evident pollution episode from April 5th to 16th of 2016, deserving the
170 investigation of the transport mechanisms. The rest of the paper is organized as follows. Section
171 2 describes briefly the WRF-Chem model, the physics parameterizations, and the model
172 configuration for this study, followed by a description of data for evaluation. The series of
173 numerical experiments at different resolutions are analyzed in Section 3. The findings are then
174 summarized and discussed in Section 4 and 5.

175

2. Methodology

2.1 Model and experiments

2.1.1 WRF-Chem model

In this study, the version of WRF-Chem updated by University of Science and Technology of China (USTC version of WRF-Chem) is used. This USTC version of WRF-Chem includes some additional capabilities such as the diagnosis of radiative forcing of aerosol species, land surface coupled biogenic volatile organic compound (VOC) emission, aerosol-snow interaction compared with the publicly released version (Zhao et al., 2013a, b, 2014, 2016; Hu et al., 2019; Du et al., 2020). The Model for Simulating Aerosol Interactions and Chemistry (MOSIAC) (Zaveri et al., 2008) and the Carbon Bond Mechanism-Z (CBM-Z) gas phase mechanisms (Zaveri and Peters, 1999) are selected. The MOSAIC aerosol scheme uses an approach of segmentation to represent aerosol size distribution with four or eight discrete size bins (Fast et al., 2006). It consists of a range of physical and chemical processes such as nucleation, condensation, coagulation, aqueous phase chemistry, and water uptake by aerosol. The parameterization of dry deposition of aerosol mass and number is according to the method of Binkowski and Shankar (1995), including particle diffusion and gravitational effects. Aerosol-cloud interactions were included in the model by Gustafson et al. (2007) for calculating the activation and re-suspension between dry aerosols and cloud droplets. The wet removal of grid-resolved stratiform clouds/precipitation includes two aspects, namely in-cloud removal (rainout) and below-cloud removal (washout) by Easter et al. (2004) and Chapman et al. (2009), respectively. Aerosol optical properties such as single scattering albedo (SSA) and scattering asymmetry and so on are calculated at each model grid through the function of wavelength. The shortwave (SW) and longwave (LW) refractive indices of aerosols use the Optical Properties of Aerosols and Clouds (OPAC) data set (Hess et al., 1998), with a detailed description of the computation of aerosol optical properties can be found in Barnard et al. (2010) and Zhao et al. (2013a). For both short wave and long wave radiation, aerosol radiation feedback combined with the Rapid Radiative Transfer Model (RRTMG) (Mlawer et al., 1997; Iacono et al., 2000) was implemented by Zhao et al. (2011). For the diagnosis of the optical properties and direct radiative forcing of various aerosol species in the atmosphere, the method described by Zhao et al (2013a) is adopted. The radiative forcing of light absorbing aerosol in surface snow is estimated with the Snow, Ice, and Aerosol Radiative model (SNICAR) (Flanner and Zender, 2005) in the land surface scheme as introduced by Zhao et al. (2014).

208 More details about the coupling between the WRF-Chem and SNICAR models can be found
209 in Zhao et al. (2014).

210

211 2.1.2 Numerical experiments

212   In this study, the WRF-Chem simulations are performed with two nested domains (one-
213 way nesting), one outer domain at 20-km horizontal resolution with 350×250 grid cells (62°E
214 -112°E, 1°N -38°N) and one inner domain at 4-km horizontal resolution with 400×300 grid
215 cells (75°E -92°E, 23°N -35°N) (Fig. 1). The inner domain roughly covers the entire Himalayas.
216 The WRF-Chem simulations conducted in this study use the terrain following coordinate
217 (Skamarock et al., 2008). To resolve the vertical structure of transport across the Himalayas,
218 the simulations are configured with 54 vertical layers and denser layers near the surface. For
219 example, averaged over a region (26°N-28°N, 76°E-80°E) near the southern Himalayas, there
220 are about 17 layers below 2 km above the ground (Fig. 2). The goal of this study is to investigate
221 the impacts of different representations of topography on the transport of BC across the
222 Himalayas. Therefore, besides this control experiment, one sensitivity (idealized) experiment
223 is also conducted with the same configuration as the control one except that the
224 ~~topography~~terrain height of the inner domain at 4-km resolution is prescribed to follow that at
225 20-km resolution similar as previous studies (e.g., Shi et al., 2008; Wu et al., 2012b; Lin et al.,
226 2018). More specifically, the sensitivity experiment applies a single value for each nested 5×5
227 grids over the inner domain as the corresponding grid of 20 km over the outer domain. The two
228 experiments are referred to the simulations with complex and smooth topography, respectively,
229 hereafter.
230   Fig. 3 shows the spatial distribution of terrain height over the inner domain with complex
231 (4-km dataset) and smooth (20-km dataset) topography. It is evident that the terrain is much
232 smoother from the 20-km dataset than from the 4-km dataset. The mountain ridges and valleys
233 can be resolved to some extent in the 4-km dataset but mostly missed or underestimated at 20-
234 km. The probability distributions of terrain height from the 20-km and 4-km datasets (Fig. S1
235 in the supporting material) show that the difference between the two datasets is small for the
236 terrain height lower than ~4.5 km but is significant for the terrain height above ~4.5 km. The
237 difference of results from the two experiments over the inner domain is analyzed as the impacts
238 of topography representations. Therefore, all the results shown below are from the simulations
239 of the inner domain at 4-km resolution with different topography if not otherwise stated. It is
240 noteworthy that this study focuses on understanding the impact of complex topography

resolved by 4 km instead of the difference between 4-km and 20-km simulations. Prescribing the topography at 4 km following the 20-km resolution distribution is just one way to smooth the topography. In fact, the sensitivity experiment at 4-km resolution with the topography from the one-degree resolution dataset is also conducted, and the result is consistent. In addition, although the topography at 4-km resolution resolves much better topography of Himalayas than that at 20-km resolution, it still cannot fully resolve the complexity of topography of Himalayas. The higher resolution (e.g., 1 km or sub-1 km) may be needed. Previous studies have found that the simulations at the resolutions between 1 km and 4 km can produce generally consistent features, but the simulation at 1 km with better representation of topography can produce a little better meteorological field compared to the observations (e.g., Karki et al., 2017 ~~km resolution with different topography if not otherwise stated.~~). One sensitivity experiment at 1.5-km resolution is also conducted in this study and found the difference between the simulations at 1.5-km and 4-km resolutions is relatively small. However, it should be noted that the simulation at 1.5-km resolution is only conducted covering a much smaller region for a shorter period due to the computational cost. The experiment at 4-km instead of 1.5-km resolution is conducted finally for the study region and period due to the balance of resolving the complex topography to some extent and affordable computational cost.

The simulations are conducted for March 29th-April 20 of 2016 for the reason as discussed in the introduction. The results of April 1th-20th are analyzed for the observed pollution episode to allow a few days spin-up for chemical initial condition. The meteorological initial and lateral boundary conditions are derived from the European Centre for Medium-Range Weather Forecasts (ECMWF) reanalysis data at $0.5° \times 0.66°$ horizontal resolution and 6 h temporal intervals (ERA-Interim dataset). The modeled u and v component wind, atmospheric temperature, and geopotential height over the outer domain are nudged towards the reanalysis data with a nudging timescale of 6 h following previous studies (e.g., Stauffer and Seaman, 1990; Seaman et al., 1995; Liu et al., 2012; Zhao et al., 2014; Karki et al., 2017; Hu et al., 2016, 2020). Spectral nudging method is applied to balance the performance of simulation at the large and small scales (Liu et al., 2012), and only to the layers above the planetary boundary layer (PBL) with nudging coefficients of 3×10^{-4} s^{-1}. A wave number of three is selected for both south-north and west-east directions. Please note that the choices of nudging coefficients and wave numbers for spectral nudging in this study are empirical. The purpose of nudging is to simulate reasonably large-scale feature so that small-scale impacts from the complex topography can be focused. Therefore, the modeling sensitivity to these choices is not tested in

274 this study. The results show that the simulations with nudging method can reproduce the large-
275 scale circulation at 700 hPa and higher over the outer domain compared to the reanalysis dataset
276 with the spatial correlation coefficient of 0.96-0.98.

277 The Mellor-Yamada-Nakanishi-Niino (MYNN) planetary boundary layer scheme
278 (Nakanishi and Niino, 2006), Community Land Model (CLM) land surface scheme (Oleson et
279 al., 2010), Morrison 2-moment microphysics scheme (Morrison et al., 2009), Kain-Fritsch
280 cumulus scheme (Kain, 2004), and Rapid Radiative Transfer Model (RRTMG) longwave and
281 shortwave radiation schemes (Iacono et al., 2000) are used in this study. The chemical initial
282 and boundary conditions are provided by a quasi-global WRF-Chem simulation for the same
283 time period to include long-range transported chemical species. The quasi-global WRF-Chem
284 simulation is performed at $1°×1°$ horizontal resolution using a quasi-global channel
285 configuration with $360×130$ grid cells (180°W-180°E, 60°S-70°N). More details about the
286 general configuration of quasi-global WRF-Chem simulation can be found in Zhao et al.
287 (2013b) and Hu et al. (2016). The detailed configuration of WRF-Chem experiments is
288 summarized in Table 1. Due to the lack of publicly available in-situ observations, this study
289 does not tend to evaluate systematically the simulated meteorological fields over the Himalayas
290 region. However, as shown in Table 1, the choice of physical parameterizations in this study
291 follows that of one previous study (Karki et al., 2017) that evaluated systematically the WRF
292 simulation for one entire year over the Himalayas region. Their results showed that the WRF
293 simulation at convection-permitting scale could generally capture the essential features of
294 meteorological fields such as precipitation, temperature, and wind over the Himalayas region.
295 Therefore, the WRF-Chem simulations in this study are reliable to investigate the impacts of
296 topography over the Himalayas region.

297

298 2.1.3 Emissions
299 Anthropogenic emissions for outer and inner simulation domains are obtained from the
300 Hemispheric Transport of Air Pollution version-2 (HTAPv2) at $0.1°×0.1°$ horizontal resolution
301 and a monthly temporal resolution for year 2010 (Janssens-Maenhout et al., 2015), except that
302 emissions of East Asia are from the MIX Asian anthropogenic emission inventory at $0.1°×0.1°$
303 horizontal resolution for 2015 (Li et al., 2017). Biomass burning emissions are obtained from
304 the Fire Inventory from National Center for Atmospheric Research (FINN) with hourly
305 temporal resolution and 1—km horizontal resolution (Wiedinmyer et al., 2011) for the
306 simulation period, and are vertically distributed following the injection heights suggested by

307 Dentener et al. (2006) from the Aerosol Comparison between Observations and Models
308 (AeroCom) project. Sea-salt emission follows Zhao et al. (2013b), which includes correction
309 of particles with radius less than 0.2 μm (Gong, 2003) and dependence of sea-salt emission on
310 sea surface temperature (Jaeglé et al., 2011). The vertical dust fluxes are calculated with the
311 Georgia Tech/Goddard Global Ozone Chemistry Aerosol Radiation and Transport (GOCART)
312 dust emission scheme (Ginoux et al., 2001), and the emitted dust particles are distributed into
313 the MOSAIC aerosol size bins following a theoretical expression based on the physics of scale-
314 invariant fragmentation of brittle materials derived by Kok (2011). More details about the dust
315 emission scheme coupled with MOSAIC aerosol scheme in WRF-Chem can be found in Zhao
316 et al. (2010, 2013b).

317 As shown in Fig. 1, anthropogenic fossil fuel emissions of BC are high over Northeast
318 India. The fossil fuel BC emissions over Nepal, the country nearby the southern Himalayas,
319 are relatively low. Instead, biomass burning emissions of BC are extremely high in Nepal and
320 Northwest India (South Himalayas, 26°N-29°N). Averaged over the South Himalayas of inner
321 domain that may significantly affect the pollutant transport into the TP, the biomass burning
322 emissions of BC are much higher than its anthropogenic fossil fuel emissions, particularly for
323 the pollution episode (Fig. 4). The anthropogenic BC emissions are set constant through April,
324 while biomass burning emissions show a strong fire event in April 5-16. During the event, the
325 biomass burning BC emissions can be ~~close to~~ a factor of 2 of the anthropogenic fossil fuel BC
326 emissions over South Himalayas.

327

328 **2.2 Dataset**

329 Three datasets are used to compare with the modeling results to demonstrate the pollutant
330 episode and spatial distribution. One is from the Moderate Resolution Imaging
331 Spectroradiometer (MODIS) instruments on Aqua and Terra satellites. The MODIS Aerosol
332 Product monitors the ambient aerosol optical thickness over the oceans globally and over the
333 continents. Daily Level 2 Aerosol Optical Depth (AOD) at 550 nm products with the spatial
334 resolution of 10 km×10 km (at nadir) from both Aqua and Terra are applied. When compared
335 with the modeling results, the simulations are sampled at the satellite overpass time and
336 location. The second one is from the Aerosol Robotic Network (AERONET) (Holben et al.,
337 1998) that has ~100 similar globally distributed sun and sky scanning ground-based automated
338 radiometers, which provide measurements of aerosol optical properties throughout the world
339 (Dubovik and King, 2000; Dubovik et al., 2002). In this study, AERONET measured AOD at
340 675 nm and 440 nm from two sites over the TP, QOMS_CAS site (86.95°E, 28.36°N) and

341   NAM_CO site (90.96°E, 30.77°N) are used to derive the AOD at 550 nm (using the Angström

342   exponent) for comparison with modeling results at 550 nm. All of the retrievals of AOD are at

343   quality level 2, and the uncertainty of AOD measurements is about 0.01 (Holben et al., 2001).

344   In this study, the available data in April 2016 are used to evaluate the modeling results during

345   the same period.

346   The third one is the measurement of near-surface BC mass concentration collected during

347   the simulation period for April 4-20 of 2016 at the Qomolangma (Mt. Everest) Station for

348   Atmospheric and Environmental Observation and Research (QOMS, 86.95°E, 28.36°N) which

349   is located at the northern slope of the HimalayasMt. Everest, about 4276 meters above sea level.

350   The BC mass concentration is measured with the widely-used instrument Aethalometer (AE-

351   33) that can provide real-time BC mass concentration measurements. The calibration of air

352   flow is routinely conducted to maintain the data quality. The instrument estimates the BC mass

353   concentration based on the optical method through measuring the reduction in light intensity

354   induced by BC. The method assumes that the relationship between attenuation and BC surface

355   loading is linear for low attenuation values. However, this relationship becomes nonlinear

356   when the attenuation values are high due to a filter saturation effect, which may lead to

357   underestimation of the high BC concentration. The detection limit of AE-33 instrument is 5

358   ng/m^3, and the uncertainty is estimated to be within 10% (e.g., Chen et al., 2018; Bansal et al.,

359   2019; Kant et al., 2019). The dataset of BC mass concentration used in this study was reported

360   by Chen et al., (2018), where more details about the measurements can be found.

361

362   3. Results

363   3.1 Spatial distribution of BC around the TP

364   Figure 5 shows the spatial distributions of column integrated BC mass within the inner

365   domain from the simulations at 4-km resolution with complex and smooth topography

366   averaged for April 1-20, 2016, and the difference between the two is also shown. For both

367   experiments, the southern Himalayas is an apparent boundary line for the distribution of BC

368   with a sharp gradient across the Himalayas. The high BC mass loading exists near the southern

369   Himalayas reaching over 10 mg/m^2, which is largely contributed by the biomass burning

370   emissions during the period (Fig. 4), while the value reduces significantly to less than 0.4

371   mg/m^2 over the TP. The BC mass loading near the central and eastern Himalayas is higher than

372   that near the western Himalayas. In general, the column BC mass loading from the simulation

373   with complex topography is higher over the TP and lower over the region to the south of

374 Himalayas compared with the smooth topography~~.~~, reflecting the stronger transport of BC from

375 the source region to the Himalayas and TP due to the complex topography (see the discussion

376 in Section 3.2). Figure 6 displays the spatial distributions of AOD from the MODIS retrievals

377 and the simulations at 4 km with two different topography averaged for April 1-20, 2016. In

378 general, both simulations reproduce the overall spatial distribution of AOD, with the large

379 values near the southern Himalayas, consistent with the BC mass loading. In addition, both the

380 simulations and satellite retrievals show higher AOD near the central and eastern Himalayas

381 than that near the western Himalayas during the study period. The difference between the

382 simulations and retrievals may be partly related to the uncertainties in emissions particularly

383 for biomass burning emissions. Other than intense emissions, the wind circulation around the

384 TP may also play an important role in accumulating BC near the southern Himalayas. Because

385 of the block of Himalayas, the wind circulation at 500 hPa is divided into two branches as

386 westerly and northwesterly. Both of them are relatively dry airflows with little effect on

387 pollutant removal, favor the accumulation of pollutants near the southern Himalayas, and carry

388 the pollutants to the TP (e.g., Dumka et al., 2010; Kang et al., 2016; Cong et al., 2015a).

389 The AOD retrieved at two AERONET sites over the TP are compared with the two

390 simulations for April 1-20, 2016 (Fig. 7). The AOD at the QOMS_CAS site near the northern

391 Himalayas is higher than that at the NAM_CO site inside of the TP. Both simulations can

392 capture this gradient. The simulation with complex topography produces higher AOD than

393 does the one with smooth topography at both sites. The modeling biases (normalized mean bias,

394 NMB) reduce from -46% (smooth topography) to 9% (complex topography) at the

395 QOMS_CAS site and from -26% (smooth topography) to -10% (complex topography) at the

396 NAM_CO site. Although the correlation coefficient between the simulations and observation

397 increases from 0.37 (smooth topography) to 0.53 (complex topography) at the QOMS_CAS

398 site, it is similar (~0.2) between the two simulations at the NAM_CO site. The correlation

399 coefficient is higher at the QOMS_CAS site near the source region than the NAM_CO site

400 farther away, which may indicate the model processes affecting the transport over the TP still

401 need examination with more observations. The NAM_CO site over the eastern TP may also be

402 affected by other sources that are not counted in this study. The modeling of temporal variations

403 of pollutants over the TP deserves further investigation with more observations.

404 There is one in-situ observational station (QOMS) near the Mt. Everest (black dot shown

405 in Fig. 1) to collect the near-surface BC concentration. The observed near-surface BC

406 concentration at this station is compared with the corresponding simulations for this period as

407 shown in Figure 8. Without local emission source, the near-surface BC concentration at QOMS

408   is primarily contributed by the transport. The temporal variation of observed near-surface BC

409   concentration correlates highly with the biomass burning emissions as shown in Fig. 4, with

410   the peak value on April 11 reaching ~3 ug/m^3. One sensitivity experiment without biomass

411   burning emissions shows that the simulated BC concentration at QOMS will be significantly

412   reduced without the peak (not shown), which further proves that the BC concentration over the

413   northern Himalayas can be largely influenced by the pollution episode near the southern

414   Himalayas. It is noteworthy that both simulations can reproduce the episode in time and

415   magnitude, and the difference at this station is small. The spatial distribution of difference in

416   near-surface BC concentration between the two simulations (Fig. S2) is more heterogeneous

417   than that of column BC mass (Fig. 5), reflecting the impact of topography on near-surface

418   transport (see the discussion in Section 3.2).

419

420   **3.2 Transport flux into the TP**

421   To further understand the difference in BC near-surface concentration and column mass

422   loading over the TP between the two simulations with different topography, Figure 9 shows

423   the longitude-height cross section of BC transport flux along the cross line (shown as the black

424   dash line in Fig. 3) from the two simulations at local time (LT) 03:00 and 15:00 averaged for

425   April 1-20 to represent nighttime and daytime transport, respectively. The PBL height along

426   the cross line is also shown as the black dash line. The transport flux is calculated by projecting

427   the wind field perpendicularly to the cross line and then multiplying the BC mass concentration

428   along the cross line. More specifically, the transport flux is calculated as following:

429    $$\text{TF} = C * (u * \sin\alpha + v * \sin\beta) \qquad (1)$$

430   Where α is the angle between east-west wind component and the cross line, β is the angle

431   between south-north wind component and the cross line, and C is the BC mass concentration

432   at the grid along the cross line. The flux is estimated at each model level. Positive values

433   represent the transport towards the TP, while negative values represent the transport away from

434   the TP. It is evident that BC is imported into the TP during the day and night on the west of

435   ~85°E, although the transport flux is much larger during the daytime than nighttime. On the

436   east of ~85°E, BC is imported into the TP during the day but exported slightly from the TP

437   during the night. The difference of transport flux between ~~on~~ the ~~west~~western and ~~east of ~85°E~~

438   eastern Himalayas is primarily due to the influence of large-scale westerly that is ~~relatively~~

439   weak ~~on~~over the ~~east of ~85°E compared with the west~~eastern Himalayas (Fig. 5). ~~If removing~~

440   ~~the mean flux during the simulation period, the~~ The transport ~~flux anomalies show evident~~

441 ~~diurnal variation between the day and night (Fig.~~ across the western Himalayas is controlled

442 ~~by~~ ~~S3 in the supporting material). This suggests that on average,~~ the large-scale westerly ~~is one~~

443 ~~of the key mechanisms transporting BC across the Himalayas into the TP~~, while ~~the circulation~~

444 ~~anomalies strengthen the prevailing import~~ local southerly dominates the transport across the

445 eastern Himalayas and also influences the transport across the central Himalayas (Fig. S3 in

446 the supporting material). ~~during the~~ The stronger diurnal variation of local southerly (towards

447 the TP in the daytime to away from the TP in the nighttime) than that of westerly near the

448 surface (Fig. S3) leads to the large difference in diurnal variation of transport between the

449 western and ~~weaken the import during the night, particularly in the west of ~85°E.~~ eastern

450 Himalayas. The strong transport is primarily within the PBL during the daytime, and the deeper

451 PBL during the daytime allows BC over the source region mixed to higher altitude, which also

452 leads to stronger import transport during the day than the night. The relatively small difference

453 in simulated PBL heights and structure between the two experiments can be due to their

454 different surface heating resulted from different topography complexity (e.g., Wagner et al.,

455 2014).

456   The difference between the simulations with two different topography is evident. The

457 mountain ridges are much higher and valleys are much deeper with the complex topography

458 than with the smooth topography. The simulation with smooth topography produces

459 overwhelming crossing-Himalayas transport towards the TP within the PBL, in particular

460 during the daytime. Although, in the simulation with complex topography, the mountain ridges

461 resolved weaken the crossing-Himalayas transport compared to the simulation with smooth

462 topography, the overall positive values near the surface indicate that the transport can overcome

463 most mountain ridges along the Himalayas. The transport fluxes near the surface from the

464 simulation with complex topography become close-to-zero only at a few mountain ridges that

465 are 6.5 km or higher. To better demonstrate the transport pathway across mountain ridges, one

466 cross-section across the mountain ridge as shown as one black solid line in Fig. 3 is taken as

467 one example. Figure 10 shows the latitude-height cross section of BC mass concentration and

468 transport flux across one mountain ridge from the simulations with complex and smooth

469 topography at local time (LT) 03:00 and 15:00 averaged for April 1-20, 2016. Near the southern

470 part of mountain, the elevated concentration of BC mass accumulates and can mix up reaching

471 as high as 5 km with the much stronger transport during the daytime. It is obvious that the

472 mountain ridge in the simulation with smooth topography is quite low. With the high mountain

473 ridge resolved by the complex topography, the simulated BC transport flux can still cross the

474 mountain. Analysis of transport flux across a few more mountain ridges indicates similar

475 results (not shown). The results above indicate that the transport of pollutants can cross a

476 majority of mountain ridges of Himalayas, which is consistent with the observation-based

477 estimate by Gong et al. (2019) that also found pollutants could overcome the blocking effect

478 of mountain ridges of Himalayas as a transport pathway. On the other hand, the resolved deeper

479 valleys in the simulation with complex topography enhance the transport flux compared to the

480 one with the smooth topography. Similarly, Figure 11 shows one example of latitude-height

481 cross section of BC mass concentration and transport flux across one valley from the

482 simulations with complex and smooth topography at local time (LT) 03:00 and 15:00 averaged

483 for April 1-20, 2016. The transport is much stronger and deeper along the valley from the

484 simulation with complex topography than the one with smooth topography. Again, analysis of

485 transport flux across a few more valleys does not show different results (not shown).

486   In order to further demonstrate the overall inflow flux across the Himalayas, the vertically

487 integrated BC mass flux along the longitudinal cross section (as shown in Fig. 9) from the

488 simulations with different topography is shown in Figure 12. The terrain heights from the two

489 simulations along the cross section are also shown as black lines. The total mass flux is

490 calculated by integrating the right-hand term of equation (1) as following:

491 $$\text{ITF} = \int_{z=z_{sfc}}^{z=z_{top}} \delta z * C * (u * \sin \alpha + v * \sin \beta) \qquad (2)$$

492 Where δz is the thickness of each vertical model level. Similarly, positive values represent

493 the transport towards the TP, while negative values represent the transport away from the TP.

494 More evidently, the positive BC inflows towards the TP occur not only through the valleys but

495 also across the mountain ridges with both topography. The negative values only exist to the

496 east of 88°E. With complex topography, higher mountain ridges can reduce the transport flux

497 to some extent compared to the smooth topography. The complex topography results in

498 significantly larger BC inflow towards the TP compared to the smooth topography, particularly

499 corresponding to the deep valleys, such as the Karnali River Valley around 82°E and the Kali

500 Gandaki Valley around 84°E.

501   One reason for the enhanced transport across the Himalayas with the complex topography

502 is the resolved deeper valleys that lead to the increased valley wind. ~~The wind across the valleys~~

503 ~~can be significantly larger with the complex topography than the smooth one (Fig. S4). The~~

504 ~~enhanced valley wind across the Himalayas has also been found by previous studies with~~

505 ~~observations and numerical simulations (Egger et al., 2000; Zängl et al., 2001; Carrera et al.,~~

506 ~~2009; Karki et al., 2017; Lin et al., 2018). The second impact of resolved complex topography~~

507 ~~on the BC transport is that more BC masses can be transported with the deeper valley channels~~

(Fig. S5a, b). With deeper valley, the column of high-concentration BC is deeper. Even with similar wind velocity, the transport flux can be larger. The third impact is through changing the small-scale circulation around the Himalayas due to the increase of topography complexity of Himalayas. The simulation with complex topography produces more near-surface winds following the direction towards the TP compared to the one with smooth topography (Fig. S6), which favors the BC transport across the Himalayas. Lastly, the simulated PBL heights from the two experiments are a little different (Fig. 9), which may also contribute partly to the different transport flux. The sensitivity of PBL height and structure to topography complexity that can result in different surface heat has been studied before (e.g., Wagner et al., 2014). The wind across some valleys can be significantly larger with the complex topography than the smooth one (Fig. S3). The enhanced valley wind across the Himalayas has also been found by previous studies with observations and numerical simulations (e.g., Egger et al., 2000; Zängl et al., 2001; Carrera et al., 2009; Karki et al., 2017; Lin et al., 2018). However, it is noteworthy that previous studies have found that the orographic drag (including gravity wave drag and turbulence orographic form drag) over the region with complex topography, such as the Himalayas and other mountainous areas, would weaken the overall near-surface wind speed (e.g., Beljaars et al., 2004; Horvath et al., 2012; Jiménez and Dudhia, 2012; Zhou et al., 2017, 2018; Lin et al., 2018; Wang et al, 2020). Therefore, the near-surface wind speed is also examined. The complex topography does lead to the overall reduction of near-surface wind speed over the Himalayas area (Fig. S4 in the supporting material), which is consistent with previous studies. However, it is interesting to note that the near-surface southerly wind during the daytime of the simulation period is overall increased over the Himalayas area with the complex topography (Fig. 13), which indicates that the transport towards the TP is strengthened with the complex topography in the daytime, particularly over the central and eastern Himalayas where the BC mass loading is higher (Fig. 5). During the night, the meridional wind is dominated by northerly over the Himalayas region in the simulation with the smooth topography. The complex topography weakens the transport away from the TP or change the wind direction from northerly to southerly over some areas of Himalayas. Both effects enhance the overall transport efficiency across the Himalayas towards the TP. Therefore, although the complex topography weakens the overall near-surface wind speed around the Himalayas, it induces more realistic small-scale mountain-valley circulation that favors the BC transport across the Himalayas towards TP during the study period. Another effect of resolving valleys is that the volume of relatively-high-concentration BC could be higher with deeper valleys (Fig. S5 in the support material), which can also result in stronger transport towards the TP even if

28

the wind condition is similar. For example, the altitude (above the ground) below which the BC mass concentration is larger than 0.3 ug/m^3 is much higher along the valleys with the complex topography than with the smooth topography (Fig. S6 in the support material). The correlation coefficient between the difference of terrain heights of valleys and of volumes of relatively-high-concentration BC can reach -0.76, indicating that the lower the valleys are, the higher the volumes of BC mass can be transported across the Himalayas. The combined influence of these factors results in significantly enhanced BC transport towards the TP with the complex topography (Fig. 12), which can also be demonstrated by the distributions of wind and BC mass concentration along the longitudinal cross section (Fig. S7a, b in the support material).

~~This~~The enhanced transport across the Himalayas turns out that the overall BC inflow with the complex topography is much stronger than that with the smooth topography. Figure ~~13~~14 shows the accumulated integrated total transport flux of BC across the Himalayas estimated from the simulations with complex and smooth topography for April 1-20, 2016. The accumulated import flux of BC increases during the period in both experiments, and the difference between the two experiments gradually increases with the time. At the end of period, the simulation with complex topography estimates a total import flux of BC of ~1.5×10^4 Ton that is ~50% higher than ~1.0×10^4 Ton estimated based on the simulation with smooth topography. The sensitivity analysis by moving the cross line (cross-section of the analysis in Fig. 9, 12, ~~13~~14) towards or away from the TP within a certain distance and re-calculating the flux indicates that the impacts of topography on the simulated results do not change significantly.

All the analysis above focuses on investigating the BC transport flux across the Himalayas. Although the inflow can reflect the impact of transport on the BC mass over the TP to some extent, the change of BC mass concentration is eventually determined by the convergence of transport. Therefore, the contribution of each model process (transport, dry-deposition, emission, PBL mixing, and wet deposition) to the increase of BC column mass averaged over the TP (with elevation > 4 km) during this episode is analyzed for both simulations following the methodology introduced by Du et al. (2020). The results show that the two main processes affecting the BC column mass over the TP during the period are transport and dry deposition. The transport is the dominant process that increases the BC column mass over the TP, while the dry deposition reduces it. The contribution of transport to the increase of BC column mass over the TP during the episode from the simulation with complex topography is significantly

larger than that with the smooth topography, which is consistent with the results shown by analyzing the transport flux across the Himalayas. Although the impacts of PBL mixing and wet deposition on the BC column mass over the TP are also different between the simulations with different topography, their impacts are much smaller than those of transport and dry deposition during the study period.

3.3 Radiative forcing of BC over the TP

The BC transported over the TP could significantly influence the regional climate and water resources over Asia through heating the atmosphere and accelerating the melting of snow and glacier (e.g., Qian et al., 2011, 2015; Lau et al., 2017). Therefore, the impact of the complex topography on estimating the BC radiative heating profile in the atmosphere and radiative forcing in surface snow deserves investigation. Figure 1415 shows the vertical profiles of BC induced radiative heating rate in the atmosphere averaged over the TP (with elevation > 4 km) within the inner domain shown in Fig.1 for April 1-20, 2016 from the simulations with complex and smooth topography. Both simulations generate higher BC heating rate near the surface and the rate gradually decreases with altitude, which is consistent with the vertical profiles of BC mass concentration averaged over the TP (Fig. S7S8 in the supporting material). The BC heating rate over the TP from the simulation with complex topography is ~0.17 K/day near the surface and reduces to ~0.08 K/day at 8 km, which is ~50% and ~30%, respectively, higher than that from the simulation with smooth topography at the corresponding altitudes. The higher BC heating rate over the TP estimated by the simulation with complex topography is consistent with its higher BC column mass (Fig. 5) and concentration profile (Fig. S7S8).

The BC radiative forcing in surface snow is controlled by both the distributions of BC mass concentration and snow coverage (e.g., Zhao et al., 2014). Figure 1516 shows the spatial distributions of snow water equivalent (SWE) averaged for April 1-20, 2016 from the simulations with two topography. The difference between the two is also shown. It shows that the simulation with complex topography generates more areas with higher SWE compared to that with the smooth topography over the TP. Along the Himalayas, the simulated SWE is higher over the mountain ridges with the complex topography, particularly for the East Himalayas, while the smooth topography leads to broader snow coverage over the West Himalayas. The difference in SWE between the two simulations is highly correlated with their difference in precipitation (Fig. S8S9 in the supporting material). Along the Himalayas, the simulated precipitation with the complex topography is larger than that with the smooth topography at the mountain ridges and smaller at the valleys. Over the TP, the overall

609 precipitation is larger with the complex topography than that with the smooth topography (Fig.

610 S8S9). Previous studies have found that the topography could significantly affect the

611 precipitation over the Himalayas region (e.g., Bookhagen and Burbank, 2010; Wulf et al., 2016;

612 Cannon et al., 2017; Karki et al., 2017).

613 Figure 1617 shows the spatial distributions of BC radiative forcing in the surface snow

614 over the TP averaged for April 1-20, 2016 from the simulations with two topography, and the

615 difference between the two is also shown. The BC radiative forcing in surface snow is largely

616 coincident with the spatial distributions of SWE as shown in Fig. 1516, mainly due to the

617 heterogeneous distributions of snow cover over the TP. The BC radiative forcing in surface

618 snow over the TP from the simulation with complex topography reaches 5 W/m^2 where the

619 snow exists, larger than that with the smooth topography. Along the Himalayas, the simulation

620 with complex topography produces higher BC snow forcing over the mountain ridges,

621 particularly over the eastern Himalayas, while the one with the smooth topography simulates

622 higher BC snow forcing over most areas of western Himalayas due to its broader snow

623 coverage there. Overall, the complex topography leads to higher BC forcing in snow over the

624 TP and the eastern Himalayas and lower BC forcing in snow over the western Himalayas, and

625 therefore results in the different distribution of BC forcing in snow over the TP and Himalayas,

626 compared to that with the smooth topography.

627

628 4. Summary and discussion

629 In this study, the model experiments with different topography are conducted to illustrate

630 the impacts of complexity of topography of Himalayas on BC transport from South Asia to the

631 TP. The observed pollution episode at the QOMS station besides the Mt. Everest during the

632 pre-monsoon season is simulated. The observed near-surface BC concentration shows a peak

633 of ~3 ug/m^3 much larger than the background value of < 0.4 ug/m^3 over the TP. The observed

634 temporal variation of near-surface BC concentrations correlates highly with that of biomass

635 burning emissions near the southern Himalayas, indicating the significant impacts of biomass

636 burning on the pollutants over the TP. The simulations can reproduce the episode in time and

637 magnitude, and are used to investigate the BC transport mechanisms and the impacts of

638 topography.

639 The high BC mass loading during the simulation period accumulates near the southern

640 Himalayas driven by the large-scale circulationwesterly and small-scale southerly circulations,

641 which is also observed by satellites. The modeling results demonstrate that the westerly

favorscirculations favor the accumulation of pollutants near the southern Himalayas, particularly over the central and eastern parts, and can carry the pollutants to the TP during the day and nightstudy period, which is consistent with previous modeling studies (e.g., Kopacz et al., 2011). The transport is stronger across the West Himalayas than that across the East. The deeper PBL during the daytime allows BC over the source region mixed to higher altitude, which also leads to stronger import transport during the day than the night. It is noteworthy that the BC accumulated near the southern Himalayas can be transported across the Himalayas overcoming a majority of mountain ridges, which is consistent with the observation-based estimate by Gong et al. (2019) that also found pollutants could overcome the blocking effect of the mountain ridges of Himalayas. However, the transport through the valleys is found much stronger and more efficient than across the mountain ridges and the enhancement effect cannot be ignored. The complex topography results in 50% higher overall transport flux across the Himalayas during the simulation period than that with the smooth topography, primarily due to the enhanced valley wind, deeper valley channels, and induced small-scale favorable circulation.strengthened efficiency of near-surface meridional transport towards the TP, enhanced wind speed at some valleys, and deeper valley channels associated with larger BC mass volume that can be transported into the TP, although the overall wind speed is weakened due to the orographic drags with the complex topography. This turns out that the simulation with complex topography produces 30-50% higher BC radiative heating rate in the atmosphere up to 10 km averaged over the TP than does the simulation with smooth topography.

Previous studies also found the induced change of circulation and transport due to the complex topography at convection permitting scales with the focus on the meteorological fields (e.g., Karki et al., 2017; Lin et al., 2018). However, most of them conducted the sub-10 km simulations over a much smaller region (e.g., 101×96 grids at 5 km in Karki et al., 2017, and 181×121 grids at 2 km in Lin et al., 2018) compared to this study (400×300 grids at 4 km). Karki et al. (2017) found that the complex topography resolving more valleys and mountain ridges yielded more realistic strong and narrower winds and also small-scale mountain-valley circulations over the Himalayas region compared to the smoother topography. Lin et al. (2018) analyzed the simulations over the region situated in the central Himalayas (87°E-89°E) with very complex terrain including several high mountains and low valleys, e.g., Mt. Everest, Mt. Kanchenjunga, and the Yadong Valley. Although Lin et al. (2018) simulated enhanced moisture flux along the valley, the overall moisture transported was lower with the complex topography (10 km resolution) compared to that with the smooth topography (30 km

For the BC radiative forcing in surface snow, the simulation with complex topography produces stronger forcing over the TP than that with the smooth one. The complex topography makes the distribution of BC forcing in surface snow quite different from the simulation with smooth topography, partly due to its different distribution of surface snow. The simulated BC radiative forcing in snow is distributed more heterogeneously than those in previous studies using global models at relatively coarse resolutions (e.g., Qian et al., 2011). He et al. (2014) used a global chemical transport model to simulate the BC forcing in snow at the horizontal resolution of ~0.2° and obtained the similar distribution as the simulation with smooth topography in this study with the high values over the western Himalayas. However, their simulated values near the Himalayas are higher than the simulated results of this study, which may be due to their estimation are averaged for November-April.

This study highlights the importance of resolving complex topography of the Himalayas in modeling the aerosol transport across the Himalayas and radiative impact over the TP. Although this study focuses on the impacts of topography on the simulated results, the additional analysis (Fig. S9-11S10-12 in the supporting material) of the outer domain simulation at 20--km resolution and the inner domain simulation at 4 km with different topography indicates that the resolution-dependent difference between 20 km and 4 km is largely contributed by their different representations of topography over the Himalayas region, consistent with previous studies (e.g., Karki et al., 2017; Lin et al., 2018). Climate models at coarser horizontal resolutions than 20 km and thus with relatively smooth topography may underestimate the aerosol transport from South Asia to the TP during the pre-monsoon season and represent inappropriately the aerosol radiative forcing in the atmosphere and surface snow over the TP.

5. Discussion

708   Previous studies also found the induced change of circulation and transport due to the
709   complex topography at convection-permitting scales with the focus on the meteorological
710   fields over the Himalayas and TP regions (e.g., Karki et al., 2017; Zhou et al., 2017, 2018; Lin
711   et al., 2018; Wang et al., 2020). Most of them either conducted the sub-10 km simulations
712   covering a relatively smaller region (e.g., 101×96 grids at 5 km in Karki et al., 2017; 181×121
713   grids at 2 km in Lin et al., 2018; ~330×230 grids at 3 km in Wang et al., 2020) compared to
714   this study (400×300 grids at 4 km) or conducted the simulations covering the entire Himalayas
715   but at the resolutions above 10 km and with the sub-grid orographic drag parameterization to
716   consider the impact of complex topography. Although some of previous studies also showed
717   that the resolved complex topography yielded more realistic small-scale mountain-valley
718   circulations and enhanced valley winds over the Himalayas region compared to the smoother
719   topography, the overall moisture transport across the Himalayas towards the TP was weaker
720   with the complex topography due to the orographic drags.

721   The difference between previous studies and this study can be due to several factors. First,
722   previous studies focused on moisture instead of air pollutants. The spatial (horizontal and
723   vertical) distributions between air pollutants and moisture are different and may contribute to
724   the different impacts of topography on the overall transport flux across the Himalayas.
725   However, the analysis of the moisture from the simulations in this study shows the increase of
726   moisture transport (not shown) and hence the increase of precipitation over the TP with the
727   complex topography (Fig. S9). Second, most of previous studies focused on monsoon season
728   instead of pre-monsoon season. Therefore, the meteorological simulations for monsoon season
729   (June-July-August) at different resolutions are also conducted in this study. The results show
730   that the moisture transport and precipitation are reduced at the higher resolution with complex
731   topography and the meridional wind is overall weakened particularly over the central and
732   eastern Himalayas and TP (not shown), which is consistent with previous studies. This may
733   indicate that the different large-scale circulations between the two seasons (much stronger
734   southerly during the monsoon season) may also lead to different impacts of complex
735   topography on meridional winds and hence cross-Himalayas transport.

736   Since this study only demonstrates the potential impacts for a relatively short period, a
737   longer-term study should be conducted to examine the impacts of topography on aerosol
738   climatic effect over the TP in both pre-monsoon and monsoon seasons. In addition, the active
739   convection during the monsoon season may also play an important role on pollutant transport
740   across the Himalayas, which deserves further investigation. Furthermore, aerosol impact on

cloud and precipitation, particularly during the monsoon season, and thus on the latent heat in the atmosphere and the associated responses may also depend on the complex topography. Previous studies based on observations found that the rain frequency and intensity reached the highest and the cloud thickness reached the deepest at the foothill of Himalayas and decreased as the elevation increased up to the TP (e.g., Chen et al., 2017; Fu et al., 2018; Zhang et al., 2018), which was explained by Fu et al. (2018) due to the blocking of the air flow by the steep slope of southern Himalayas. However, the large amount of transported aerosol along the slope from the foothill up to the TP may also play a role. These potential impacts of aerosols on regional hydro-climate around the TP and over Asia using high-resolution model that can resolve the complex topography of Himalayas and TP deserve further investigation.

Data availability

The released version of WRF-Chem can be downloaded from http://www2.mmm.ucar.edu/wrf/users/download/get_source.html. The updated USTC version of WRF-Chem can be downloaded from http://aemol.ustc.edu.cn/product/list/ or contact chunzhao@ustc.edu.cn. Also, the code modifications will be incorporated the release version of WRF-Chem in future.

Author contributions

Meixin Zhang and Chun Zhao designed the experiments, conducted and analyzed the simulations. All authors contributed to the discussion and final version of the paper.

Acknowledgements

Reference

Bansal, O., Singh, A., and Singh, D.: Characteristics of Black Carbon aerosols over Patiala Northwestern part of the IGP: Source apportionment using cluster and CWT analysis, Atmospheric Pollution Research, 10, 244–256, doi:10.1016/j.apr.2018.08.001, 2019.

Barnard, J. C., Fast, J. D., Paredes-Miranda, G., Arnott, W. P., and Laskin, A.: Technical Note: Evaluation of the WRF-Chem "Aerosol Chemical to Aerosol Optical Properties" Module using data from the MILAGRO campaign, Atmos. Chem. Phys., 10, 7325–7340, doi:10.5194/acp-10-7325-2010, 2010.

Beljaars, A. C., Brown, A. R., and Wood, N.: A new parametrization of turbulent orographic form drag, QJ Roy. Meteorol. Soc., 130, 1327-1347, doi: 10.1256/qj.03.73, 2004.

Barnett, T. P., Adam, J. C., and Lettenmaier, D. P.: Potential impacts of a warming climate on water availability in snow-dominated regions, Nature, 438, 303–309, doi:10.1038/nature04141, 2005.

Binkowski, F. S. and Shankar, U.: The Regional Particulate Matter Model: 1. Model description and preliminary results, J. Geophys. Res., 100, 26191, doi:10.1029/95JD02093, 1995.

Bookhagen, B. and Burbank, D. W.: Toward a complete Himalayan hydrological budget: Spatiotemporal distribution of snowmelt and rainfall and their impact on river discharge, J. Geophys. Res., 115, 39, doi:10.1029/2009JF001426, 2010.

Boos, W. R. and Kuang, Z.: Sensitivity of the South Asian monsoon to elevated and non-elevated heating, Scientific reports, 3, 1192, doi:10.1038/srep01192, 2013.

Cannon, F., Carvalho, L. M. V., Jones, C., Norris, J., Bookhagen, B., and Kiladis, G. N.: Effects of topographic smoothing on the simulation of winter precipitation in High Mountain Asia, J. Geophys. Res. Atmos., 122, 1456–1474, doi:10.1002/2016JD026038, 2017.

Cao, J., Tie, X., Xu, B., Zhao, Z., Zhu, C., Li, G., and Liu, S.: Measuring and modeling black carbon (BC) contamination in the SE Tibetan Plateau, Journal of Atmospheric Chemistry, 67, 45-60, doi:10.1007/s10874-011-9202-5, 2010.

Carrera, M. L., Gyakum, J. R., and Lin, C. A.: Observational Study of Wind Channeling within the St. Lawrence River Valley, J. Appl. ~~Meteor. Climatol~~Meteorol. Clim., 48, 2341–2361, doi:10.1175/2009JAMC2061.1, 2009.

Chapman, E. G., Gustafson, W. I., Easter, R. C., Barnard, J. C., Ghan, S. J., Pekour, M. S., and Fast, J. D.: Coupling aerosol-cloud-radiative processes in the WRF-Chem model:

808   Investigating the radiative impact of elevated point sources, Atmos. Chem. Phys., 9, 945–

809   964, doi:10.5194/acp-9-945-2009, 2009.

810 Chen, J. and Bordoni, S.: Orographic Effects of the Tibetan Plateau on the East Asian Summer

811   Monsoon: An Energetic Perspective, J. Climate, 27, 3052–3072, doi:10.1175/JCLI-D-13-

812   00479.1, 2014.

813 Chen, X., Kang, S., Cong, Z., Yang, J., and Ma, Y.: Concentration, temporal variation, and

814   sources of black carbon in the Mt. Everest region retrieved by real-time observation and

815   simulation, Atmos. Chem. Phys., 18, 12859–12875, doi:10.5194/acp-18-12859-2018, 2018.

816 Chen, Y., Fu, Y., Xian, T., and Pan, X.: Characteristics of cloud cluster over the steep southern

817   slopes of the Himalayas observed by CloudSat, Int. J. Climatol., 37, 4043–4052,

818   doi:10.1002/joc.4992, 2017.

819 Cong, Z., Kang, S., and Qin, D.: Seasonal features of aerosol particles recorded in snow from

820   Mt. Qomolangma (Everest) and their environmental implications, Journal of environmental

821   sciences (China), 21, 914–919, doi:10.1016/S1001-0742(08)62361-X, 2009.

822 Cong, Z., Kang, S., Kawamura, K., Liu, B., Wan, X., Wang, Z., Gao, S., and Fu, P.:

823   Carbonaceous aerosols on the south edge of the Tibetan Plateau: concentrations, seasonality

824   and sources, Atmos. Chem. Phys., 15, 1573–1584, doi:10.5194/acp-15-1573-2015, 2015a.

825 Cong, Z., Kawamura, K., Kang, S., and Fu, P.: Penetration of biomass-burning emissions from

826   South Asia through the Himalayas: new insights from atmospheric organic acids, Scientific

827   reports, 5, 9580, doi:10.1038/srep09580, 2015b.

828 Dentener, F., Kinne, S., Bond, T., Boucher, O., Cofala, J., Generoso, S., Ginoux, P., Gong, S.,

829   Hoelzemann, J. J., Ito, A., Marelli, L., Penner, J. E., Putaud, J. P., Textor, C., Schulz, M.,

830   van der Werf, G. R., and Wilson, J.: Emissions of primary aerosol and precursor gases in the

831   years 2000 and 1750, prescribed data-sets for AeroCom, Atmos. Chem. Phys., 6, 4321–4344,

832   doi:10.5194/acp-6-4321-2006, 2006.

833 Ding, Y., Sun, Y., Wang, Z., Zhu, Y., and Song, Y.: Inter-decadal variation of the summer

834   precipitation in China and its association with decreasing Asian summer monsoon Part II:

835   Possible causes, Int. J. Climatol., 29, 1926–1944, doi:10.1002/joc.1759, 2009.

836 Du, Q., Zhao, C., Zhang, M., Dong, X., Chen, Y., Liu, Z., Hu, Z., Zhang, Q., Li, Y., Yuan, R.

837   , and Miao, S.: Modelling diurnal variation of surface PM2.5 concentration over East China

838   with WRF-Chem: Impacts from boundary layer mixing and anthropogenic

839   emission, Atmos. Chem. Phys. Discuss., https://doi.org/10.5194/acp-2019-

840   739, in review, 2020.

841   Duan, A. M. and Wu, G. X.: Role of the Tibetan Plateau thermal forcing in the summer climate

842   patterns over subtropical Asia, Climate Dynamics, 24, 793–807, doi:10.1007/s00382-004-

843   0488-8, 2005.

844   Dubovik, O. and King, M. D.: A flexible inversion algorithm for retrieval of aerosol optical

845   properties from Sun and sky radiance measurements, J. Geophys. Res., 105, 20673–20696,

846   doi:10.1029/2000JD900282, 2000.

847   Dubovik, O., Holben, B., Eck, T. F., Smirnov, A., Kaufman, Y. J., King, M. D., Tanré, D., and

848   Slutsker, I.: Variability of Absorption and Optical Properties of Key Aerosol Types

849   Observed in Worldwide Locations, J. Atmos. Sci., 59, 590–608, doi:10.1175/1520-

850   0469(2002)059<0590:VOAAOP>2.0.CO;2, 2002.

851   Dumka, U. C., Moorthy, K. K., Kumar, R., Hegde, P., Sagar, R., Pant, P., Singh, N., and Babu,

852   S. S.: Characteristics of aerosol black carbon mass concentration over a high altitude location

853   in the Central Himalayas from multi-year measurements, Atmospheric Research, 96, 510–

854   521, doi:10.1016/j.atmosres.2009.12.010, 2010.

855   Easter, R. C., Ghan, S. J., Zhang, Y., Saylor, R. D., Chapman, E. G., Laulainen, N. S., Abdul-

856   Razzak, H., Leung, L. R., Bian, X., and Zaveri, R. A.: MIRAGE: Model Description and

857   Evaluation of Aerosols and Trace Gases, J. Geophys. Res., 109, D20210,

858   doi:10.1029/2004JD004571, 2004.

859   Egger, J., Bajracharya, S., Egger, U., Heinrich, R., Reuder, J., Shakya, P., Wendt, H., and Wirth,

860   V.: Diurnal winds in the Himalayan Kali Gandaki Valley. Part I: Observations, Mon.

861   Weather Rev., 128, 1106–1122, 2000.

862   Engling, G. and Gelencser, A.: Atmospheric Brown Clouds: From Local Air Pollution to

863   Climate Change, Elements, 6, 223–228, doi:10.2113/gselements.6.4.223, 2010.

864   Fan, J., Rosenfeld, D., Yang, Y., Zhao, C., Leung, L. R., and Li, Z.: Substantial contribution

865   of anthropogenic air pollution to catastrophic floods in Southwest China, Geophys. Res. Lett.,

866   42, 6066–6075, doi:10.1002/2015GL064479, 2015.

867   Fast, J. D., Gustafson Jr, W. I., Easter, R. C., Zaveri, R. A., Barnard, J. C., Chapman, E. G.,

868   Grell, G. A., and Peckham, S. E.: Evolution of ozone, particulates, and aerosol direct

869   radiative forcing in the vicinity of Houston using a fully coupled meteorology-chemistry-

870   aerosol model, J. Geophys. Res., 111, D21305, doi:10.1029/2005JD006721, 2006.

871   Feng, Y., Kotamarthi, V. R., Coulter, R., Zhao, C., and Cadeddu, M.: Radiative and

872   thermodynamic responses to aerosol extinction profiles during the pre-monsoon month over

873   South Asia, Atmos. Chem. Phys., 16, 247–264, doi:10.5194/acp-16-247-2016, 2016.

874 Flanner, M. G. and Zender, C. S.: Snowpack radiative heating: Influence on Tibetan Plateau

875 climate, Geophys. Res. Lett., 32, L06501, doi:10.1029/2004GL022076, 2005.

876 Fu, Y., Pan, X., Xian, T., Liu, G., Zhong, L., Liu, Q., Li, R., Wang, Y., and Ma, M.:

877 Precipitation characteristics over the steep slope of the Himalayas in rainy season observed

878 by TRMM PR and VIRS, Climate dynamics, 51, 1971-1989, doi: 10.1007/s00382-017-

879 3992-3, 2018.

880 Gao, Y., Zhao, C., Liu, X., Zhang, M., and Leung, L. R.: WRF-Chem simulations of aerosols

881 and anthropogenic aerosol radiative forcing in East Asia, Atmospheric Environment, 92,

882 250–266, doi:10.1016/j.atmosenv.2014.04.038, 2014.

883 Ginoux, P., Chin, M., Tegen, I., Prospero, J. M., Holben, B., Dubovik, O., and Lin, S.-J.:

884 Sources and distributions of dust aerosols simulated with the GOCART model, J. Geophys.

885 Res., 106, 20255–20273, doi:10.1029/2000JD000053, 2001.

886 Gong, P., Wang, X., Pokhrel, B., Wang, H., Liu, X., Liu, X., and Wania, F.: Trans-Himalayan

887 Transport of Organochlorine Compounds: Three-Year Observations and Model-Based Flux

888 Estimation, Environ. Sci. Technol., 53, 6773–6783, doi:10.1021/acs.est.9b01223, 2019.

889 Gong, S. L.: A parameterization of sea-salt aerosol source function for sub- and super-micron

890 particles, Global Biogeochem. Cycles, 17, n/a-n/a, doi:10.1029/2003GB002079, 2003.

891 Grell, G. A., Peckham, S. E., Schmitz, R., McKeen, S. A., Frost, G., Skamarock, W. C., and

892 Eder, B.: Fully coupled "online" chemistry within the WRF model, Atmospheric

893 Environment, 39, 6957–6975, doi:10.1016/j.atmosenv.2005.04.027, 2005.

894 Gustafson, W. I., E. G. Chapman, S. J. Ghan, R. C. Easter, and J. D. Fast: Impact on modeled

895 cloud characteristics due to simplified treatment of uniform cloud condensation nuclei

896 during NEAQS 2004, Geophys. Res. Lett., 34, L19809, doi:10.1029/2007GL030021, 2007.

897 Hansen, J. and Nazarenko, L.: Soot climate forcing via snow and ice albedos, Proceedings of

898 the National Academy of Sciences, 101, 423–428, doi:10.1073/pnas.2237157100, 2004.

899 He, C., Li, Q., Liou, K. N., Takano, Y., Gu, Y., Qi, L., Mao, Y., and Leung, L. R.: Black carbon

900 radiative forcing over the Tibetan Plateau, Geophys. Res. Lett., 41, 7806–7813,

901 doi:10.1002/2014GL062191, 2014.

902 He, C., Wang, Z., Zhou, T., and Li, T.: Enhanced Latent Heating over the Tibetan Plateau as a

903 Key to the Enhanced East Asian Summer Monsoon Circulation under a Warming Climate,

904 J. Climate, 32, 3373–3388, doi:10.1175/JCLI-D-18-0427.1, 2019.

905 Hess, M., Koepke, P., and Schult, I.: Optical Properties of Aerosols and Clouds: The Software

906 Package OPAC, Bull. Amer. Meteor. Soc., 79, 831–844, doi:10.1175/1520-

907 0477(1998)079<0831:OPOAAC>2.0.CO;2, 1998.

Hindman, E. E. and Upadhyay, B. P.: Air pollution transport in the Himalayas of Nepal and Tibet during the 1995–1996 dry season, Atmospheric Environment, 36, 727–739, doi:10.1016/S1352-2310(01)00495-2, 2002.

Holben, B. N., Eck, T. F., Slutsker, I., Tanré, D., Buis, J. P., Setzer, A., Vermote, E., Reagan, J. A., Kaufman, Y. J., Nakajima, T., Lavenu, F., Jankowiak, I., and Smirnov, A.: AERONET—A Federated Instrument Network and Data Archive for Aerosol Characterization, Remote Sensing of Environment, 66, 1–16, doi:10.1016/S0034-4257(98)00031-5, 1998.

Holben, B. N., Tanre, D., Smirnov, A., ECK T. F., Slutsker, I., Abuhassan, N., Newcomb, W., Schafer, J., Chatenet, B., Lavenu, F., Kaufman, Y., Vande Castle, J., Setzer, A., Markham, B., Clark, D., Frouin, R., Halthore, R., Karneli, A., O'Neill, N., Pietras, C., Pinker, R., Voss, K., and Zibordi, G.: An emerging ground-based aerosol climatology: Aerosol optical depth from AERONET, J. Geophys. Res., 106, 12067-12097, doi:10.1029/2001JD900014, 2001.

Horvath, K., Koracin, D., Vellore, R., Jiang, J., and Belu, R.: Sub‐kilometer dynamical downscaling of near‐surface winds in complex terrain using WRF and MM5 mesoscale models, J. Geophys. Res. Atmos., 117, D11111, doi:10.1029/2012JD017432, 2012

Hu, Z., Huang, J., Zhao, C., Bi, J., Jin, Q., Qian, Y., Leung, L. R., Feng, T., Chen, S., and Ma, J.: Modeling the contributions of Northern Hemisphere dust sources to dust outflow from East Asia, Atmospheric Environment, 202, 234–243, doi:10.1016/j.atmosenv.2019.01.022, 2019.

Hu, Z., Huang, J., Zhao, C., Jin, Q., Ma, Y., and Yang, B.: Modeling dust sources, transport, and radiative effects at different altitudes over the Tibetan Plateau, Atmos. Chem. Phys. Discuss., https://doi.org/10.5194/acp-2019-431, in press, 2020.

Hu, Z., Zhao, C., Huang, J., Leung, L. R., Qian, Y., Yu, H., Huang, L., and Kalashnikova, O.V.: Trans-pacific transport and evolution of aerosols: Evaluation of quasi global WRF-Chem simulation with multiple observations, Geosci. Model Dev., 9, 1725–1746, doi:10.5194/gmd-9-1725-2016, 2016.

Huang, X., Song, Y., Zhao, C., Cai, X., Zhang, H., and Zhu, T.: Direct Radiative Effect by Multicomponent Aerosol over China, J. Climate, 28, 3472–3495, doi:10.1175/JCLI-D-14-00365.1, 2015.

Iacono, M. J., Mlawer, E. J., Clough, S. A., and Morcrette, J. J.: Impact of an improved longwave radiation model, RRTM, on the energy budget and thermodynamic properties of

the NCAR community climate model, CCM3, J. Geophys. Res., 105, 14873–14890, doi:10.1029/2000JD900091, 2000.

Immerzeel, W. W., van Beek, L. P. H., and Bierkens, M. F. P.: Climate change will affect the Asian water towers, Science (New York, N.Y.), 328, 1382–1385, doi:10.1126/science.1183188, 2010.

Jaeglé, L., Quinn, P. K., Bates, T. S., Alexander, B., and Lin, J. T.: Global distribution of sea salt aerosols: new constraints from in situ and remote sensing observations, Atmos. Chem. Phys., 11, 3137–3157, doi:10.5194/acp-11-3137-2011, 2011.

Janssens-Maenhout, G., Crippa, M., Guizzardi, D., Dentener, F., Muntean, M., Pouliot, G., Keating, T., Zhang, Q., Kurokawa, J., Wankmüller, R., van der Denier Gon, H., Kuenen, J. J. P., Klimont, Z., Frost, G., Darras, S., Koffi, B., and Li, M.: HTAP_v2.2: a mosaic of regional and global emission grid maps for 2008 and 2010 to study hemispheric transport of air pollution, Atmos. Chem. Phys., 15, 11411–11432, doi:10.5194/acp-15-11411-2015, 2015.

Ji, Z. M.: Modeling black carbon and its potential radiative effects over the Tibetan Plateau, Advances in Climate Change Research, 7, 139–144, doi:10.1016/j.accre.2016.10.002, 2016.

Ji, Z., Kang, S., Cong, Z., Zhang, Q., and Yao, T.: Simulation of carbonaceous aerosols over the Third Pole and adjacent regions: distribution, transportation, deposition, and climatic effects, Clim Dyn, 45, 2831–2846, doi:10.1007/s00382-015-2509-1, 2015.

Jiménez, P. A. and Dudhia, J.: Improving the representation of resolved and unresolved topographic effects on surface wind in the WRF model, J. Appl. Meteorol. Clim., 51, 300-316, doi:10.1175/JAMC-D-11-084.1, 2012.

Kain, J. S.: The Kain–Fritsch Convective Parameterization: An Update, J. Appl. Meteor., 43, 170–181, doi:10.1175/1520-0450(2004)043<0170:TKCPAU>2.0.CO;2, 2004.

Kang, S, Chen P, Li C, Liu B, Cong Z: Atmospheric Aerosol Elements over the Inland Tibetan Plateau: Concentration, Seasonality, and Transport, Aerosol Air Qual. Res., 16, 789–800, doi:10.4209/aaqr.2015.02.0307, 2016.

Kang, S., Q. Zhang, Y. Qian, Z. Ji, C. Li, Z. Cong, Y. Zhang, J. Guo, W. Du, J. Huang, Q. You, A. K. Panday, M. Rupakheti, D. Chen, O. Gustafsson, M. H. Thiemens, and D. Qin: Linking atmospheric pollution to cryospheric change in the Third Pole region: current progress and future prospects, National Science Review, 6, 796–809, doi:10.1093/nsr/nwz031, 2019.

Kant, Y., Shaik, D. S., Mitra, D., Chandola, H. C., Babu, S. S., and Chauhan, P.: Black carbon aerosol quantification over north-west Himalayas: Seasonal heterogeneity, source

975   apportionment and radiative forcing, Environmental pollution (Barking, Essex 1987),
976   113446, doi:10.1016/j.envpol.2019.113446, 2019.

977   Karki, R., ul Hasson, S., Gerlitz, L., Schickhoff, U., Scholten, T., and Böhner, J.: Quantifying
978   the added value of convection-permitting climate simulations in complex terrain: a
979   systematic evaluation of WRF over the Himalayas, Earth Syst. Dynam., 8, 507–528,
980   doi:10.5194/esd-8-507-2017, 2017.

981   Kok, J. F.: A scaling theory for the size distribution of emitted dust aerosols suggests climate
982   models underestimate the size of the global dust cycle, Proceedings of the National Academy
983   of Sciences of the United States of America, 108, 1016–1021, doi:10.1073/pnas.1014798108,
984   2011.

985   Kopacz, M., Mauzerall, D. L., Wang, J., Leibensperger, E. M., Henze, D. K., and Singh, K.:
986   Origin and radiative forcing of black carbon transported to the Himalayas and Tibetan
987   Plateau, Atmos. Chem. Phys., 11, 2837–2852, doi:10.5194/acp-11-2837-2011, 2011.

988   Kuhlmann, J. and Quaas, J.: How can aerosols affect the Asian summer monsoon? Assessment
989   during three consecutive pre-monsoon seasons from CALIPSO satellite data, Atmos. Chem.
990   Phys., 10, 4673–4688, doi:10.5194/acp-10-4673-2010, 2010.

991   Lau, K. M. and Kim, K. M.: Observational relationships between aerosol and Asian monsoon
992   rainfall, and circulation, Geophys. Res. Lett., 33, D22101, doi: 10.1029/2006GL027546,
993   2006b.

994   Lau, K. M., Kim, M. K., and Kim, K. M.: Asian summer monsoon anomalies induced by
995   aerosol direct forcing: the role of the Tibetan Plateau, Clim Dyn, 26, 855–864, doi:
996   10.1007/s00382-006-0114-z, 2006a.

997   Lau, W. K. and Kim, K. M.: Impact of Snow Darkening by Deposition of Light-Absorbing
998   Aerosols on Snow Cover in the Himalayas–Tibetan Plateau and Influence on the Asian
999   Summer Monsoon: A Possible Mechanism for the Blanford Hypothesis, Atmosphere, 9, 438,
1000 doi:10.3390/atmos9110438, 2018.

1001 Lau, W. K. M., Kim, K. M., Shi, J. J., Matsui, T., Chin, M., Tan, Q., Peters-Lidard, C., and
1002 Tao, W. K.: Impacts of aerosol–monsoon interaction on rainfall and circulation over
1003 Northern India and the Himalaya Foothills, Clim Dyn, 49, 1945–1960, doi:10.1007/s00382-
1004 016-3430-y, 2017.

1005 Lau, W. K. M., Kim, M. K., Kim, K. M., and Lee, W. S.: Enhanced surface warming and
1006 accelerated snow melt in the Himalayas and Tibetan Plateau induced by absorbing aerosols,
1007 Environ. Res. Lett., 5, 25204, doi:10.1088/1748-9326/5/2/025204, 2010.

Lee, W. S., Bhawar, R. L., Kim, M. K., and Sang, J.: Study of aerosol effect on accelerated snow melting over the Tibetan Plateau during boreal spring, Atmospheric Environment, 75, 113–122, doi:10.1016/j.atmosenv.2013.04.004, 2013.

Li, C., Bosch, C., Kang, S., Andersson, A., Chen, P., Zhang, Q., Cong, Z., Chen, B., Qin, D., and Gustafsson, Ö.: Sources of black carbon to the Himalayan–Tibetan Plateau glaciers, Nat Commun, 7, 4825, doi:10.1038/ncomms12574, 2016.

Li, M., Zhang, Q., Kurokawa, J. i., Woo, J. H., He, K., Lu, Z., Ohara, T., Song, Y., Streets, D. G., Carmichael, G. R., Cheng, Y., Hong, C., Huo, H., Jiang, X., Kang, S., Liu, F., Su, H., and Zheng, B.: MIX: a mosaic Asian anthropogenic emission inventory under the international collaboration framework of the MICS-Asia and HTAP, Atmos. Chem. Phys., 17, 935–963, doi:10.5194/acp-17-935-2017, 2017.

Li, R. and Min, Q. L.: Impacts of mineral dust on the vertical structure of precipitation, J. Geophys. Res., 115, 1337, doi:10.1029/2009JD011925, 2010.

Li, R., Dong, X., Guo, J., Fu, Y., Zhao, C., Wang, Y., and Min, Q.: The implications of dust ice nuclei effect on cloud top temperature in a complex mesoscale convective system, Sci Rep, 7, 291, doi:10.1038/s41598-017-12681-0, 2017.

Li, R., Shao, W., Guo, J., Fu, Y., Wang, Y., Liu, G., Zhou, R., and Li, W.: A Simplified Algorithm to Estimate Latent Heating Rate Using Vertical Rainfall Profiles Over the Tibetan Plateau, J. Geophys. Res. Atmos., 124, 942–963, doi:10.1029/2018JD029297, 2019.

Lin, C., Chen, D., Yang, K., and Ou, T.: Impact of model resolution on simulating the water vapor transport through the central Himalayas: implication for models' wet bias over the Tibetan Plateau, Clim Dyn, 51, 3195–3207, doi:10.1007/s00382-018-4074-x, 2018.

Liu, P., Tsimpidi, A. P., Hu, Y., Stone, B., Russell, A. G., and Nenes, A.: Differences between downscaling with spectral and grid nudging using WRF, Atmos. Chem. Phys., 12, 3601–3610, doi:10.5194/acp-12-3601-2012, 2012.

Liu, Y., Sato, Y., Jia, R., Xie, Y., Huang, J., and Nakajima, T.: Modeling study on the transport of summer dust and anthropogenic aerosols over the Tibetan Plateau, Atmos. Chem. Phys., 15, 12581–12594, doi:10.5194/acp-15-12581-2015, 2015.

Liu, Z., Ming, Y., Zhao, C., Lau, N. C., Guo, J., Bollasina, M., and Yim, S. H. L.: Contribution of local and remote anthropogenic aerosols to a record-breaking torrential rainfall event in Guangdong Province, China, Atmos. Chem. Phys., 20, 223–241, doi:10.5194/acp-20-223-2020, 2020.

1040   Lu, Z., Streets, D. G., Zhang, Q., and Wang, S.: A novel back-trajectory analysis of the origin

1041   of black carbon transported to the Himalayas and Tibetan Plateau during 1996-2010,

1042   Geophys. Res. Lett., 39, n/a-n/a, doi:10.1029/2011GL049903, 2012.

1043   Lüthi, Z. L., Škerlak, B., Kim, S. W., Lauer, A., Mues, A., Rupakheti, M., and Kang, S.:

1044   Atmospheric brown clouds reach the Tibetan Plateau by crossing the Himalayas, Atmos.

1045   Chem. Phys., 15, 6007–6021, doi:10.5194/acp-15-6007-2015, 2015.

1046   Lutz, A. F., Immerzeel, W. W., Shrestha, A. B., and Bierkens, M. F. P.: Consistent increase in

1047   High Asia's runoff due to increasing glacier melt and precipitation, Nature Clim Change, 4,

1048   587–592, doi:10.1038/nclimate2237, 2014.

1049   Marinoni, A., Cristofanelli, P., Laj, P., Duchi, R., Calzolari, F., Decesari, S., Sellegri, K.,

1050   Vuillermoz, E., Verza, G. P., and Villani, P.: Aerosol mass and black carbon concentrations,

1051   a two year record at NCO-P (5079 m, Southern Himalayas), Atmos. Chem. Phys., 10, 8551–

1052   8562, doi:10.5194/acp-10-8551-2010, 2010.

1053   Menon, S., Koch, D., Beig, G., Sahu, S., Fasullo, J., and Orlikowski, D.: Black carbon aerosols

1054   and the third polar ice cap, Atmos. Chem. Phys., 10, 4559–4571, doi:10.5194/acp-10-4559-

1055   2010, 2010.

1056   Ming, J., Xiao, C., Cachier, H., Qin, D., Qin, X., Li, Z., and Pu, J.: Black Carbon (BC) in the

1057   snow of glaciers in west China and its potential effects on albedos, Atmospheric Research,

1058   92, 114–123, doi:10.1016/j.atmosres.2008.09.007, 2009.

1059   Mlawer, E. J., Taubman, S. J., Brown, P. D., Iacono, M. J., and Clough, S. A.: Radiative

1060   transfer for inhomogeneous atmospheres: RRTM, a validated correlated-k model for the

1061   longwave, J. Geophys. Res., 102, 16663–16682, doi:10.1029/97JD00237, 1997.

1062   Morrison, H., Thompson, G., and Tatarskii, V.: Impact of Cloud Microphysics on the

1063   Development of Trailing Stratiform Precipitation in a Simulated Squall Line: Comparison

1064   of One- and Two-Moment Schemes, Mon. Wea. Rev., 137, 991–1007,

1065   doi:10.1175/2008MWR2556.1, 2009.

1066   Nakanishi, M. and Niino, H.: An Improved Mellor–Yamada Level-3 Model: Its Numerical

1067   Stability and Application to a Regional Prediction of Advection Fog, Boundary-Layer

1068   Meteorol, 119, 397–407, doi:10.1007/s10546-005-9030-8, 2006.

1069   Oleson, K. W., Lawrence, D. M., Bonan, G. B., Flanner, M. G., Kluzek, E., Lawrence, P. J.,

1070   Levis, S., Swenson, S. C., Thornton, P. E., Dai, A., Decker, M., Dickinson, R., Feddema, J.,

1071   Heald, C. L., Hoffman, F., Lamarque, J. F., Mahowald, N., Niu, G. Y., Qian, T., Randerson,

1072   J., Running, S., Sakaguchi, K., Slater, A., Stockli, R., Wang, A., Yang, Z. L., Zeng, X., and

1073   Zeng, X.: Technical Description of version 4.0 of the Community Land Model (CLM), Tech.

1074   Rep. NCAR/TN-478+STR, National Center for Atmospheric Research, Boulder, Colorado,
1075   USA, 2010.

1076 Prasad, A. K. and Singh, R. P.: Comparison of MISR-MODIS aerosol optical depth over the
1077   Indo-Gangetic basin during the winter and summer seasons (2000–2005), Remote Sensing
1078   of Environment, 107, 109–119, doi:10.1016/j.rse.2006.09.026, 2007.

1079 Qian, Y., Flanner, M. G., Leung, L. R., and Wang, W.: Sensitivity studies on the impacts of
1080   Tibetan Plateau snowpack pollution on the Asian hydrological cycle and monsoon climate,
1081   Atmos. Chem. Phys., 11, 1929–1948, doi:10.5194/acp-11-1929-2011, 2011.

1082 Qian, Y., Yasunari, T. J., Doherty, S. J., Flanner, M. G., Lau, W. K. M., Ming, J., Wang, H.,
1083   Wang, M., Warren, S. G., and Zhang, R.: Light-absorbing particles in snow and ice:
1084   Measurement and modeling of climatic and hydrological impact, Adv. Atmos. Sci., 32, 64–
1085   91, doi:10.1007/s00376-014-0010-0, 2015.

1086 Qiu, J.: China: The third pole, Nature, 454, 393–396, doi:10.1038/454393a, 2008.

1087 Ramanathan, V. and Carmichael, G.: Global and regional climate changes due to black carbon,
1088   Nature Geosci, 1, 221–227, doi:10.1038/ngeo156, 2008.

1089 Ramanathan, V., Ramana, M. V., Roberts, G., Kim, D., Corrigan, C., Chung, C., and Winker,
1090   D.: Warming trends in Asia amplified by brown cloud solar absorption, Nature, 448, 575–
1091   578, doi:10.1038/nature06019, 2007.

1092 Sarangi, C., Qian, Y., Rittger, K., Bormann, K. J., Liu, Y., Wang, H., Lin, G., and Painter, T.
1093   H.: Impact of light-absorbing particles on snow albedo darkening and associated radiative
1094   forcing over high-mountain Asia: high-resolution WRF-Chem modeling and new satellite
1095   observations. Atmos. Chem. Phys., 19, 7105–7128, doi:10.5194/acp-19-7105-2019, 2019.

1096 Seaman, N. L., Stauffer, D. R., and Lario-Gibbs, A. M.: A Multiscale Four-Dimensional Data
1097   Assimilation System Applied in the San Joaquin Valley during SARMAP. Part I: Modeling
1098   Design and Basic Performance Characteristics, J. Appl. Meteor., 34, 1739–1761,
1099   doi:10.1175/1520-0450(1995)034<1739:AMFDDA>2.0.CO;2, 1995.

1100 Shi, X., Wang, Y., and Xu, X.: Effect of mesoscale topography over the Tibetan Plateau on
1101   summer precipitation in China: A regional model study, Geophys. Res. Lett., 35, 255,
1102   doi:10.1029/2008GL034740, 2008.

1103 Singh, P. and Bengtsson, L.: Hydrological sensitivity of a large Himalayan basin to climate
1104   change, Hydrol. Process., 18, 2363–2385, doi:10.1002/hyp.1468, 2004.

1105 Skamarock, W. C., Klemp, J. B., Dudhia, J., Gill, D. O., Barker, D. M., Duda, M., Huang, X.
1106   Y., Wang, W., and Powers, J. G.: A Description of the Advanced Research WRF Version 3,

1107 NCAR Technical Note, NCAR/TN-468+STR, available at: http://wrf-
1108 model.org/wrfadmin/docs/arw v2.pdf, 2008.

1109 Stauffer, D. R. and Seaman, N. L.: Use of Four-Dimensional Data Assimilation in a Limited-
1110 Area Mesoscale Model. Part I: Experiments with Synoptic-Scale Data, Mon. Wea. Rev., 118,
1111 1250–1277, doi:10.1175/1520-0493(1990)118<1250:UOFDDA>2.0.CO;2, 1990.

1112 Wagner, J. S., Gohm, A., and Rotach, M. W.: The Impact of Horizontal Model Grid Resolution
1113 on the Boundary Layer Structure over an Idealized Valley, Mon. Wea. Rev., 142, 3446–
1114 3465, doi:10.1175/MWR-D-14-00002.1, 2014.

1115 Wang, X., Gong, P., Sheng, J., Joswiak, D. R., and Yao, T.: Long-range atmospheric transport
1116 of particulate Polycyclic Aromatic Hydrocarbons and the incursion of aerosols to the
1117 southeast Tibetan Plateau, Atmospheric Environment, 115, 124–131,
1118 doi:10.1016/j.atmosenv.2015.04.050, 2015.

1119 Wang, Y., Yang, K., Zhou, X., Chen, D., Lu, H., Ouyang, L., Chen, Y., Lazhu., and Wang, B.:
1120 Synergy of orographic drag parameterization and high resolution greatly reduces biases of
1121 WRF-simulated precipitation in central Himalaya, Climate Dynamics, 54, 1729–1740,
1122 doi:10.1007/s00382-019-05080-w, 2020.

1123 Wiedinmyer, C., Akagi, S. K., Yokelson, R. J., Emmons, L. K., Al-Saadi, J. A., Orlando, J. J.,
1124 and Soja, A. J.: The Fire INventory from NCAR (FINN): a high resolution global model to
1125 estimate the emissions from open burning, Geosci. Model Dev., 4, 625–641,
1126 doi:10.5194/gmd-4-625-2011, 2011.

1127 Wu, G., Liu, Y., Dong, B., Liang, X., Duan, A., Bao, Q., and Yu, J.: Revisiting Asian monsoon
1128 formation and change associated with Tibetan Plateau forcing: I. Formation, Clim Dyn, 39,
1129 1169–1181, doi:10.1007/s00382-012-1334-z, 2012a.

1130 Wu, G., Liu, Y., He, B., Bao, Q., Duan, A., and Jin, F. F.: Thermal controls on the Asian
1131 summer monsoon, Scientific reports, 2, 404, doi:10.1038/srep00404, 2012b.

1132 Wu, G., Liu, Y., Zhang, Q., Duan, A., Wang, T., Wan, R., Liu, X., Li, W., Wang, Z., and Liang,
1133 X.: The Influence of Mechanical and Thermal Forcing by the Tibetan Plateau on Asian
1134 Climate, J. Hydrometeor., 8, 770–789, doi:10.1175/JHM609.1, 2007.

1135 Wu, L., Su, H., and Jiang, J. H.: Regional simulation of aerosol impacts on precipitation during
1136 the East Asian summer monsoon, J. Geophys. Res. Atmos., 118, 6454–6467,
1137 doi:10.1002/jgrd.50527, 2013.

1138 Wulf, H., Bookhagen, B., and Scherler, D.: Differentiating between rain, snow, and glacier
1139 contributions to river discharge in the western Himalaya using remote-sensing data and

1140   distributed hydrological modeling, Advances in Water Resources, 88, 152–169,
1141   doi:10.1016/j.advwatres.2015.12.004, 2016.

1142   Yang, J., Kang, S., Ji, Z., and Chen, D.: Modeling the Origin of Anthropogenic Black Carbon
1143   and Its Climatic Effect Over the Tibetan Plateau and Surrounding Regions, J. Geophys. Res.
1144   Atmos., 123, 671–692, doi:10.1002/2017JD027282, 2018.

1145   Yasunari, T. J., Bonasoni, P., Laj, P., Fujita, K., Vuillermoz, E., Marinoni, A., Cristofanelli, P.,
1146   Duchi, R., Tartari, G., and Lau, K.-M.: Estimated impact of black carbon deposition during
1147   pre-monsoon season from Nepal Climate Observatory – Pyramid data and snow albedo
1148   changes over Himalayan glaciers, Atmos. Chem. Phys., 10, 6603–6615, doi:10.5194/acp-
1149   10-6603-2010, 2010.

1150   Ye, D. Z. and Wu, G. X.: The role of the heat source of the Tibetan Plateau in the general
1151   circulation, Meteorl. Atmos. Phys., 67, 181–198, doi:10.1007/BF01277509, 1998.

1152   Zängl, G., Egger, J., and Wirth, V.: Diurnal Winds in the Himalayan Kali Gandaki Valley. Part
1153   II: Modeling, Mon. Wea. Rev., 129, 1062–1080, doi:10.1175/1520-
1154   0493(2001)129<1062:DWITHK>2.0.CO;2, 2001.

1155   Zaveri, R. A. and Peters, L. K.: A new lumped structure photochemical mechanism for large-
1156   scale applications, J. Geophys. Res., 104, 30387–30415, doi:10.1029/1999JD900876, 1999.

1157   Zaveri, R. A., Easter, R. C., Fast, J. D., and Peters, L. K.: Model for Simulating Aerosol
1158   Interactions and Chemistry (MOSAIC), J. Geophys. Res., 113, 1591,
1159   doi:10.1029/2007JD008782, 2008.

1160   Zhang, A., Fu, Y., Chen, Y., Liu, G., and Zhang, X.: Impact of the surface wind flow on
1161   precipitation characteristics over the southern Himalayas: GPM observations, Atmospheric
1162   Research, 202, 10–22, doi:10.1016/j.atmosres.2017.11.001, 2018.

1163   Zhang, R., Wang, H., Qian, Y., Rasch, P. J., Easter, R. C., Ma, P. L., Singh, B., Huang, J., and
1164   Fu, Q.: Quantifying sources, transport, deposition, and radiative forcing of black carbon over
1165   the Himalayas and Tibetan Plateau, Atmos. Chem. Phys., 15, 6205–6223, doi:10.5194/acp-
1166   15-6205-2015, 2015.

1167   Zhang, R., Wang, Y., He, Q., Chen, L., Zhang, Y., Qu, H., Smeltzer, C., Li, J., Alvarado, L. M.
1168   A., Vrekoussis, M., Richter, A., Wittrock, F., and Burrows, J. P.: Enhanced trans-Himalaya
1169   pollution transport to the Tibetan Plateau by cut-off low systems, Atmos. Chem. Phys., 17,
1170   3083–3095, doi:10.5194/acp-17-3083-2017, 2017.

1171   Zhang, Y., Kang, S., Cong, Z., Schmale, J., Sprenger, M., Li, C., Yang, W., Gao, T., Sillanpää,
1172   M., Li, X., Liu, Y., Chen, P., and Zhang, X.: Light-absorbing impurities enhance glacier

1173   albedo reduction in the southeastern Tibetan plateau, J. Geophys. Res. Atmos., 122, 6915–
1174   6933, doi:10.1002/2016JD026397, 2017.

1175 Zhang, Y., Kang, S., Sprenger, M., Cong, Z., Gao, T., Li, C., Tao, S., Li, X., Zhong, X., Xu,
1176   M., Meng, W., Neupane, B., Qin, X., and Sillanpää, M.: Black carbon and mineral dust in
1177   snow cover on the Tibetan Plateau, The Cryosphere, 12, 413–431, doi:10.5194/tc-12-413-
1178   2018, 2018.

1179 Zhao, C., Chen, S., Leung, L. R., Qian, Y., Kok, J., Zaveri, R., and Huang, J.: Uncertainty in
1180   modeling dust mass balance and radiative forcing from size parameterization, Atmos. Chem.
1181   Phys., 13, 10733–10753, doi:doi:10.5194/acp-13-10733-2013, 2013b.

1182 Zhao, C., Hu, Z., Qian, Y., Leung, L. R., Huang, J., Huang, M., Jin, J., Flanner, M., Zhang, R.,
1183   Wang, H., Yan, H., Lu, Z., and Streets, D. G.: Simulating black carbon and dust and their
1184   radiative forcing in seasonal snow: a case study over North China with field campaign
1185   measurements, Atmos. Chem. Phys., 14, 11475–11491, doi:10.5194/acp-14-11475-2014,
1186   2014.

1187 Zhao, C., Huang, M., Fast, J. D., Berg, L. K., Qian, Y., Guenther, A., Gu, D., Shrivastava, M.,
1188   Liu, Y., and Walters, S.: Sensitivity of biogenic volatile organic compounds to land surface
1189   parameterizations and vegetation distributions in California, Geosci. Model Dev, 9, 1959–
1190   1976, doi:10.5194/gmd-9-1959-2016, 2016.

1191 Zhao, C., Liu, X., and Leung, L. R.: Impact of the Desert dust on the summer monsoon system
1192   over Southwestern North America, Atmos. Chem. Phys., 12, 3717–3731, doi:10.5194/acp-
1193   12-3717-2012, 2012.

1194 Zhao, C., Liu, X., Leung, L. R., and Hagos, S.: Radiative impact of mineral dust on monsoon
1195   precipitation variability over West Africa, Atmos. Chem. Phys., 11, 1879–1893,
1196   doi:10.5194/acp-11-1879-2011, 2011.

1197 Zhao, C., Liu, X., Leung, L. R., Johnson, B., McFarlane, S. A., Gustafson, W. I., Fast, J. D.,
1198   and Easter, R.: The spatial distribution of mineral dust and its shortwave radiative forcing
1199   over North Africa: modeling sensitivities to dust emissions and aerosol size treatments,
1200   Atmos. Chem. Phys., 10, 8821–8838, doi:10.5194/acp-10-8821-2010, 2010.

1201 Zhao, C., Ruby Leung, L., Easter, R., Hand, J., and Avise, J.: Characterization of speciated
1202   aerosol direct radiative forcing over California, J. Geophys. Res. Atmos., 118, 2372–2388,
1203   doi:10.1029/2012JD018364, 2013a.

1204 Zhao, P., Zhou, X., Chen, J., Liu, G., and Nan, S.: Global climate effects of summer Tibetan
1205   Plateau, Science Bulletin, 64, 1–3, doi:10.1016/j.scib.2018.11.019, 2019.

Zhou, X., Beljaars, A., Wang, Y., Huang, B., Lin, C., Chen, Y., and Wu, H.: Evaluation of WRF simulations with different selections of subgrid orographic drag over the Tibetan Plateau, J. Geophys. Res. Atmos., 122, 9759–9772, doi:10.1002/ 2017JD027212, 2017.

Zhou, X., Yang, K., and Wang, Y.: Implementation of a turbulent orographic form drag scheme in WRF and its application to the Tibetan Plateau, Climate dynamics, 50, 2443-2455, doi: 10.1007/s00382-017-3677-y, 2018.

Zhao, Z., Cao, J., Shen, Z., Xu, B., Zhu, C., Chen, L. W. A., Su, X., Liu, S., Han, Y., Wang, G., and Ho, K.: Aerosol particles at a high-altitude site on the Southeast Tibetan Plateau, China: Implications for pollution transport from South Asia, J. Geophys. Res. Atmos., 118, 11,360-11,375, doi:10.1002/jgrd.50599, 2013.

Zhong, S., Qian, Y., Zhao, C., Leung, R., Wang, H., Yang, B., Fan, Ji., Yan, H., Yang, X., and Liu, D.: Urbanization-induced urban heat island and aerosol effects on climate extremes in the Yangtze River Delta region of China, Atmos. Chem. Phys., 17, 5439–5457, doi:10.5194/acp-17-5439-2017, 2017.

1234

1235

1236

1237

1238
1239
1240
1241
1242
1243

1244 **Table 1.** Summary of model configurations.

Description	Selection	References
Horizontal grid spacing	20 km (D1), 4 km (D2)	
Grid dimensions	250×350, 300×400	
Topography	30 arcsec (USGS)	
Vertical layers	54 (roughly 17 layers below 2 km)	
Model top pressure	50 hPa	
Nesting approach	One-way	
Aerosol scheme	MOSAIC 8 bin	Zaveri et al., 2008
Gas-phase chemistry	CBM-Z	Zaveri and Peters, 1999
Long wave Radiation	RRTMG	Iacono et al., 2000; Zhao et
Short-wave Radiation	RRTMG	al., 2011, 2013a
Cloud Microphysics	Morrison 2-moment	Morrison et al., 2009
Cumulus Cloud	Kain-Fritsch	Kain, 2004
Planetary boundary layer	MYNN level 2.5	Nakanishi and Niino, 2006
Land surface	CLM	Oleson et al., 2010
Meteorological Forcing	ERA-Interim, 0.5°×0.66°, 6 hourly	

1245

1246

1247

1248

1249

1250

1251

1252

1253

1254

1255

1256

1257

1258

1259

1260

1261

1262

1263

1264
1265
1266
1267
1268
1269
1270
1271
1272
1273
1274
1275
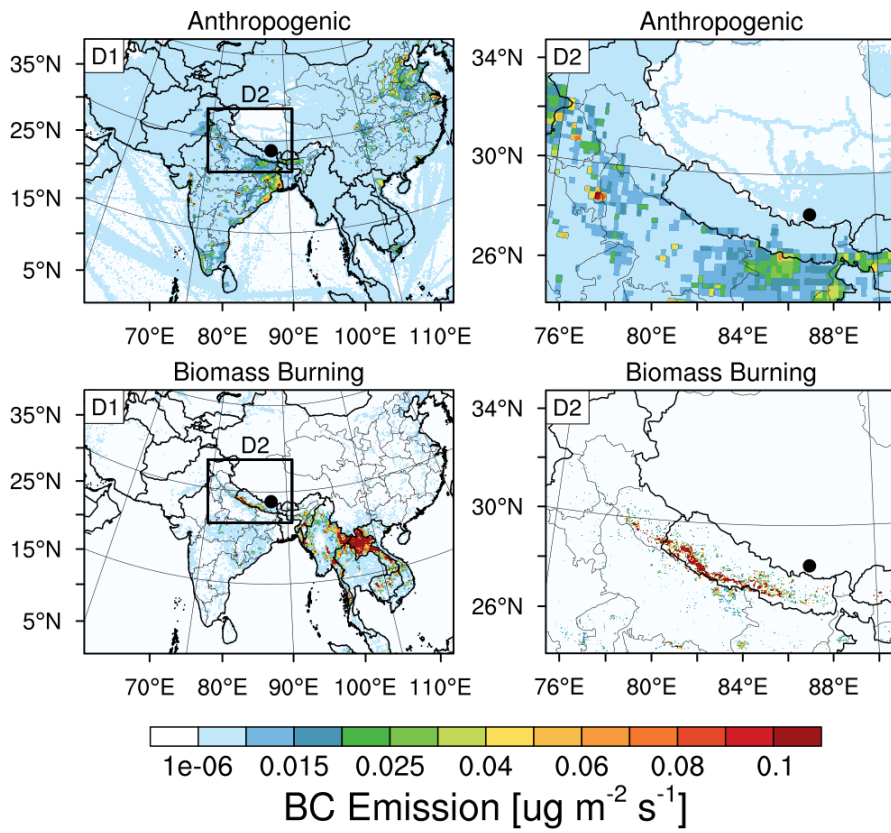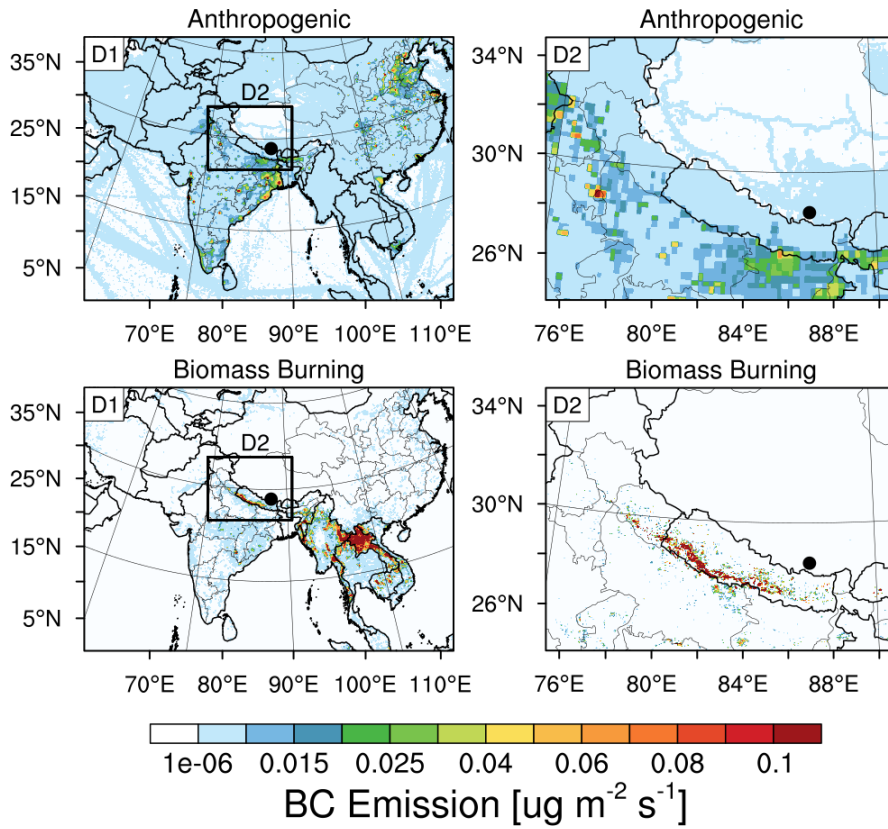
Figure 1. Anthropogenic and fire emissions over the entire simulated regions of 20-km and 4-km resolutions, the black dot represents the Qomolangma Station (QOMS, 86.95°E, 28.36°N).
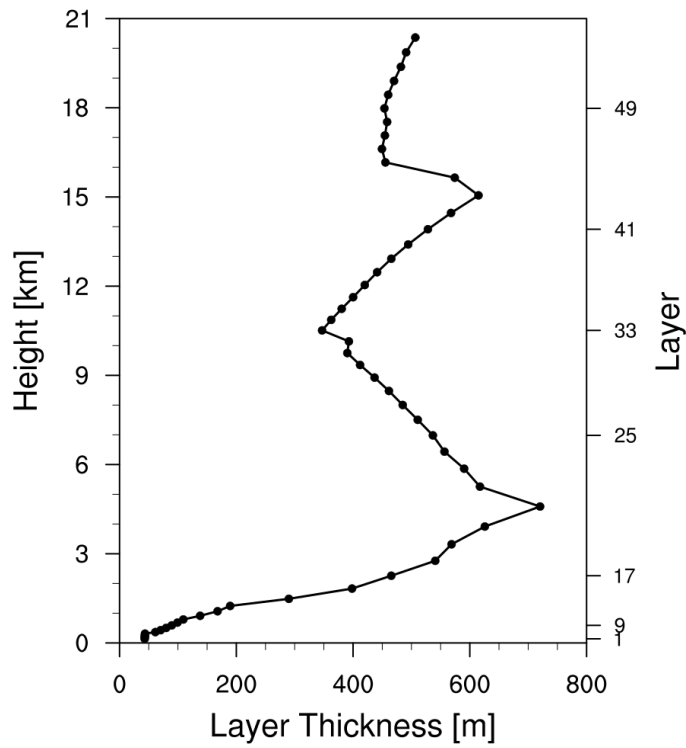
1303
Figure 2. The thickness of each vertical layer in the simulations (54 layers in total).

1304
1305
1306
1307
1308
1309
1310
1311
1312
1313
1314
1315
1316
1317
1318
1319
1320
1321
1322
1323
1324
1325
1326
1327
1328
1329
1330
1331
1332
1333
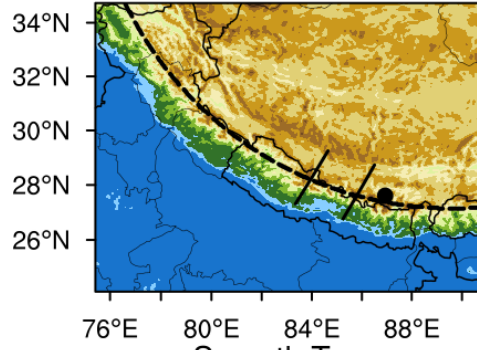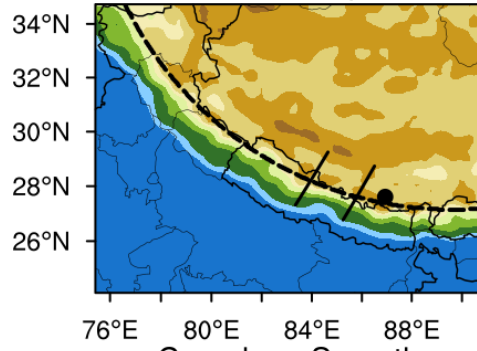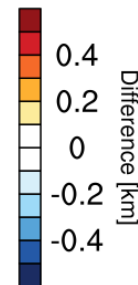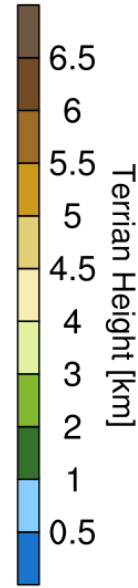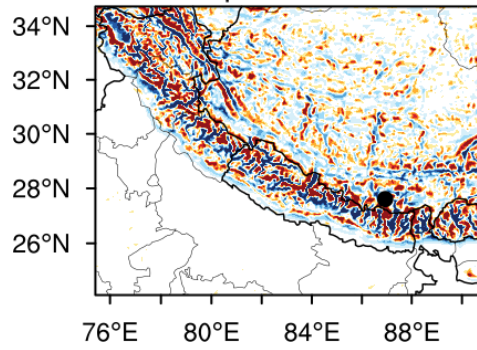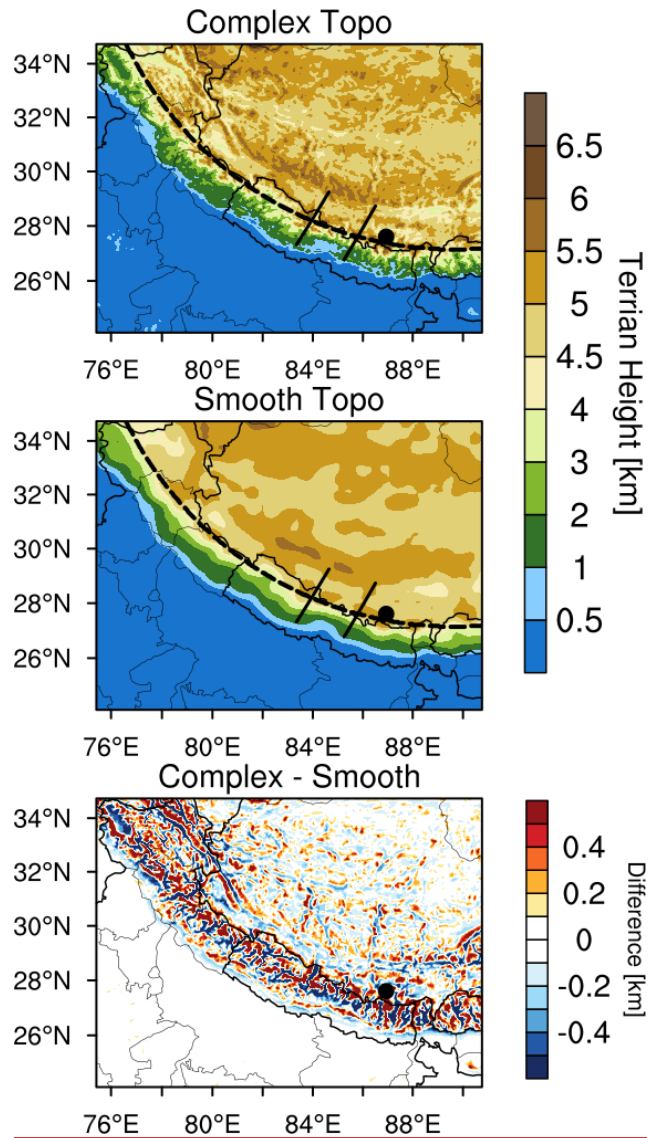
Figure 3. Spatial distributions of terrain height from the dataset at 20 km (Smooth Topo) and 4 km (Complex Topo). The one dash line and two solid lines represent the cross sections for analysis in the following.
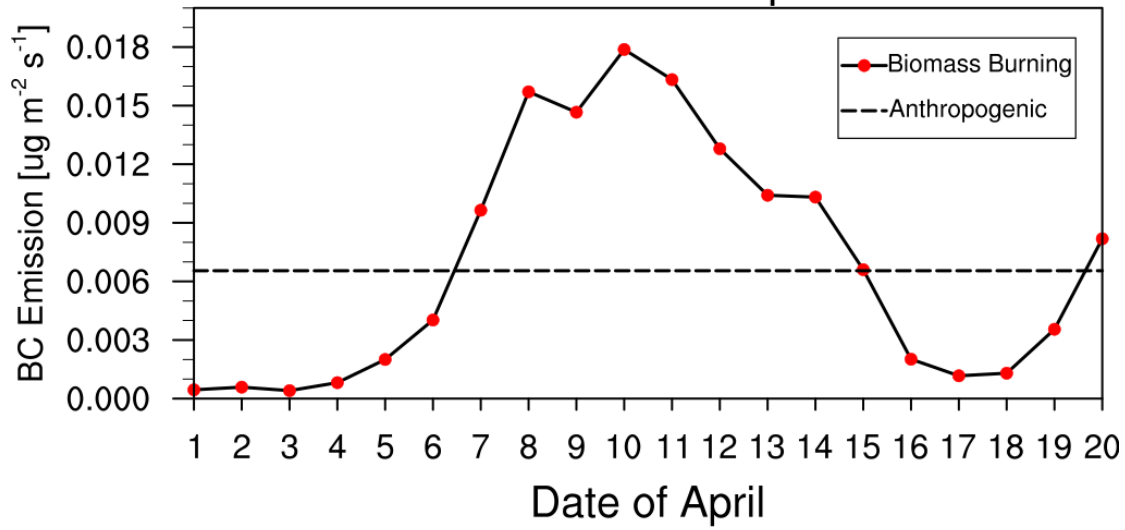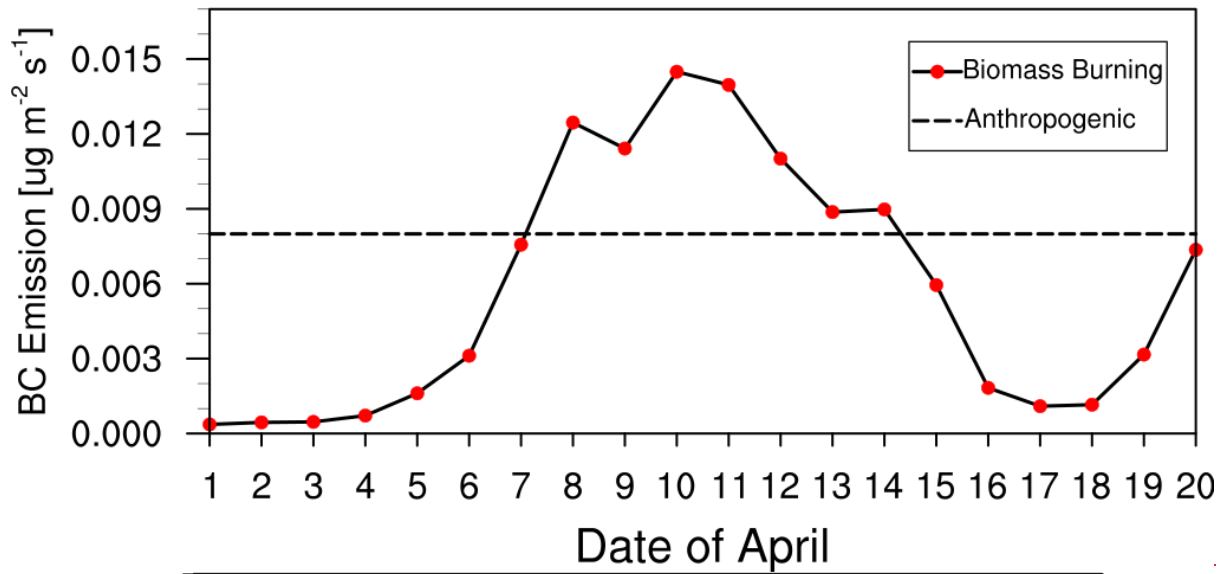
Figure 4. Time series of area-averaged daily fire emissions between 26°N and 29°N over the simulation domain at 4-km resolution (The dash line in the figure represents the anthropogenic emissions).

1377
1378
1379
1380
1381
1382
1383
1384
1385
1386
1387
1388
1389
1390
1391
1392
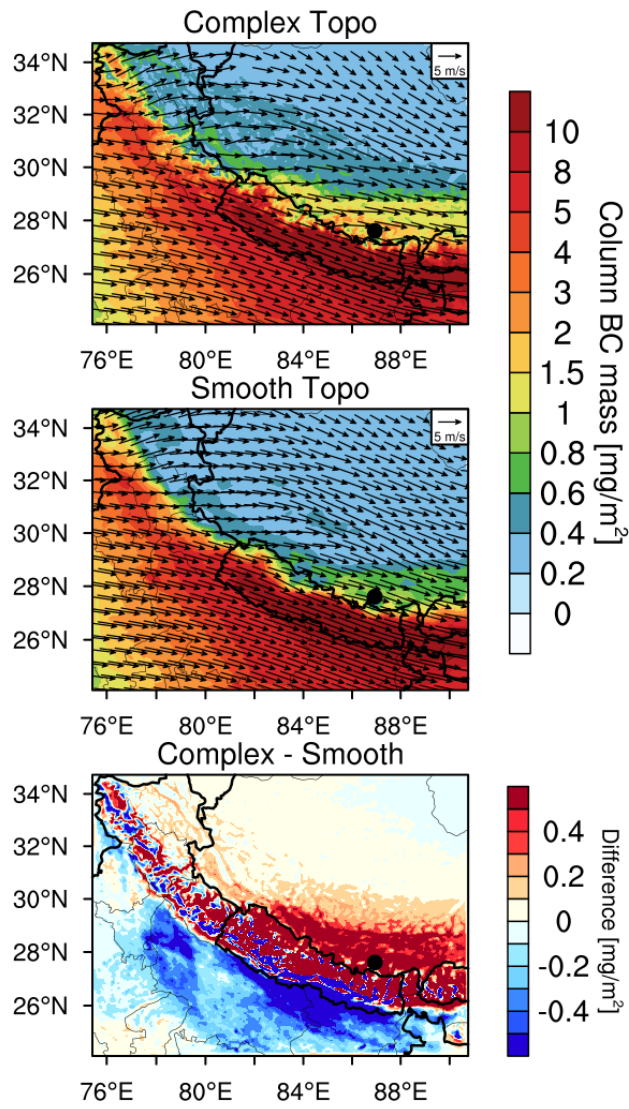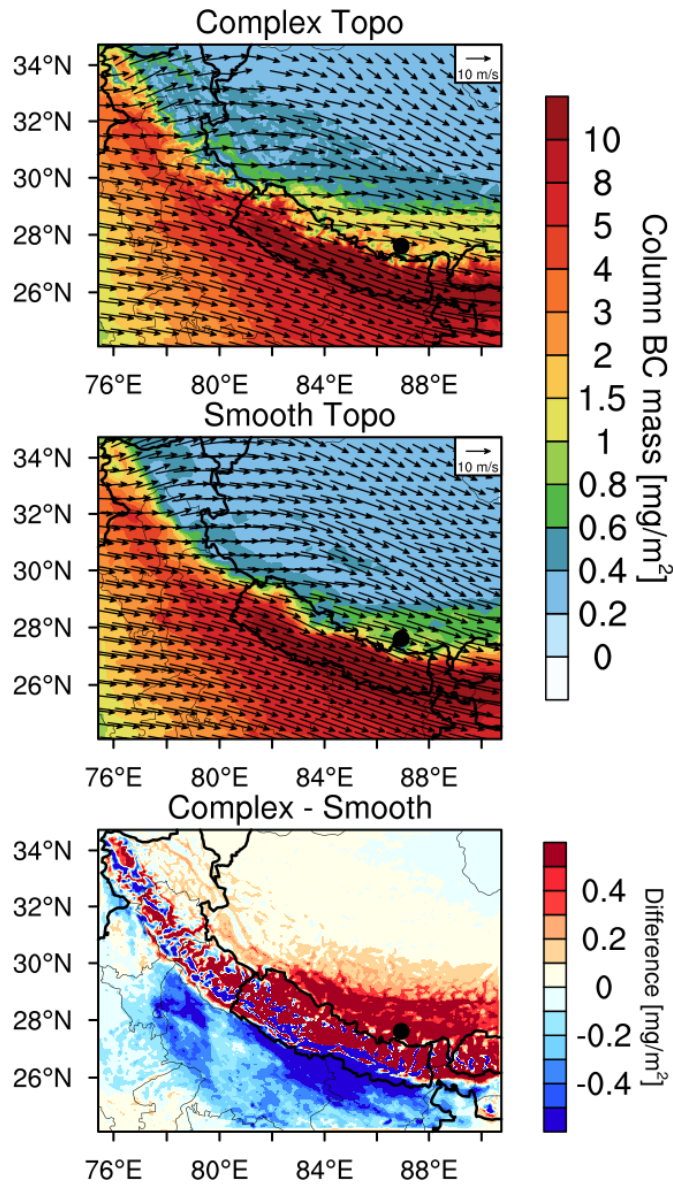
Figure 5. Spatial distributions of column integrated BC mass and the horizontal wind field at 500 hPa from the simulations with complex and smooth topography (Complex Topo and Smooth Topo) averaged for April 1-20, 2016. The difference between the two is also shown.

1413
1414
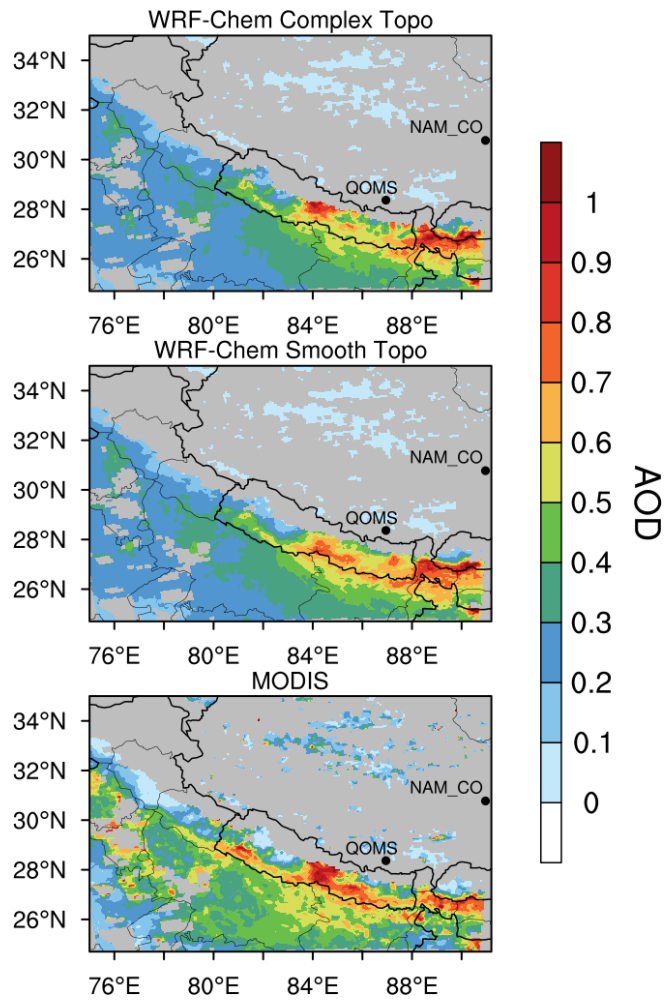
1415
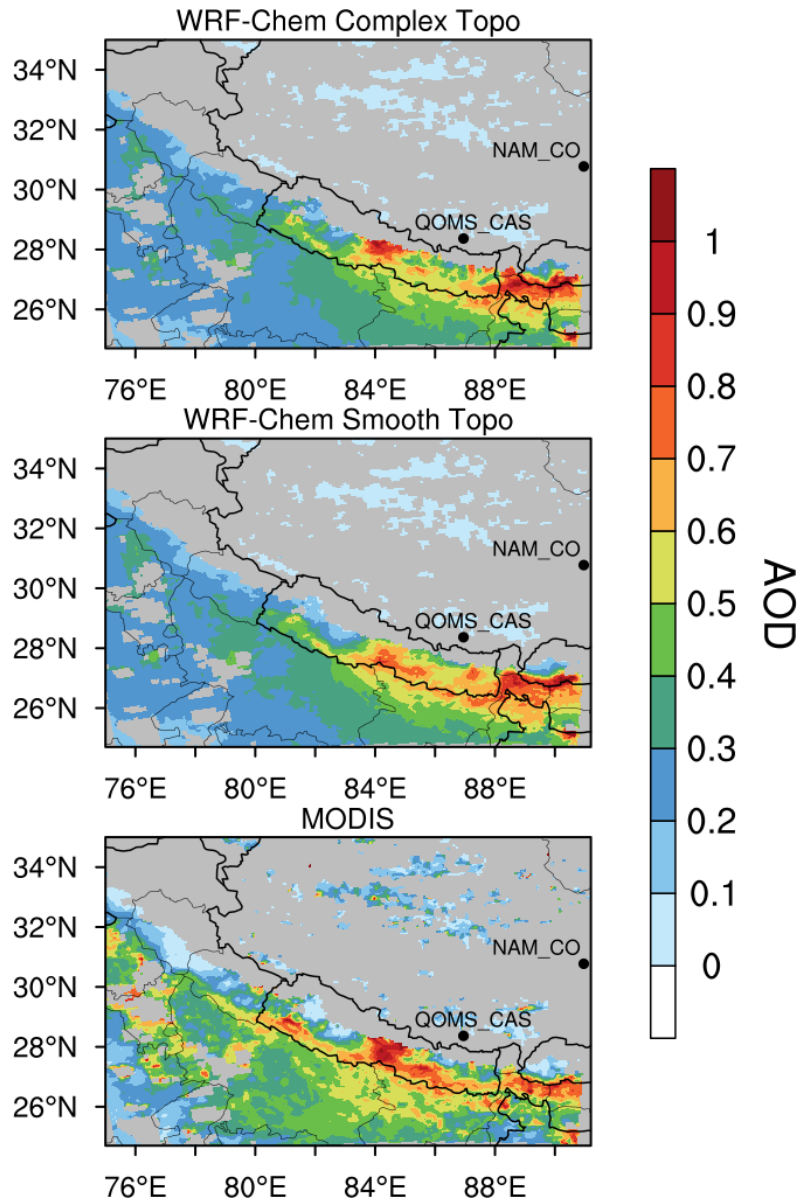
Figure 6. Spatial distributions of AOD from the MODIS retrievals and the simulations with complex and smooth topography averaged for April 1-20, 2016. The two black dots represent the two AERONET sites over the TP (QOMS_CAS, 86.95°E, 28.36°N; NAM_CO, 90.96°E, 30.77°N).

60
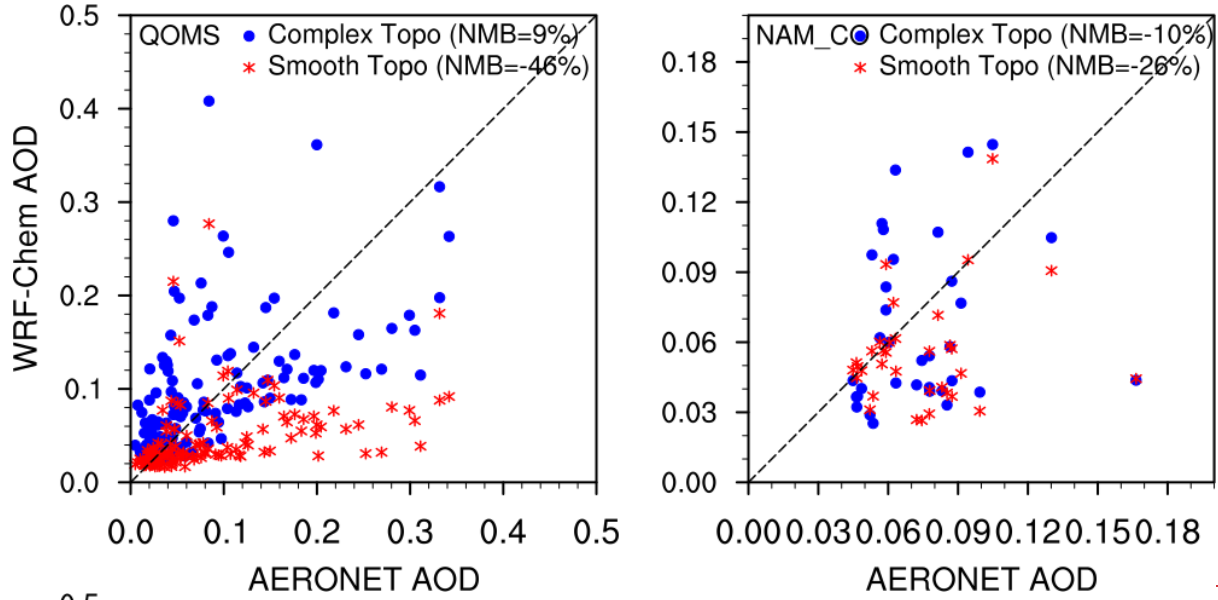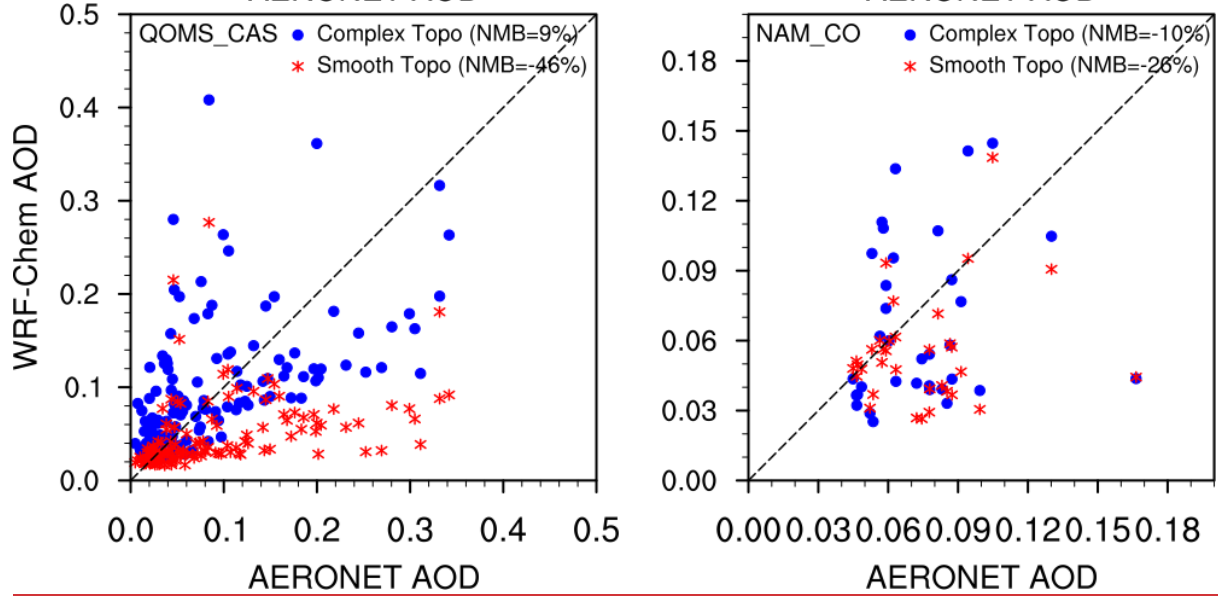
Figure 7. Hourly AOD from the measurements of AERONET and simulations by WRF-Chem at the two sites over the TP (QOMS_CAS, 86.95°E, 28.36°N; NAM_CO, 90.96°E, 30.77°N) for April 1-20, 2016.

61

1454
1455
1456
1457
1458
1459
1460
1461
1462
1463
1464
1465
1466
1467
1468
1469
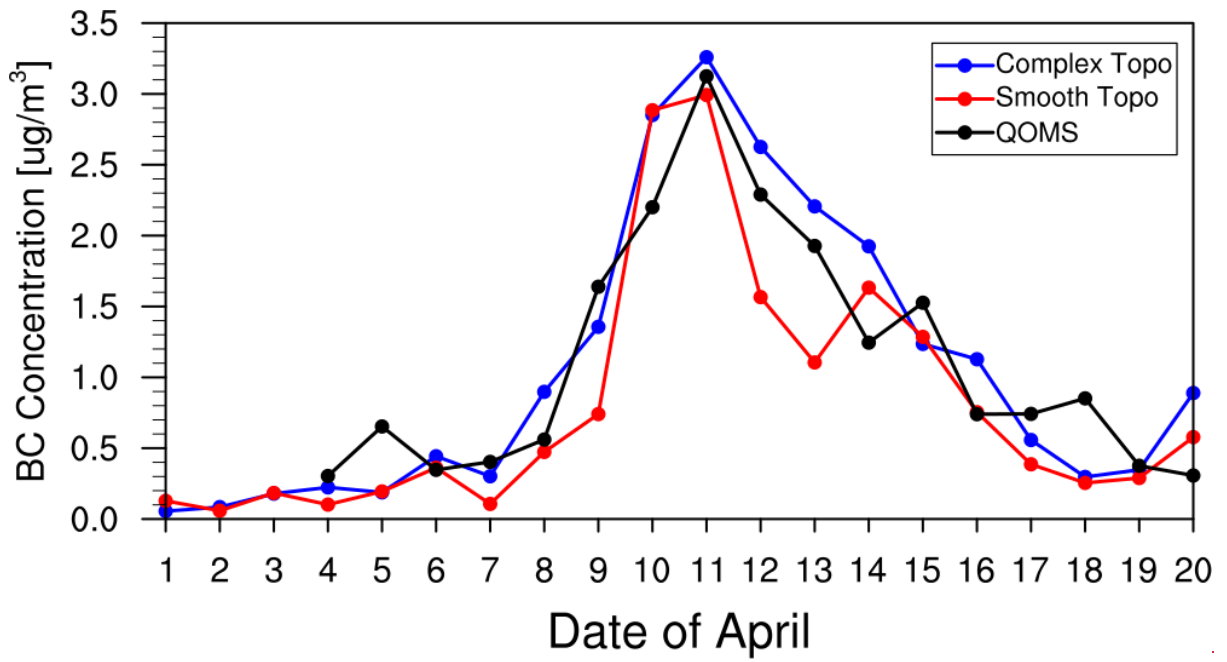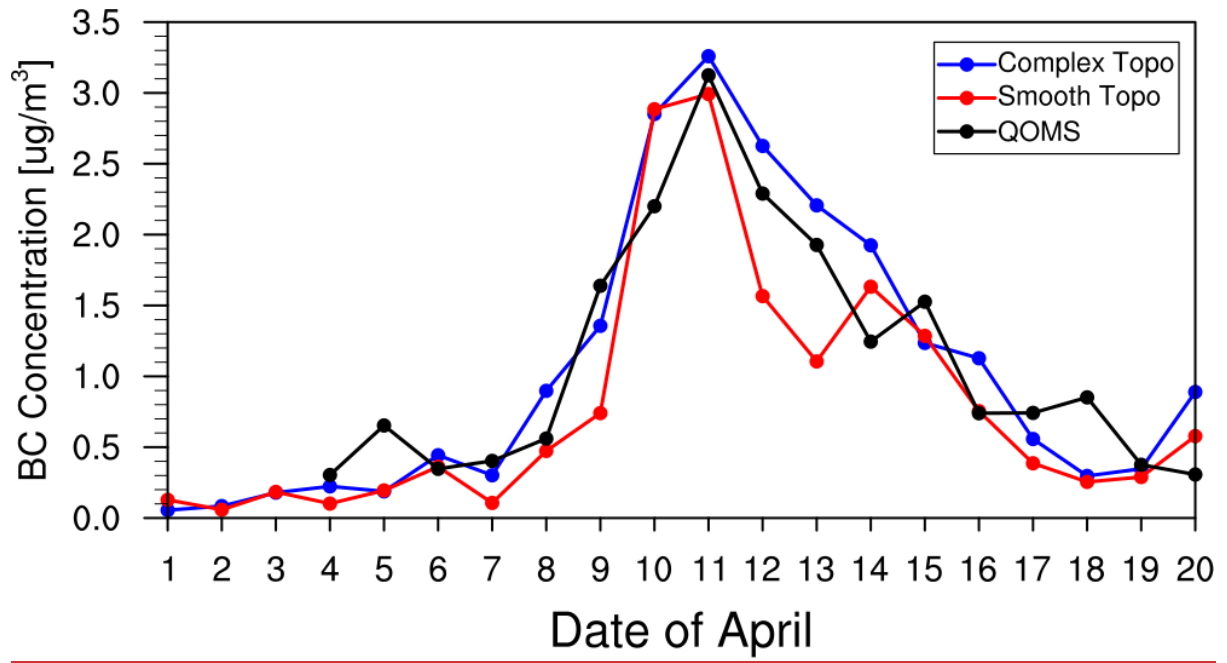
Figure 8. The simulated (colored) and observed (black) temporal variability of near-surface BC mass concentration at the measurement station during April 1-20 in 2016.

Figure 8. The simulated (colored) and observed (black) temporal variability of near-surface BC mass concentration at the measurement station during April 1-20 in 2016.
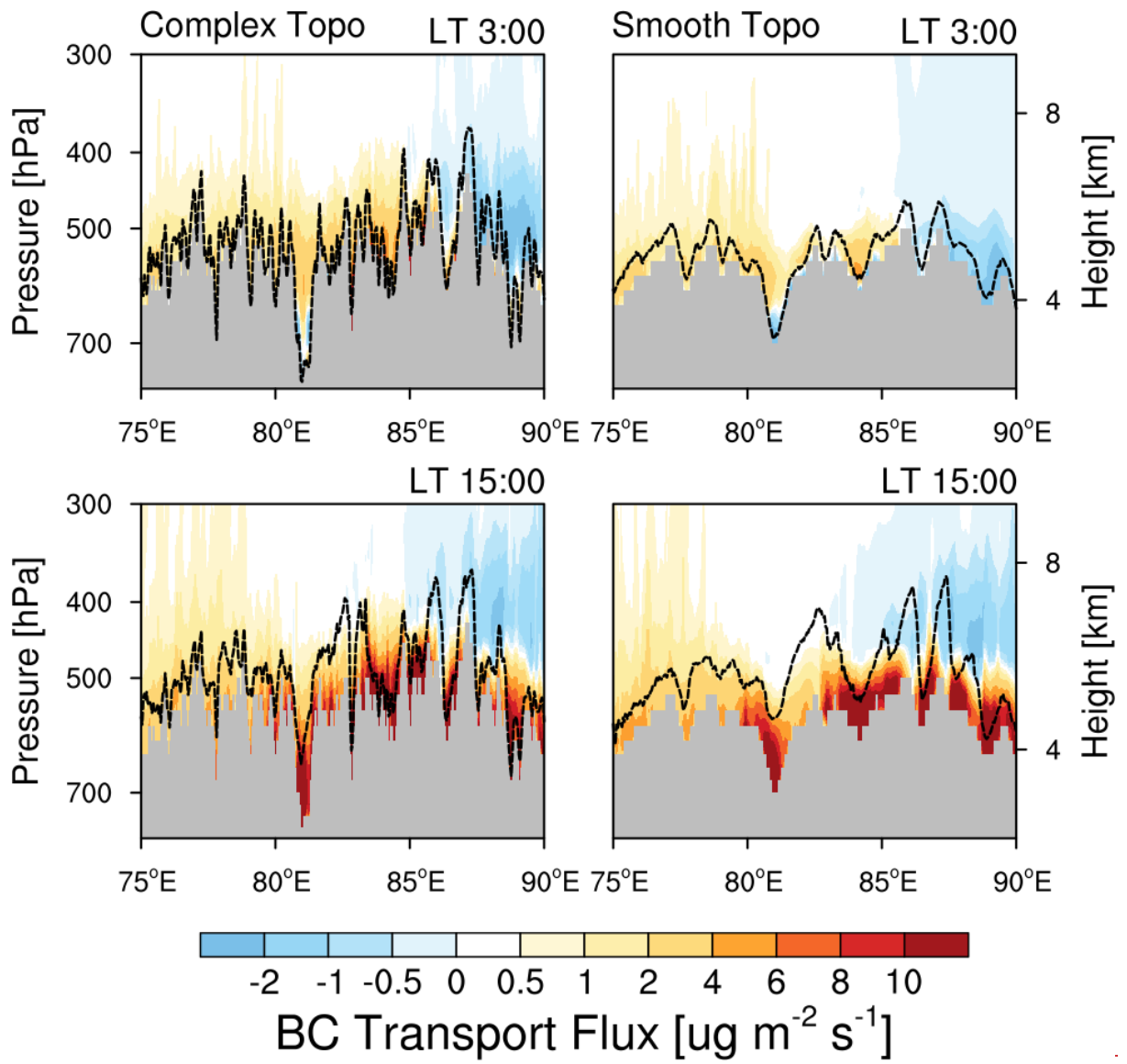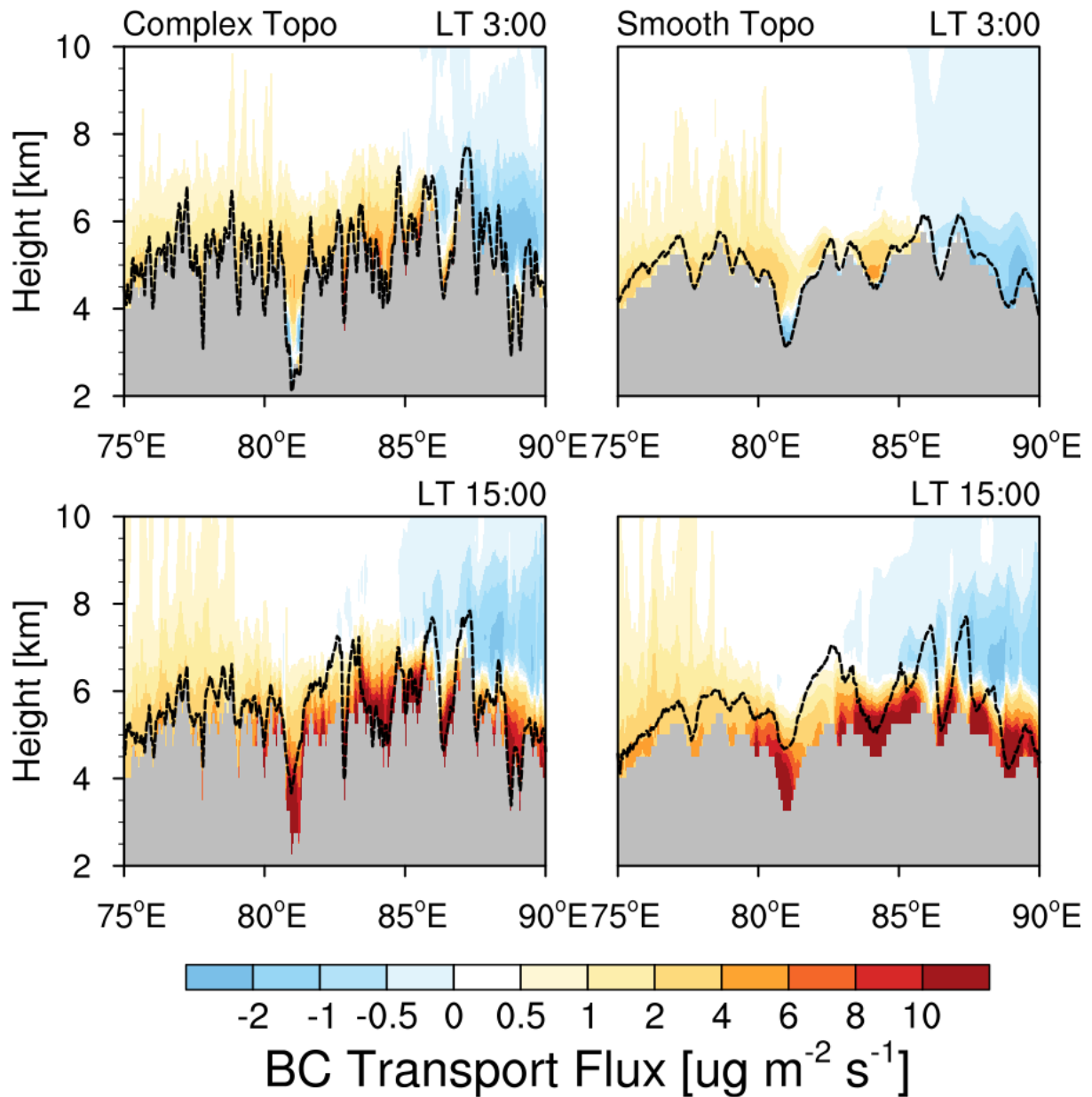
Figure 9. Longitude-height cross section of BC transport flux along the cross line (shown as the black dash line in Fig. 3) from the simulations with complex and smooth topography at local time (LT) 03:00 and 15:00 averaged for April 1-20. The PBL height along the cross section is shown here as the black dash line.
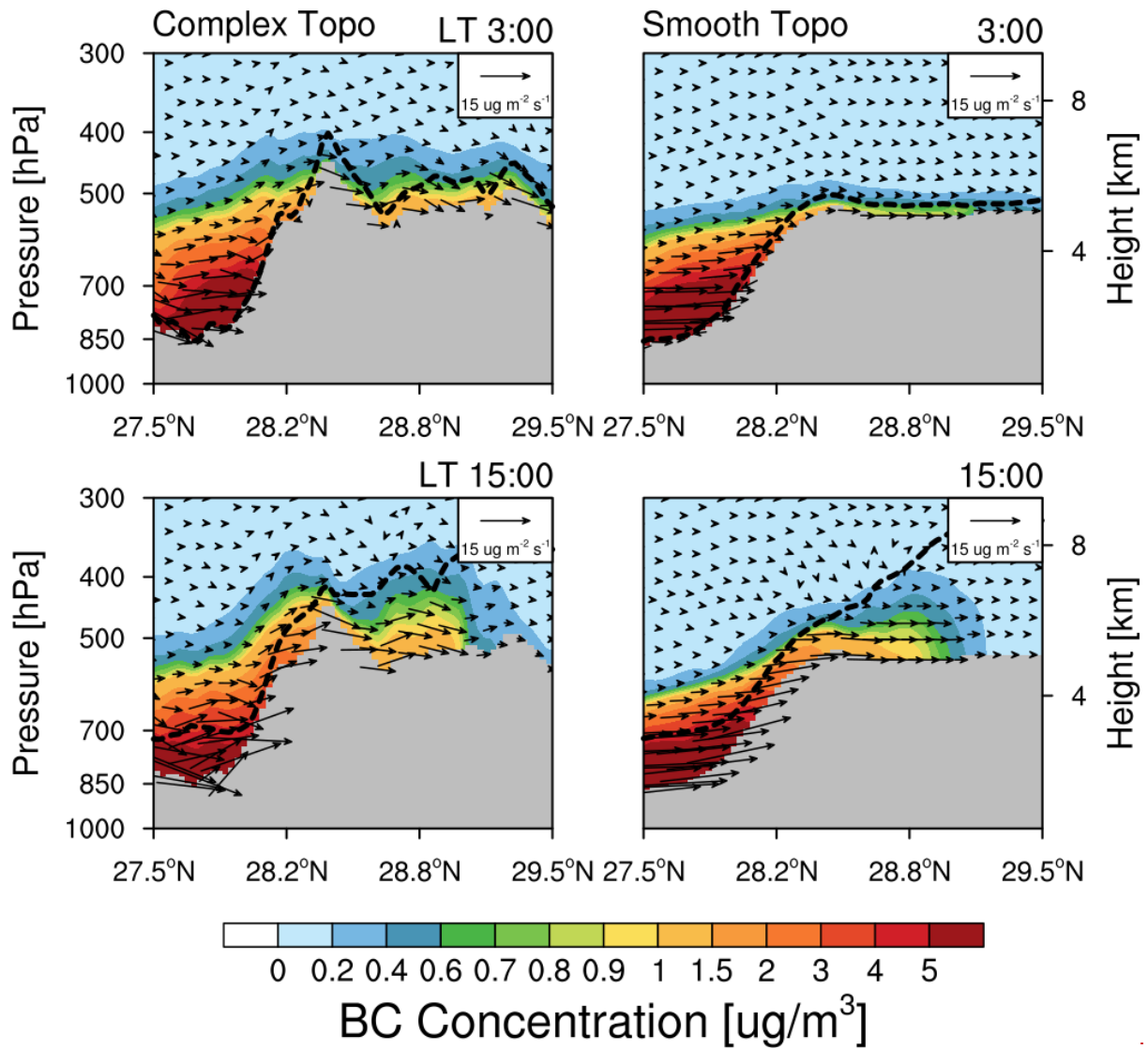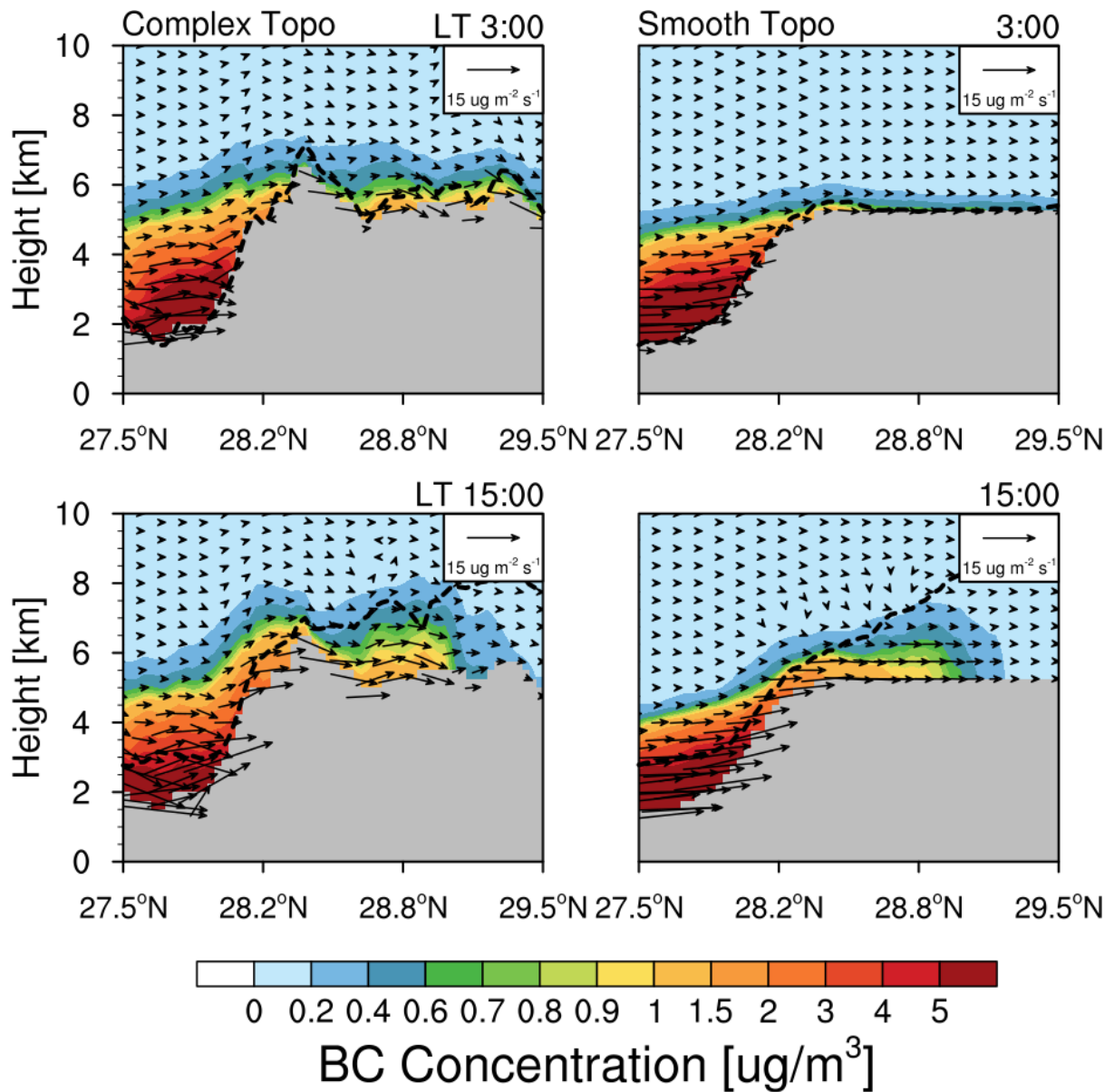
66

Figure 10. Latitude-height cross section of BC flux (vector) across the mountain (shown as the East black solid line in Fig.3) from the simulations with complex and smooth topography at local time (LT) 03:00 and 15:00 averaged for April 1-20, 2016. Contour represents the BC concentration.

68
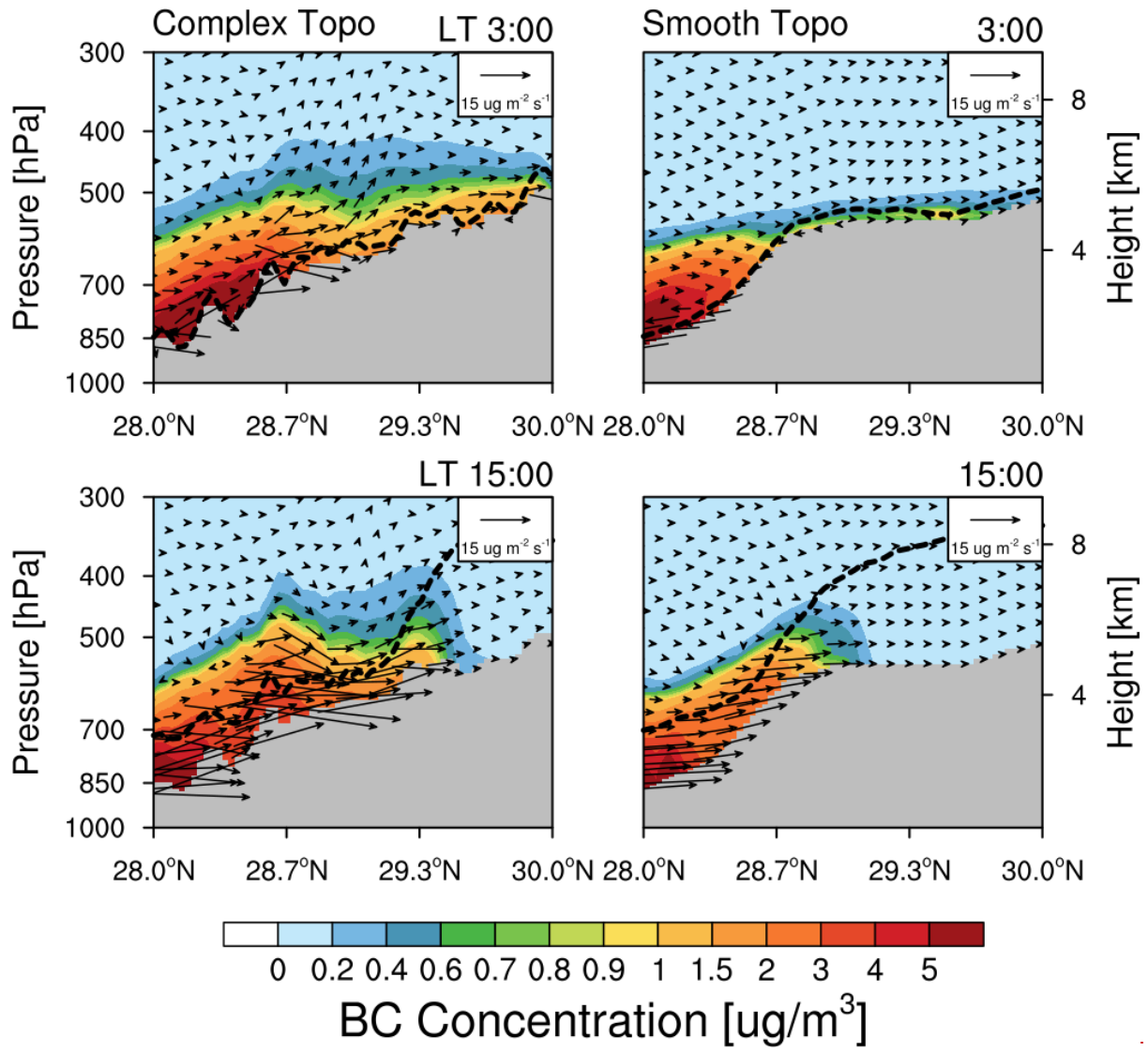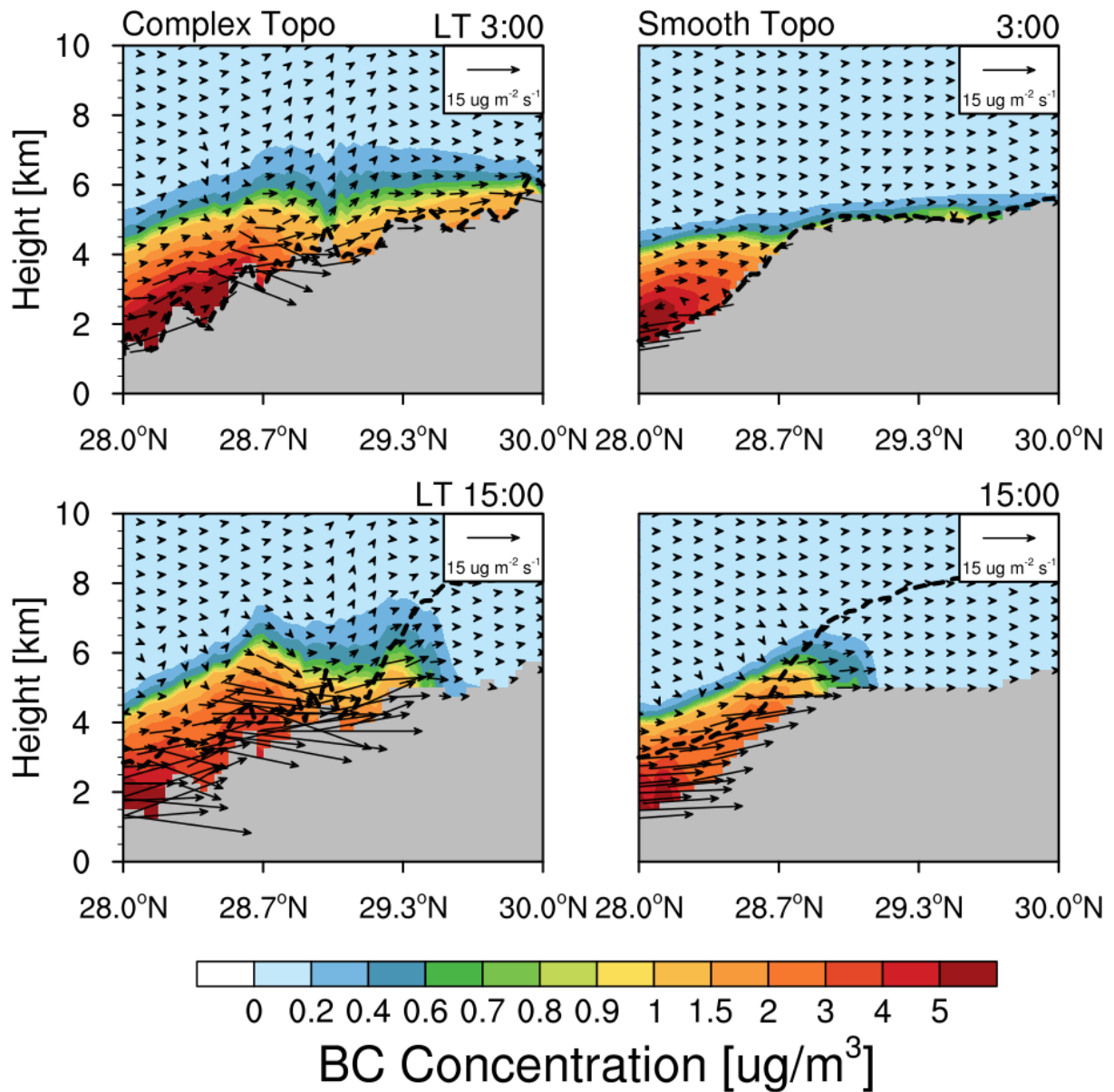
Figure 11. Latitude-height cross section of BC flux (vector) along the valley (shown as the West black solid line in Fig. 3) from the simulations with complex and smooth topography at local time (LT) 03:00 and 15:00 averaged for April 1-20, 2016. Contour represents the BC concentration.
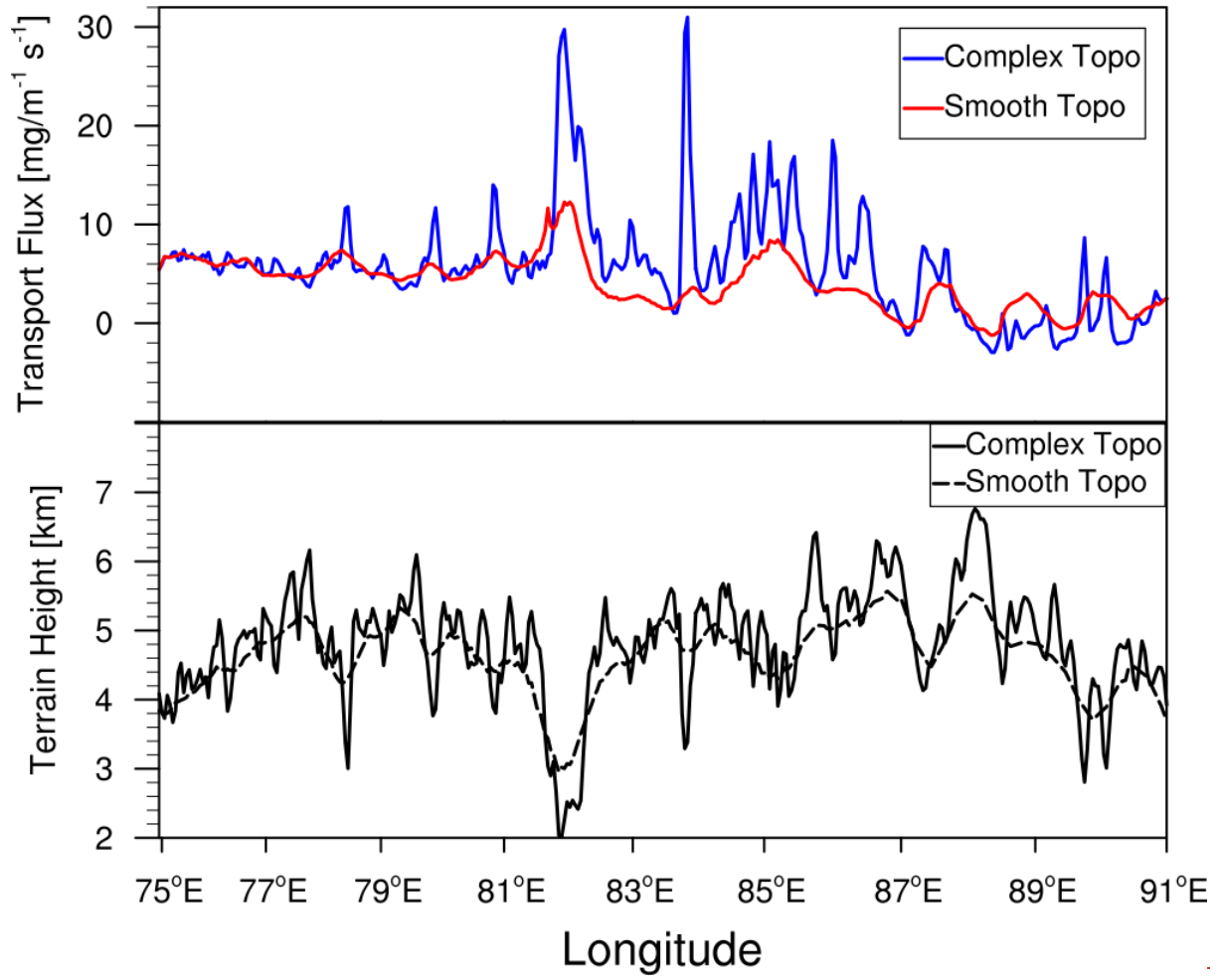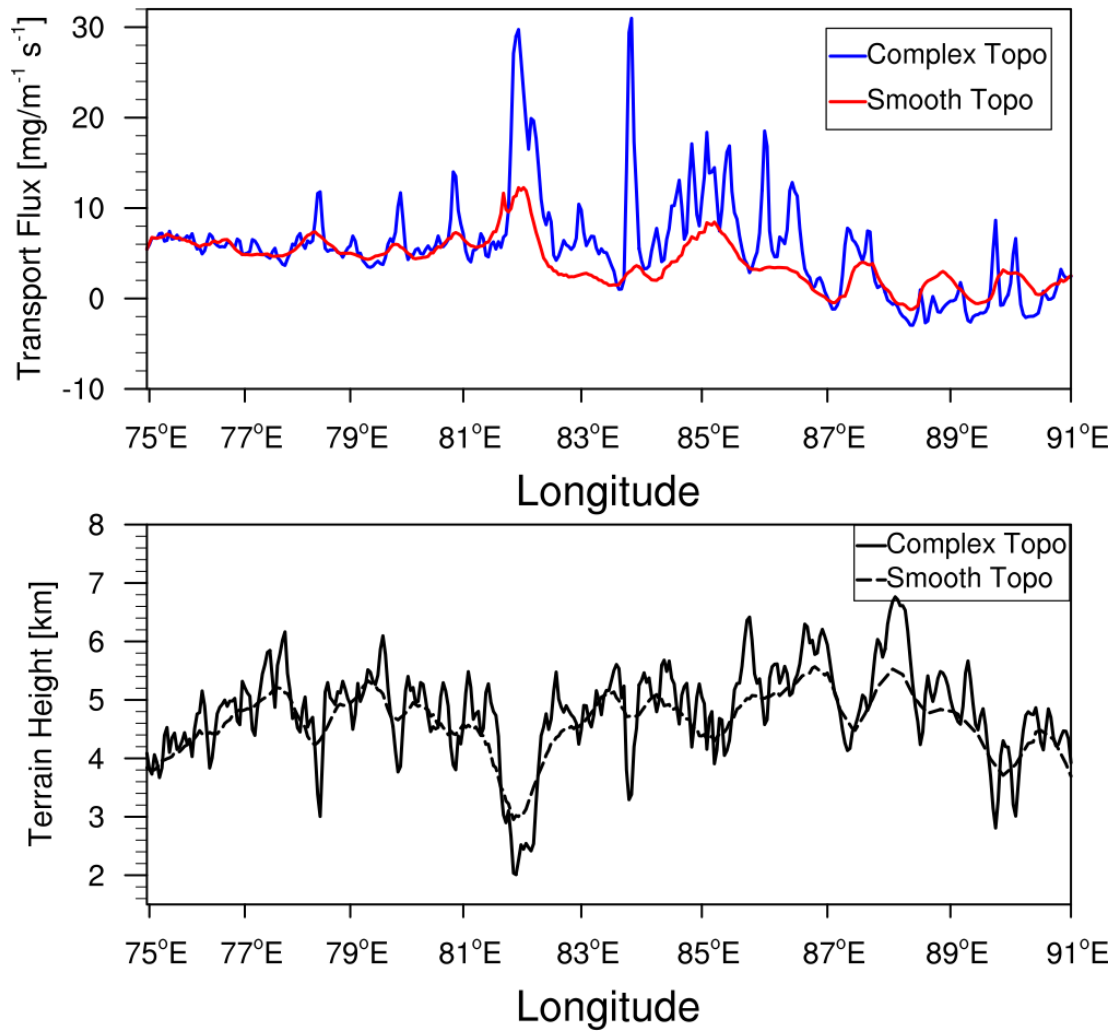
Figure 12. Longitudinal distribution of integrated BC mass flux along the cross section in Fig. 3 from the simulations with complex and smooth topography. The black lines represent the terrain heights with different topography.

1593
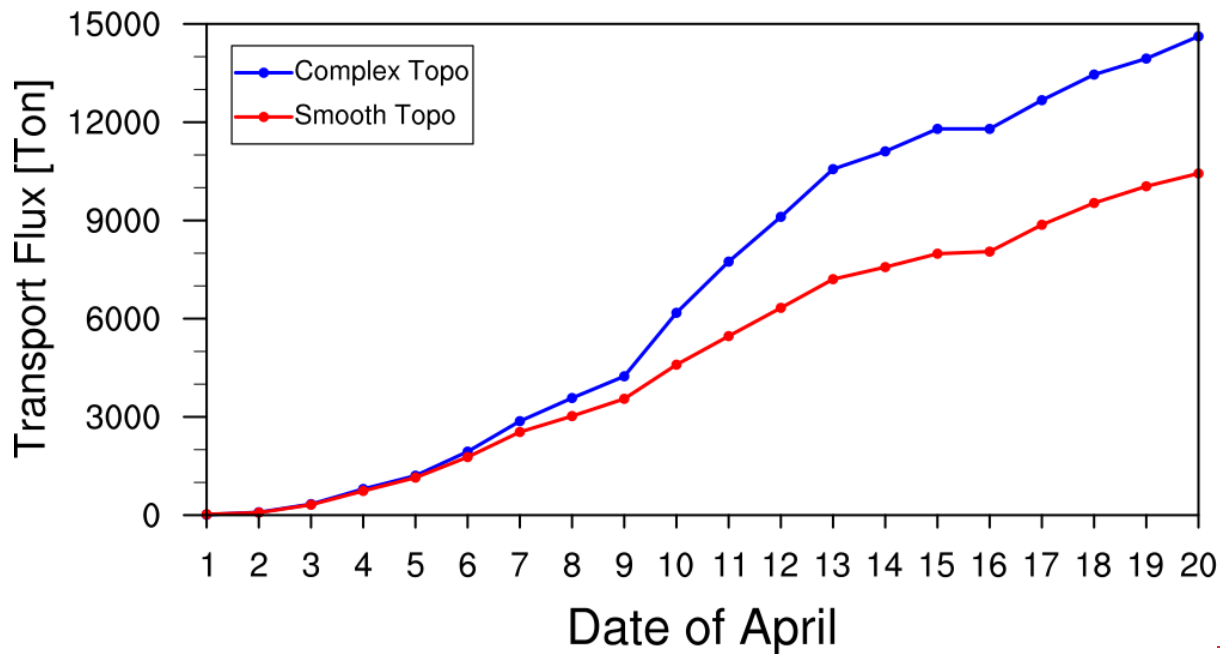
1594
1595 **Figure 13.**
1596
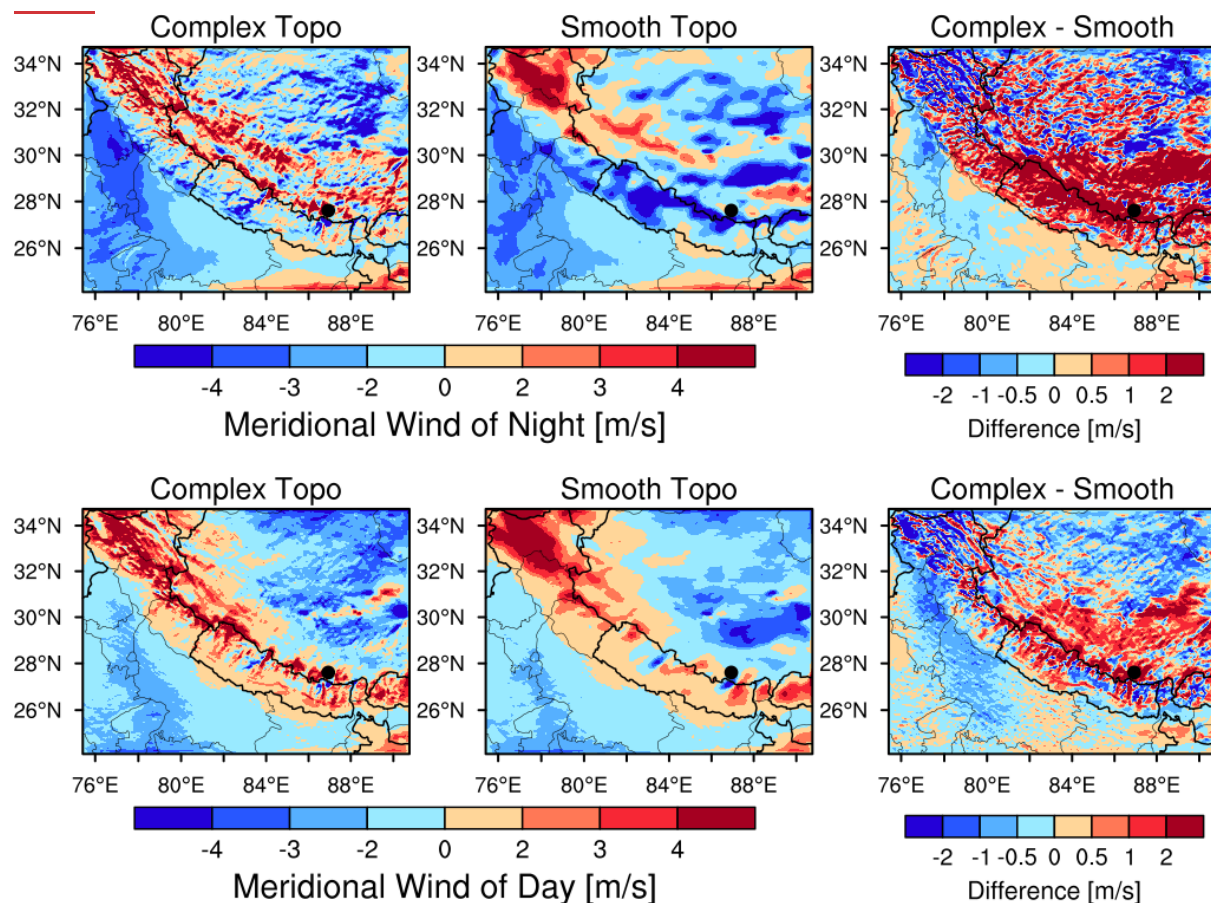
1597
1598 **Figure 13.** Spatial distributions of meridional wind speed averaged within 500 m above the
1599 ground for day and night during April 1-20, 2016 from the simulations with complex and
1600 smooth topography. The difference between the two is also shown. Nighttime is defined as
1601 local time 21:00-6:00, and daytime is defined as 9:00-18:00. Positive value denotes southerly,
1602 and negative value denotes northerly.

1603
1604
1605
1606
1607
1608
1609
1610
1611
1612
1613
1614
1615
1616
1617
1618
1619
1620
1621
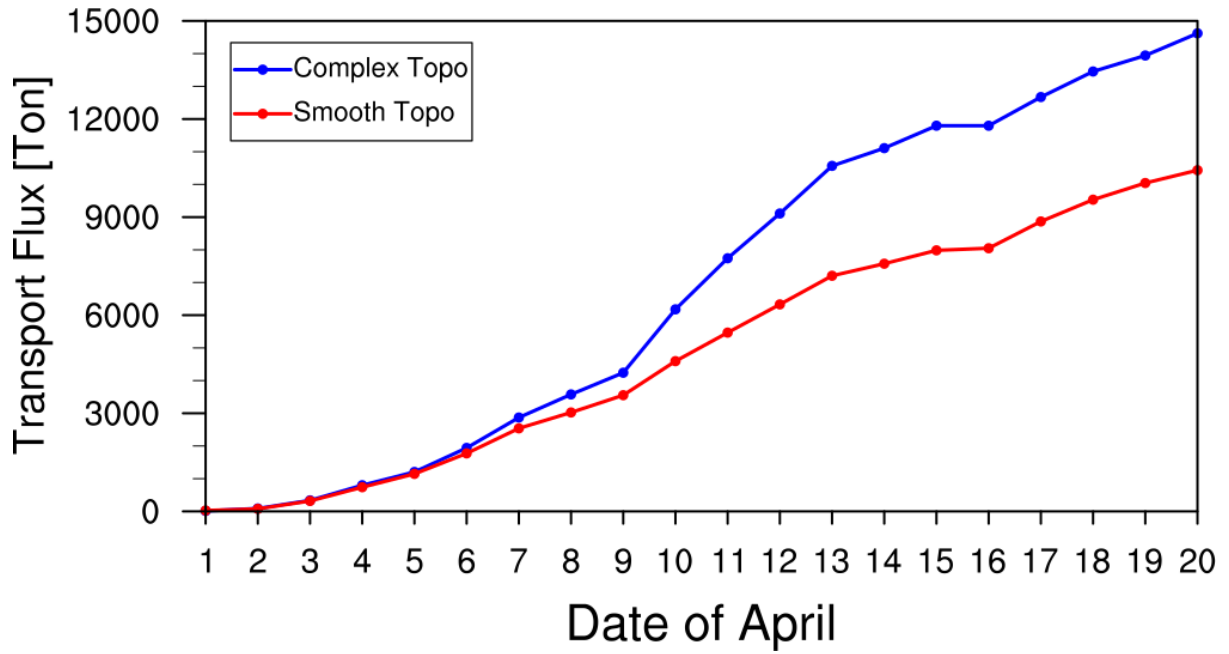
1622
1623
1624
1625
1626
1627
1628
1629
1630
1631
1632
1633
1634
1635

Figure 14. Accumulated integrated total transport flux of BC across the Himalayas estimated from the simulations with complex and smooth topography during April 1-20, 2016.

1636
1637
1638
1639
1640
1641
1642
1643
1644
1645
1646
1647
1648
1649
1650
1651
1652
1653
1654
1655
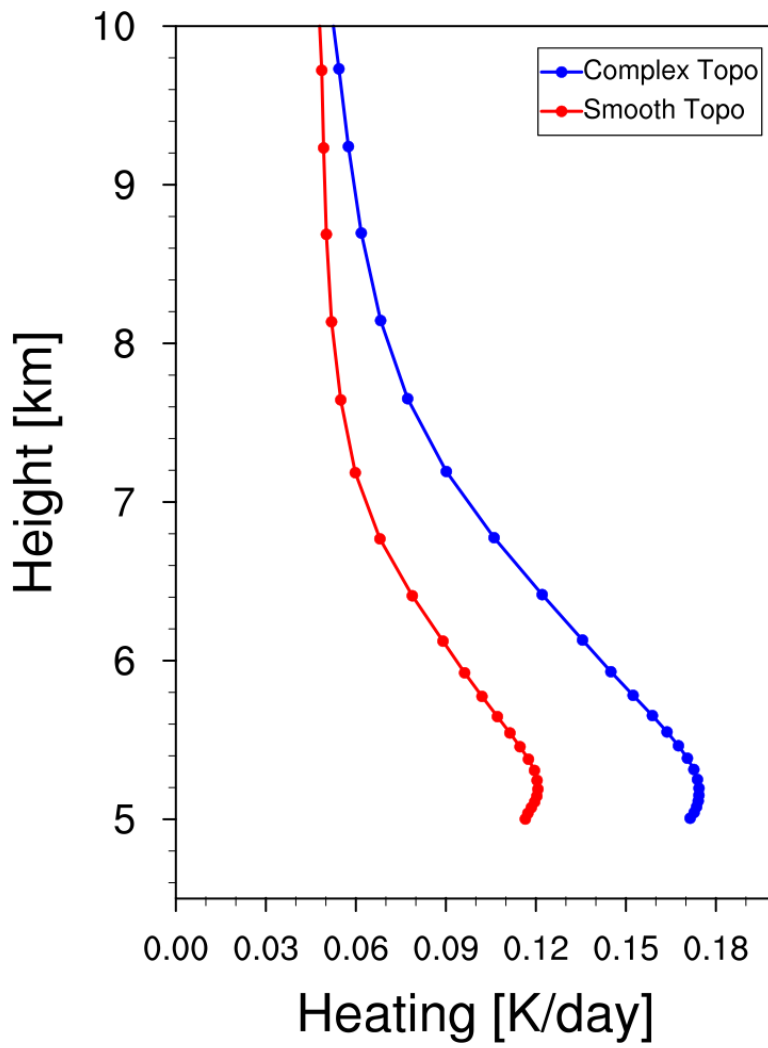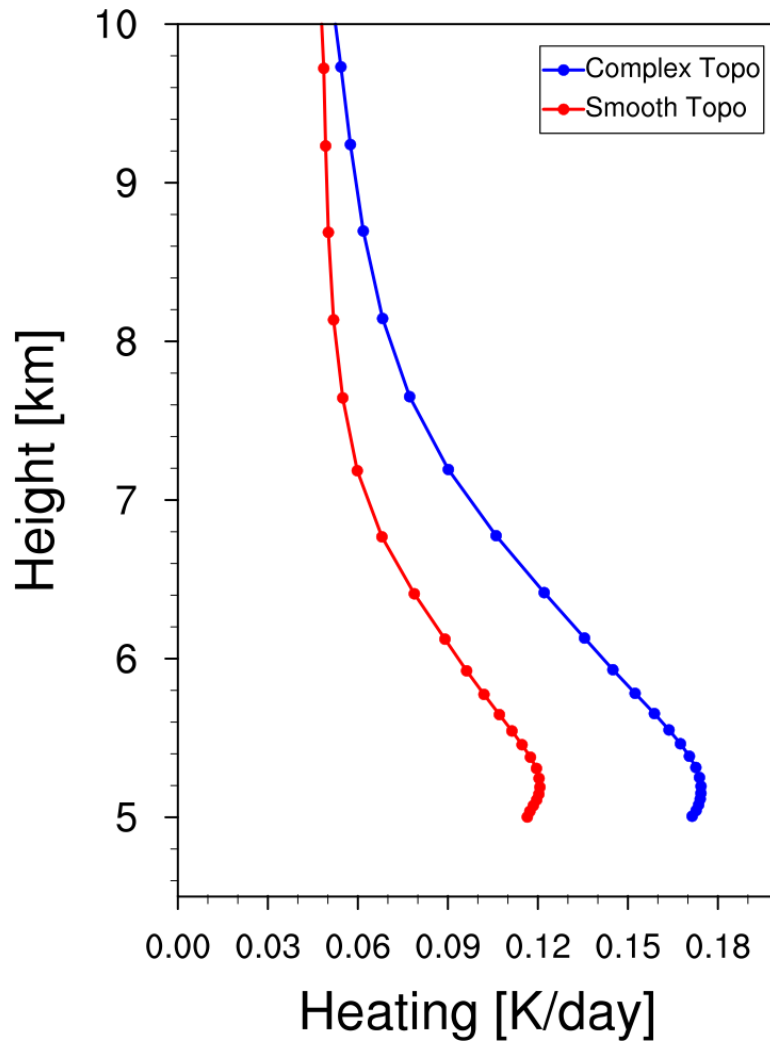
Figure ~~14~~15. Vertical profiles of BC induced radiative heating rate in the atmosphere averaged over the TP (with elevation > 4 km) from the simulations with complex and smooth topography during April 1-20, 2016.
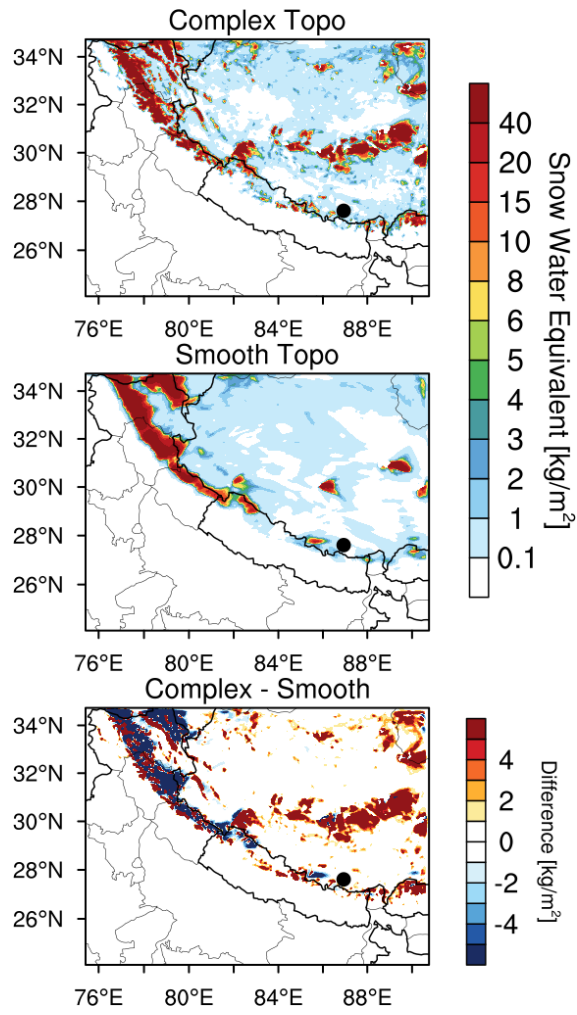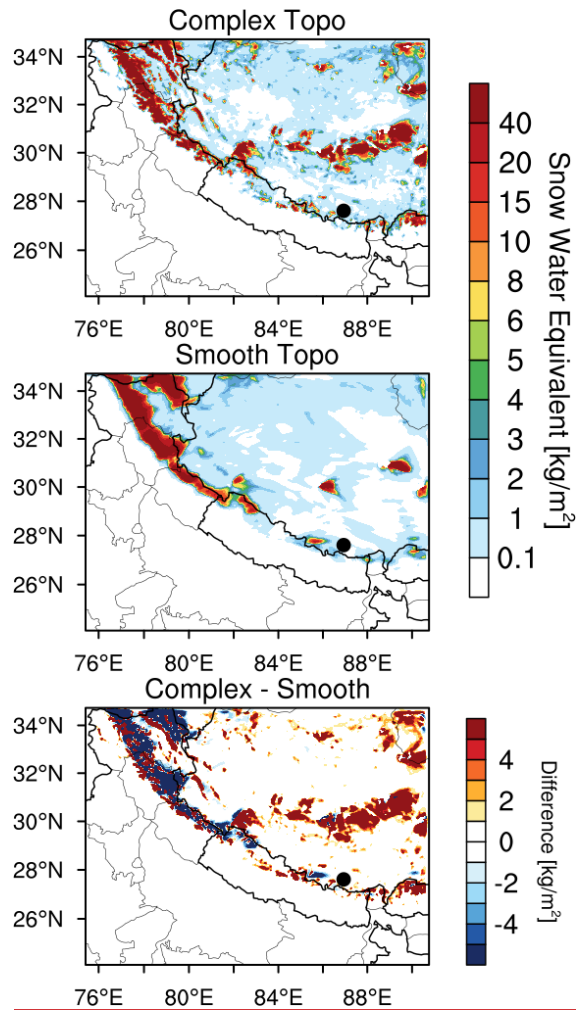
Figure ~~15~~16. Spatial distributions of snow water equivalent averaged for April 1-20, 2016 from the simulations with complex and smooth topography. The difference between the two is also shown.
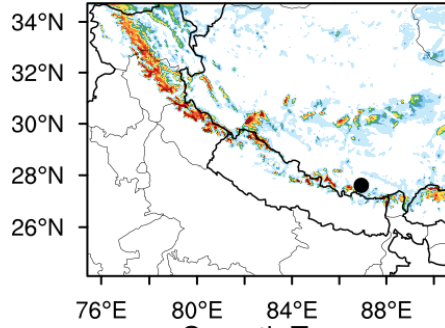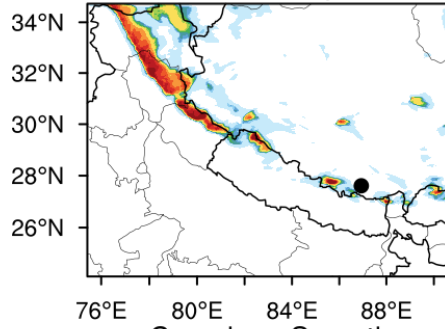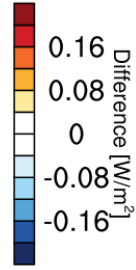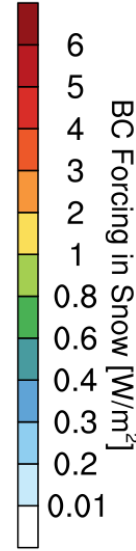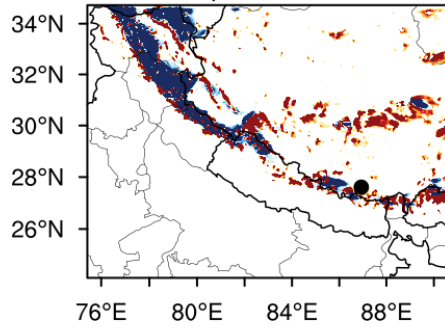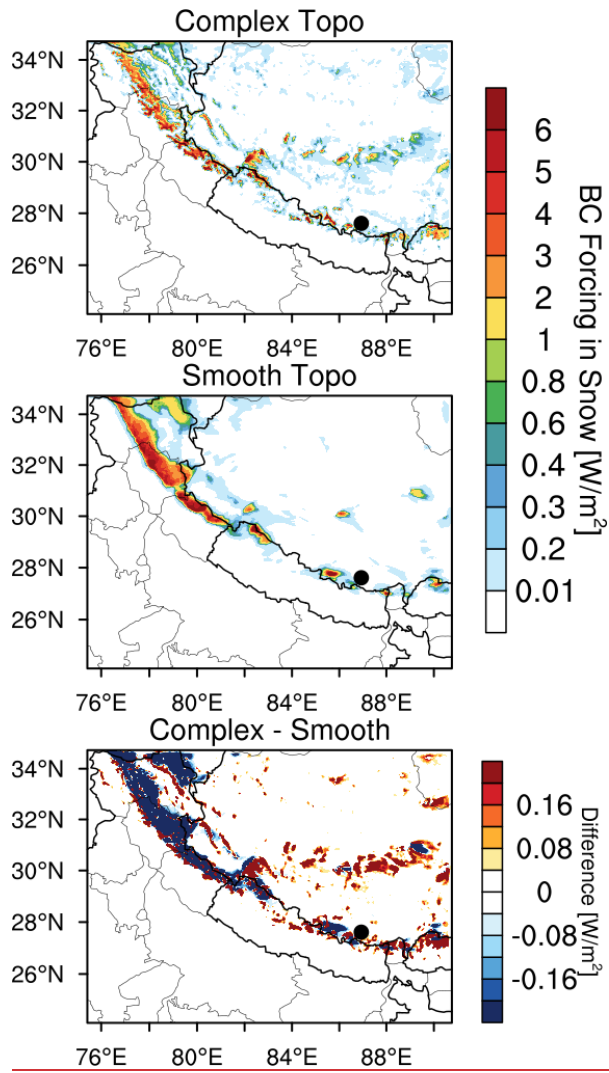
Figure ~~16~~17. Spatial distributions of BC radiative forcing in the surface snow averaged for April 1-20, 2016 from the simulations with complex and smooth topography. The difference between the two is also shown.